Doctoral Dissertation

博士論文

Evaluation of rainfall-induced mass movements and sediment yields in Taiwan

(台湾における降雨で生じたマスムーブメントと土砂流出の評価)

Chi-Wen CHEN

陳 麒文

Department of Natural Environmental Studies,

Graduate School of Frontier Sciences,

The University of Tokyo

東京大学大学院新領域創成科学研究科

自然環境学専攻

Abstract

Rainfall-induced mass movements are significant natural hazards in Taiwan. However, few studies have explored the rainfall conditions associated with mass movements for a broad area in Taiwan. This dissertation presents results of studies for the whole of Taiwan, to establish the relationship between the initiation of mass movements and rainfall conditions, apply a useful index to Taiwan which may contribute to a future warning system of mass movements, identify dimensional characteristics of landslides, and discuss the effects of landslides on the sediment discharge in rivers.

This study analyzed mass movements caused by rainfall events in Taiwan during a seven-year period from 2006 to 2012. Data from 263 mass movement events, including 172 landslides and 107 debris flows (16 events with both), were collected from the reports of the Soil and Water Conservation Bureau of Taiwan. After confirming the location of each event, we compiled relevant rainfall data by interpolating data from >400 rain gauges. Subsequently, the rainfall intensity–duration (*I*–*D*) relationship was examined to establish the rainfall threshold for mass movements using random sampling: $I = 18.10(\pm 2.67)D^{-0.17(\pm 0.04)}$, where *I* is mean rainfall intensity (mm/h) and *D* is the time between the beginning of a rainfall event and resulting mass movements (h). Significant differences in the rainfall intensity and the thresholds were detected between landslides and debris flows. For short duration rainfall events, higher mean rainfall intensities were required to trigger debris flows. Contrastingly, for long duration rainfall events, similar mean rainfall intensities triggered both landslides and debris flows. We also rescaled mean rainfall intensity using mean annual precipitation (*MAP*), which defined a new threshold calculated as

I_{MAP} = 0.0060(±0.0009)$D^{-0.17(\pm0.04)}$, where I_{MAP} is the rainfall intensity rescaled by a *MAP* value of 3,000 mm, the minimum *MAP* of mountainous areas in Taiwan. Although the *I–D* threshold for Taiwan was high relative to those for other areas around the world, the I_{MAP}–*D* threshold tended to be lower. Our results indicate that Taiwan is highly prone to rainfall-induced mass movements. This study also shows that most of the mass movements occurred around the period when rainfall intensity was highest, but some events occurred significantly before and after the rainfall peak. Both the antecedent and peak rainfall played important roles in triggering landslides, whereas debris flow occurrence was more related to peak rainfall than antecedent rainfall.

We also used the soil water index (*SWI*) which can represent the conceptual soil water contents as influenced by the present and antecedent rainfall. *SWI* is used by the Japan Meteorological Agency to assess mass movement hazards in Japan. Previous studies show that *SWI* can successfully predict the occurrence of mass movements in Japan. Therefore, this study examines whether *SWI* can be also applied to Taiwan. We used the mass movement data in 2006–2012 for analyses and those in 2013 (n = 19) for verification. The values of *SWI* before the rainfall events which triggered mass movements were used as the indicator of the antecedent rainfall condition. We found that under different values of *SWI* before rainfall events, the rainfall conditions needed for triggering mass movements, such as the rainfall intensity, duration, and cumulative rainfall, are different. Then we classified rainfall conditions for triggering mass movements into two types, short duration–high intensity (SH) and long duration–low intensity (LL), based on the principal component analysis. The SH type is associated with a rapid increase of *SWI* within a short duration, and the LL type is with a gradual rise and subsequent constancy of *SWI*. Based on this result, we modeled the general trend of changes in *SWI* for the two types. We then verified the model by analyzing

the mass movements in 2013, with 14 SH types and five LL types. We also checked hourly changes in *SWI* for these events and found that they all followed the general trend of the inferred SH and LL curves. From these results, it seems possible to predict a mass movement of the SH or LL type at an early stage of a rainfall event. Our results indicate that *SWI* is applicable to Taiwan in assessing regional mass movement hazards.

Both *I–D* thresholds and *SWI* contribute to mass movement warnings. For the *I–D* threshold, once the rainfall conditions exceed the threshold, it can provide warnings of a potential mass movement hazard. According to our results, both antecedent rainfall and peak rainfall intensity play important roles in triggering mass movements. The results of *SWI* also showed that soil water contents for many cases of LL type increased rapidly before mass movements. However, this phenomenon cannot be found in the *I–D* threshold because it is defined as the minimum-level of the rainfall conditions, and the *I–D* plots represent average rainfall event conditions and do not necessarily reflect some sporadic high rainfall intensities. Thus, predicting the exact time of mass movements using only the *I–D* threshold is difficult. On the other hand, *SWI* is a long-term and dynamic index that reflects effects of antecedent rainfall and temporal rainfall intensity variations. Therefore, real-time monitoring using *SWI* together with the *I–D* conditions allows local authorities to make appropriate decisions about mass movement warnings.

Among the 263 mass movements during 2006–2012, this study identified dimensional characteristics of 172 landslides. The area of each landslide was mapped and calculated using FORMOSA–II satellite images. The volume and depth were also calculated using empirical formula. Comparing the landslide size with rainfall conditions, this study found that deep landslides usually occurred due to long duration and moderate intensity rainfall, whereas shallow landslides occurred due to short

duration and high intensity rainfall. This observation is consistent with some previous studies and is ascribable to the fact that deep landslides need a high groundwater level, soil moisture, and pore water pressure caused by a prolonged rainfall. Concerning the area of landslides, their frequency–area distribution correlates well with a power-law relation having an exponent of −1.1, over the range 6.3×10^2 m^2 < A_L < 3.1×10^6 m^2. The slope of the power-law relation for Taiwan is lower than those for other areas around the world. It indicates that for the same total area or total number of landslides, the proportion of large landslides will be higher in Taiwan than in other areas. To assess landslide events particularly historical ones, this study has also proposed a landslide-event magnitude scale m_L = log V_a, where V_a is the average volume of landslides associated with an event. The average m_L for all landslides during 2006–2012 was estimated to be 6.4.

Debris sourced from mass movements will result in environmental problems such as increased sediment discharge in rivers. This study analyzed the sediment discharge of the 17 main rivers during the 15 typhoon events that caused the mass movements collected in this study. The measured suspended sediment and water discharge, collected from hydrometric stations of the Water Resources Agency of Taiwan, were used to establish rating-curve relationships. Then sediment discharge during typhoon events were estimated using the rating-curve method and the measured data of daily water discharge. Positive correlations between sediment discharge and rainfall conditions for each river indicate that sediment discharge increased when there was a greater amount of rainfall or a higher intensity rainfall during a typhoon event. In addition, the amount of sediment discharge during a typhoon event is mainly controlled by the total amount of rainfall, not peak rainfall. Differences in the correlation equations among the rivers suggest that the catchments with larger areas and steeper slopes produce more sediment. Catchments with

relatively low sediment discharge show more distinct increase in sediment discharge in response to increase in average daily rainfall.

The positive correlation between the average sediment discharge and the average area of landslides during typhoon events indicates that when larger landslides are caused by heavier rainfall during a typhoon event, more loose materials from latest landslide debris are flushed into rivers resulting in higher sediment discharge. However, the correlation between landslides and sediment discharge is not very high and is lower than the correlation between sediment discharge and rainfall conditions. This means that the latest landslides caused by each of the 14 typhoon events are not an only single source of sediment discharge. Previous studies in Taiwan pointed out that the latest landslide debris have not been delivered completely to rivers but have been successively delivered to rivers by following heavy storms. Therefore, the condition of landslide debris staying on slopes since previous heavy storms also affects sediment discharge. According to our result of the frequency–area distribution of landslides, the proportion of large landslides is high in Taiwan. Previous studies in Taiwan indicated that when the lowest point of a landslide reaches a location with the drainage area > 1 km^2, produced sediment are delivered to channels. This means that debris of large landslides have higher opportunity to reach such locations and supply sediment to rivers. Therefore, large landslides in Taiwan contribute significantly to the high annual sediment yield of the world top class, in spite of the small area of Taiwan.

Contents

List of figures

List of tables

Chapter 1 Introduction

Mass movements such as landslides and debris flows are common natural hazards in mountainous areas of the world (Aleotti and Chowdhury, 1999; Guzzetti et al., 1999; Dai et al., 2002; Dou et al. 2014). These hazards not only cause considerable loss of property and life but also cause ecological and environmental problems such as increased soil erosion rates and sediment discharge (Hovius et al., 1997; Claessens et al., 2007). They are caused mainly by three triggers: earthquakes, rainfall and rapid snowmelt (Keefer, 1984; Guzzetti et al., 2002; Malamud et al., 2004a,b) and influenced by numerous factors such as topography, lithology, geological structure, soil moisture content, and anthropic influence (Crozier, 1999; Glade et al., 2000). Numerous methodologies have been developed to solve the problems of mass movements. Such methodologies generally employ hydrological and/or statistical models to assess and map mass movement susceptibility and probability. Hydrological models assess slope stability on the basis of topographical, hydrological, and soil texture parameters, and calculate the factor of safety along a critical slip surface using the ordinary method of slices or its variations (Fellenius, 1927; Bishop, 1955; Janbu et al., 1956; Morgenstem and Price, 1965; Spencer, 1967). Other factors or methods have also been used with hydrological models to determine slope stability – for example, vegetation-root cohesion (Sidle, 1992), colluvial soil thickness (Dietrich et al., 1995), and the contact element method (Jiang et al., 2006). In contrast, statistical models assess slope stability by means of multivariate analysis of selected and weighted site factors such as geology, topography, climate, land use, and vegetation. Several methods have been proposed to establish statistical models and assess mass movement susceptibility for different areas. These models include

logistic regression (Guzzetti et al., 1999; Dai and Lee, 2002; Ayalew and Yamagishi, 2005), weight of evidence (Lee and Choi, 2004), likelihood ratio (Lee et al., 2007), discriminant analysis (Guzzetti et al., 2006), frequency ratio (Lee and Lee, 2006), analytical hierarchy processing (Komac, 2006; Yalcin, 2008; Wu and Chen, 2009), artificial neural networks (Chang and Chao, 2006; Lee, 2007; Lee et al., 2007; Melchiorre et al., 2008), and decision-tree models (Pal and Mather, 2003; Xu et al., 2005; Bou Kheir et al., 2008; Schneevoigt et al., 2008; Saito et al., 2009). Assuming that mass movements will occur in the future because of the same conditions that triggered them in the past, susceptibility assessments can be used to predict geographical locations of future mass movements (Guzzetti et al., 1999, 2005, 2006). However, this kind of approach does not allow us to predict the time of mass movement occurrence.

Rainfall is the primary factor triggering mass movements in countries like Japan and Taiwan, and also a key factor in predicting where and when mass movements will occur. Therefore, this study analyzes rainfall-induced mass movements in Taiwan and focuses on rainfall parameters as the most important aspect of mass movement hazards. This relatively simple approach can be applied to the whole of Taiwan. Several studies have used rainfall characteristics, such as intensity, duration, cumulative rainfall, and antecedent rainfall during a particular period, to identify the threshold value for mass movement initiation (Caine, 1980; Keefer et al., 1987; Crozier, 1999; Glade et al., 2000; Aleotti, 2004; Guzzetti et al., 2007; Saito et al., 2010a). This study also follows the same approach. Although other factors such as terrain shape also affect the occurrence of mass movements, Lin et al. (2009) pointed out that the areas in and around the Central Mountain Range of Taiwan are characterized by highly similar V-shaped valleys with a typical inclination value of 35°. This particular characteristic for Taiwan permits us to focus on the effects of

rainfall conditions.

This paper also deals with sediment discharge from major rivers in Taiwan. Sediment discharge in rivers is an important indicator for not noly erosion in river catchments but also sedimentation in downstream areas and ocean floors (Hovius et al., 2000; Fuller et al., 2003; Dadson et al., 2004). In mountainous areas of Taiwan, landslides and debris flows are highly important erosional processes of river catchments as the main sources of sediment in rivers (Lin et al., 2008; Chuang et al., 2009).

1.1 Review on rainfall-induced mass movements and sediment discharge

1.1.1 Rainfall thresholds

Mass movements, especially shallow landslides and debris flows, are often triggered by heavy rainfall. Sitar et al. (1992) pointed out that a sudden rise in pore water pressure of soil is critical for the occurrence of debris flows. Wieczorek et al. (2000) found that necessary rainfall conditions for the occurrence of debris flows are high rainfall intensity and sufficiently long rain duration. Finlay et al. (1997) found the relationship between the occurrence probability of landslides and rainfall expressed by linear, quadratic, and cubic curves fitted to data of 791 landslides in Hong Kong during 1984–1997.

Many studies have investigated rainfall thresholds for the initiation of mass movements across the globe using both physical and empirical models, because such thresholds are essential for predicting future mass movements. Physical models mainly use slope stability models and are used widely in the field of engineering

geology (Wu and Sidle, 1995; Iverson, 2000). In order to connect rainfall patterns and data into the slope stability/instability conditions, slope stability models and infiltration models are sometimes used simultaneously (Salvucci and Entekabi, 1994). Wilson (1989) proposed the "leaky barrel" model which can estimate the amount of cumulative groundwater via infiltration. This model was used in San Francisco to predict the occurrence of debris flows (Wilson and Wieczorek, 1995). Physical models can determine the needed amount of rainfall to trigger mass movements and predict the location and time of mass movement occurrences as a warning system. However, it requires detailed information of hydrology, lithology, topography and soil characteristics. These are difficult to collect precisely over a large area.

Although the simplicity of empirical approaches neglects detailed hydrological controls, it offers a straightforward means for issuing regional-scale mass movement warnings based solely on rainfall data. Caine (1980) first used the rainfall intensity and rainfall duration plotting on logarithmic coordinates to create the rainfall threshold for shallow landslides and debris flows. He considered that rainfall threshold is more precise than the external geomorphological threshold (Schumm, 1973). It can be further quantified and calculated for shallow landslides and debris flows. Keefer et al. (1987) successfully predicted the time of major landslides during a rainstorm event by using the rainfall threshold using data from rain gauges and the national weather forecast. Aleotti (2004) used the annual average rainfall in their study area to rescale the rainfall intensity and cumulative rainfall to better reflect local rainfall characteristics. The rainfall threshold was also considered with the needed time for evacuation of people to establish a warning system. Saito et al. (2010a) used 1174 landslides which occurred during 2006 to 2008 in Japan to establish a rainfall threshold and compared it with known thresholds for other areas in the world. They found that rainfall thresholds of shallow landslides for Japan are lower than those for

the other areas. This is mainly due to the fact that Japan is located on the subtropical monsoon climate zone with high-relief topography and complex geological conditions.

In order to derive empirical rainfall thresholds for mass movements, many studies have focused on rainfall parameters such as the rainfall intensity, duration, cumulative rainfall, and antecedent rainfall (see Guzzetti et al., 2007, 2008 for detailed reviews). Among these, the relationship between rainfall intensity (*I*) and duration (*D*) is most commonly used to estimate rainfall thresholds (e.g., Caine, 1980; Guzzetti et al., 2007, 2008; Brunetti et al., 2010; Saito et al., 2010a; Saito et al., 2014). Several studies have also examined the importance of peak rainfall intensity in the initiation of mass movements; e.g., the occurrence of peak rainfall intensity and the initiation of mass movements are often concurrent (Aleotti, 2004; Chien-Yuan et al., 2005; Guzzetti et al., 2007, 2008; Dahal and Hasegawa, 2008; Saito et al., 2010a,b). Although antecedent rainfall also plays an important role in mass movement initiation (Kim et al., 1992; Glade, 1997; Crozier, 1999; Glade et al., 2000; Guzzetti et al., 2007, 2008; Dahal and Hasegawa, 2008), intensity–duration (*I–D*) thresholds and/or the peak rainfall intensity are often used to predict mass movements and to warn the appropriate authorities of potential mass movement hazards (Onodera et al., 1974; Keefer et al., 1987; Aleotti, 2004; Hong et al., 2005; Jan and Chen, 2005; Cannon et al., 2008; Coe et al., 2008; Dahal and Hasegawa, 2008; Guzzetti et al., 2008).

Okada et al. (2001) from the Japan Meteorological Agency (JMA) proposed the soil water index (*SWI*) as the conceptual soil water contents influenced by present and antecedent rainfall. This index uses a calculated value of the total water depth of a three-layer tank model with fixed parameters (Sugawara et al., 1974; Ishihara and Kobatake, 1979). Previous studies for Japan show that *SWI* can successfully predict the occurrence of mass movements (Osanai et al., 2010; Saito et al., 2010b). Using

SWI, the Japanese Government has established a nationwide early-warning system for mass movement disasters in 2005. The system sets a criterion for the occurrence of mass movements based on 60-mins cumulative rainfall and *SWI* in each 5-km grid cell covering all areas of Japan (Osanai et al., 2010).

Saito et al. (2010b) proposed the normalized soil water index (*NSWI*) which is *SWI* divided by the highest value of *SWI* over the past decade. They identified two types of rainfall conditions for shallow landslide initiations in Japan: short-duration–high-intensity (SH) type and long-duration–low-intensity (LL) type. This classification can be used for predicting shallow landslides resulting from the rapid increase of *NSWI* with short duration in the SH type, and from the gentle rise of *NSWI* followed by heavy rainfall with long duration in the LL type. *NSWI* was then used for a regional case study of landslide disasters triggered by a record-breaking rainfall due to Typhoon Talas that caused enormous damages in the Kii Peninsula, Japan, in September 2011. Most of landslides occurred in an area where the maximum *NSWI* was high (Saito and Matsuyama, 2012).

In some previous studies, *SWI* was used to assess the influence of antecedent rainfall. For example, the investigation team of landslide disasters triggered by the 2004 Mid-Niigata Prefecture earthquake in Japan used *SWI* to analyze the influence of rainfall before the earthquake (Sassa, 2005). The heavy rainfall prior to the Mid-Niigata Prefecture earthquake resulted in numerous landslides which significantly differed from another case, the Nikawa landslide due to the Hyogoken-Nambu earthquake with a long travel distance and almost no antecedent rainfall.

There are some unique approaches related to rainfall thresholds of mass movements in Taiwan. For example, Chang and Chiang (2009) combined slope stability and statistical models to establish a landslide probability model based on

geographical and hydrological data for landslides triggered by typhoon events, and they validated the model using data from an additional typhoon event. Lin and Chen (2012) used a rainfall kinetic energy conversion formula and rainfall intensity data from typhoon events between 1994 and 2008 to determine that 2,000 J/m^2 is the landslide rainfall threshold for the mountainous areas of central Taiwan. In order to validate this threshold, they utilized rainfall, sediment discharge, and flow discharge data from another typhoon event.

1.1.2 Geomorphological and geological characteristics of mass movements

Rock strength and discontinuities density of geological materials will control the distribution of mass movements. Using statistical data of landslides, Keefer (2000) found that landslide density is higher in areas with weak rocks than areas with hard rocks. Clague and Evans (2003) pointed out that in the sedimentary formation with alternation of sand and shale, when the pore water pressure of sandstone increased by rainfall, the formation becomes vulnerable to failures due to disintegration. In addition, Chen et al. (1999) found that developed discontinuities are the main factor for the occurrence of debris flows in Hualien, eastern Taiwan. Developed discontinuities on valley sides are also the major source of materials for debris flows. When heavy rainfall raises soil moisture contents and groundwater table, the safety factor of slopes will drop drastically and cause failures (Chen and Su, 2001). Chuang et al. (2009) also found that areas with higher density of discontinuities in rocks are more prone to rainfall-induced mass movements.

A lot of studies have examined landslides in terms of their number, area, and volume. Regarding rainfall-induced landslides, Lumb (1975) correlated the

characteristics of landslides in Hong Kong with the 24-h rainfall and the 15-day antecedent rainfall. He found that disastrous events with more than 50 landslides per day occurred when the 24-h rainfall exceeded 100 mm and the 15-day antecedent rainfall exceeded 350 mm. Several events causing 10–50 landslides per day were triggered by rainfall of 100 mm/day following 200 mm of antecedent rainfall. Dai and Lee (2001) also studied rainfall-induced landslides in Hong Kong and found that the 12-hour rolling rainfall is the most important in predicting the number of landslides; but in terms of failure volume, the most important rainfall period seems to be 24 hours. Saito et al. (2014) found that rainfall totals appear to be a suitable predictor of landslide volumes mobilized during typhoons and frontal storms in Japan. Some studies have also pointed out that deep slides in soils usually occurred only for long duration, moderate intensity storms, whereas very shallow slides of soil over bedrock also occurred for short duration, high intensity storms (Wieczorek, 1987; Larsen and Simon, 1993).

In terms of the landslide area, it was found that the frequency–area distribution of landslides correlates well with a power-law relation (Hovius et al., 2000; Guzzetti et al., 2002; Malamud et al., 2004a,b). In addition, Malamud et al. (2004a) and Guzzetti et al. (2009) proposed the use of the total number or total volume of landslides to measure the magnitude of a landslide event.

1.1.3 Sediment discharge in Taiwan

Mass movements produce debris that will enter rivers and will be transported to the ocean. Therefore, by analyzing sediment yield, we can identify not only the average exhumation rate of an area but also the effect of mass movements on surface morphology. Mass movements can directly or indirectly affect sediment discharge in

rivers (Hovius et al., 1997; Claessens et al., 2007). There are about 384 Mt of sediment transported into the ocean every year in Taiwan (Dadson et al., 2003). Among these, about 30–42% of sediment was discharged at hyperpycnal sediment concentrations, typically during typhoon events (Dadson et al., 2005). However, it is difficult to estimate how much the proportion of materials, produced by the latest mass movements, enters rivers. Few previous studies have directly discussed the relationship between mass movements and sediment discharge in Taiwan.

Dadson et al. (2004) used the drainage area of the lowest point reached by each landslide to estimate the proportion of materials, produced by the latest mass movements, which entered a river. The result shows that when a landslide reaches a location with the drainage area > 1 km^2, the delivered sediment enters a river. In the Chenyoulan river catchment, Taiwan, about 80% of materials produced by the Chi-Chi earthquake were not delivered to rivers immediately, but successively delivered to rivers by following typhoons (Dadson et al., 2004). In addition, Lin et al. (2011) studied landslides in the upstream area of the Shihmen Reservoir, Taiwan, and pointed out that high landslide ratios do not correspond to high sediment discharge, probably because sediment discharge is controlled by water discharge and landslide debris may still stay on slopes.

1.2 Objectives of the dissertation

Taiwan represents an area extremely susceptible to mass movements because of the steep mountainous topography, complex geological conditions, frequent heavy rainfall, and frequent earthquakes. Thus, as noted above, many studies have been performed on mass movements in Taiwan. However, these studies typically examined specific events or locations. Surprisingly few studies have explored the rainfall

conditions associated with mass movements for Taiwan as a whole. Although Chien-Yuan et al. (2005) investigated the *I–D* threshold of debris flows for Taiwan, their data were generally sourced from specific areas in northern and central Taiwan and was relatively old (1989–2001) and, thus, possibly less credible than more recent data.

Since mass movements are densely and widely distributed in Taiwan, it is important to firmly establish the relationship between the initiation of mass movements and rainfall conditions. Therefore, the first objective of this dissertation was to analyze rainfall conditions associated with mass movements for the whole of Taiwan and to establish the *I–D* threshold using relatively abundant recent data.

In order to combine the effects of antecedent and current rainfall intensities and contribute to mass movement warnings, the second objective was to apply *SWI* for analyzing mass movements in Taiwan and to verify its effectiveness.

Then to understand characteristics of landslides in Taiwan and its effects on sediment discharge in rivers, the third and fourth objectives were to identify dimensional characteristics of landslides in Taiwan, and to identify sediment discharge of main rivers during typhoon events in Taiwan and to find out the relationship between sediment discharge and landslides.

Chapter 2 Study area

Taiwan is located on a convergent plate boundary between the Eurasian Continental and the Philippine Sea plates, with the Philippine Sea plate moving towards the Eurasian Continental plate at a rate of 80 mm/yr (Yu et al., 1997). The subduction of the Philippine Sea plate beneath the Eurasian Continental plate resulted in the formation of an active mountain belt called the Central Range with over 200 peaks higher than 3,000 m a.s.l. (Ho, 1986; Teng, 1990) (Fig. 2.1). It is also responsible for frequent large earthquakes and an orogenic uplift rate of about 5 to 7 mm/yr (Li, 1976; Willett et al., 2003). According to the elevation histogram derived from a 10-m DTM of Taiwan, about 32% of the country is above 1,000 m. The slope of mountainous areas is mostly between 30° and 50° (Fig. 2.2).

Because of the long and narrow shape of Taiwan, most rivers are sourced from the Central Range and radially flow into the ocean in all orientations. Among these rivers, 17 are main representative rivers (Fig. 2.1). They include three rivers (Xindian, Tahan, and Touchien Rivers) in the northern part of Taiwan, four (Taan, Tachia, Wu, and Choshui Rivers) in the central part, five (Tsengwen, Erhjen, Kaoping, Linpien, and Sihjhong Rivers) in the southern part, and five (Peinan, Hsiukuluan, Hualien, Hoping, and Lanyang Rivers) in the eastern part.

The geological map provided by the Central Geological Survey of Taiwan (Ho, 1988) illustrates the seven major geological zones of Taiwan (Fig. 2.3). The western region and part of the northeastern coastal region are mainly underlain by Tertiary marine sedimentary rocks. Central Taiwan is composed of metamorphic rocks. The pre-Tertiary metamorphic complex is exposed mainly in the eastern Central Range, while the majority of the western Central Range consists of Tertiary indurated

metamorphosed argillaceous sedimentary rocks (Ho, 1988). The eastern coastal region is underlain by volcanic-arc sediments, orogenic sediments, and a subduction-collision complex formed in the Pliocene to Pleistocene. Northern Taiwan consists mainly of agglomerates-masses of igneous rock fragments. Finally, lowlands such as alluvial fans and coastal plains are mostly composed of Quaternary sediments.

Taiwan is located between 120°E and 122°E and between 22°N and 25°N, and the boundary between tropical and subtropical-monsoon climates is located in the south of Taiwan (Wang and Ho 2002). The average temperature over the Taiwanese lowlands during the wet season (May to October) is above 20°C, while that during the dry season (November to April) is between 14°C and 20°C. Central and southern Taiwan is mountainous, making the average temperature lower than in other regions of the country (Fig. 2.4). On average, four typhoons strike Taiwan every year (Wu and Kuo, 1999), causing heavy and concentrated rainfall. Annual rainfall over Taiwan averages 2,500 mm. However, annual rainfall in mountainous regions can surpass 3,000 mm (Shieh, 2000). Approximately 60% to 80% of rainfall falls during the wet season (Fig. 2.4).

Heavy rainfall, steep topography and high seismicity in Taiwan have contributed to an erosion rate of 3 to 7 mm/yr (Dadson et al. 2003). Mass movements triggered by frequent rainfall and earthquakes, particularly landslides and debris flows, represent the primary mechanisms of this erosion and are important for maintaining balance between erosion and uplift (Dadson et al. 2003). Taiwan also has a fragile geological environment, and areas that display a high density of geological discontinuity are more prone to mass movements (Chen et al., 1999; Chen and Su, 2001; Chuang et al., 2009). Interestingly, the number and magnitude of rainfall-induced mass movements increased after the 1999 Chi-Chi earthquake, because slopes became more vulnerable due to intense ground shaking (Chang and Slaymaker, 2002; Dadson et al., 2004;

Cheng et al., 2005), reducing both the maximum rainfall intensity and critical cumulative rainfall required to trigger mass movements (Lin et al., 2003; Chang et al., 2009; Shieh et al., 2009; Chen, 2011).

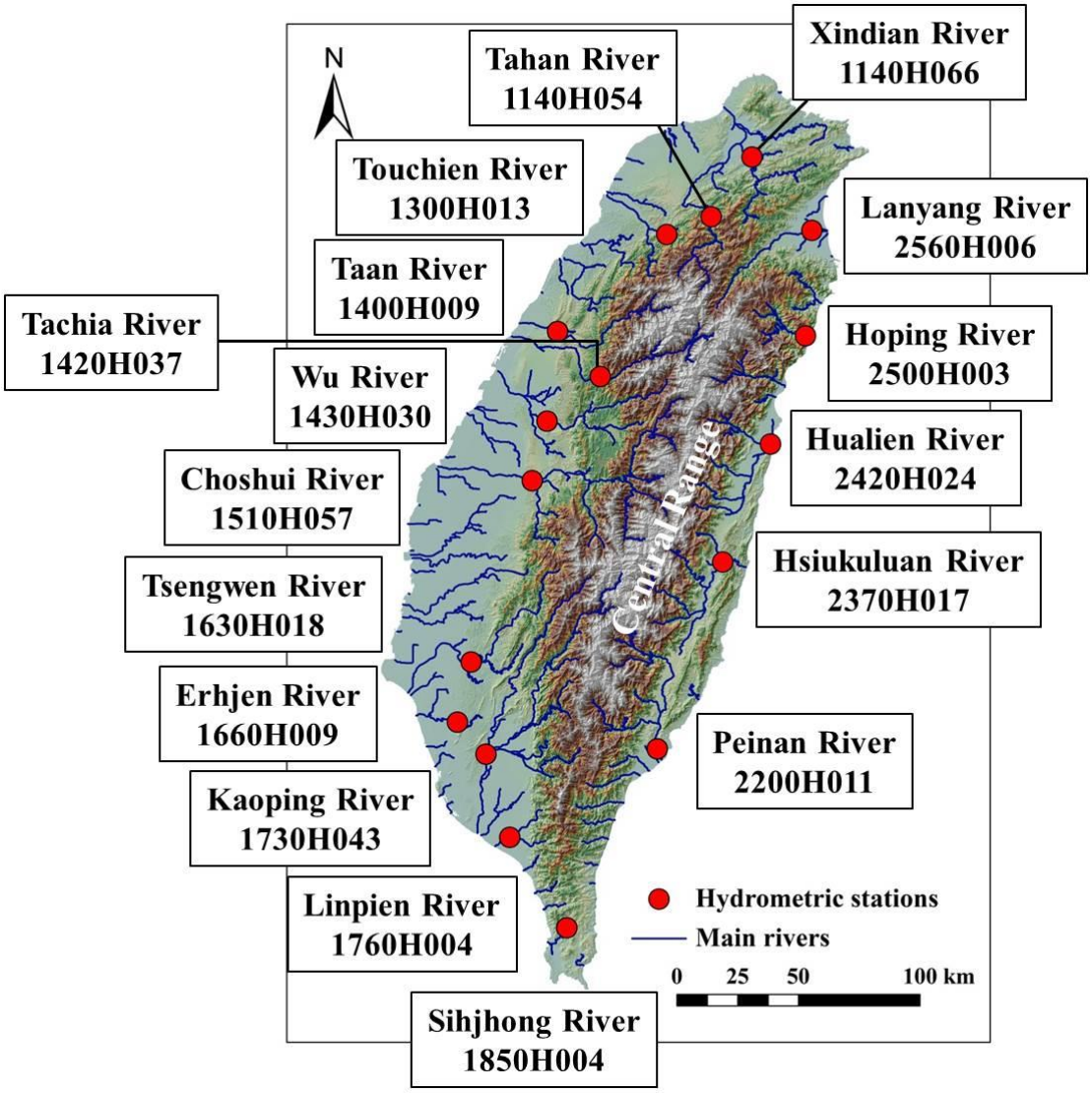

Fig. 2.1 Main rivers and representative hydrometric stations in Taiwan.

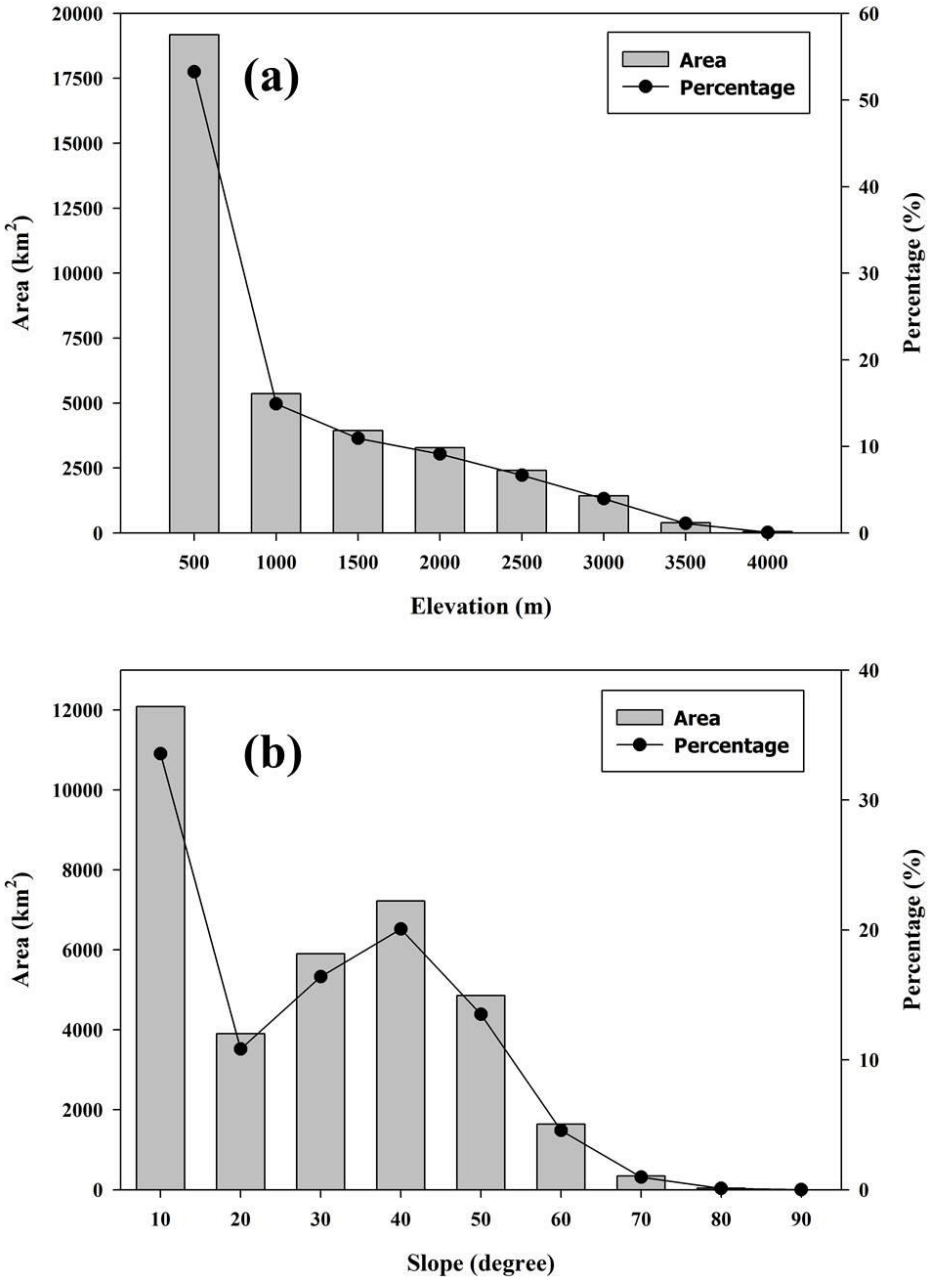

Fig. 2.2 Distribution of (a) elevation, and (b) slope in Taiwan.

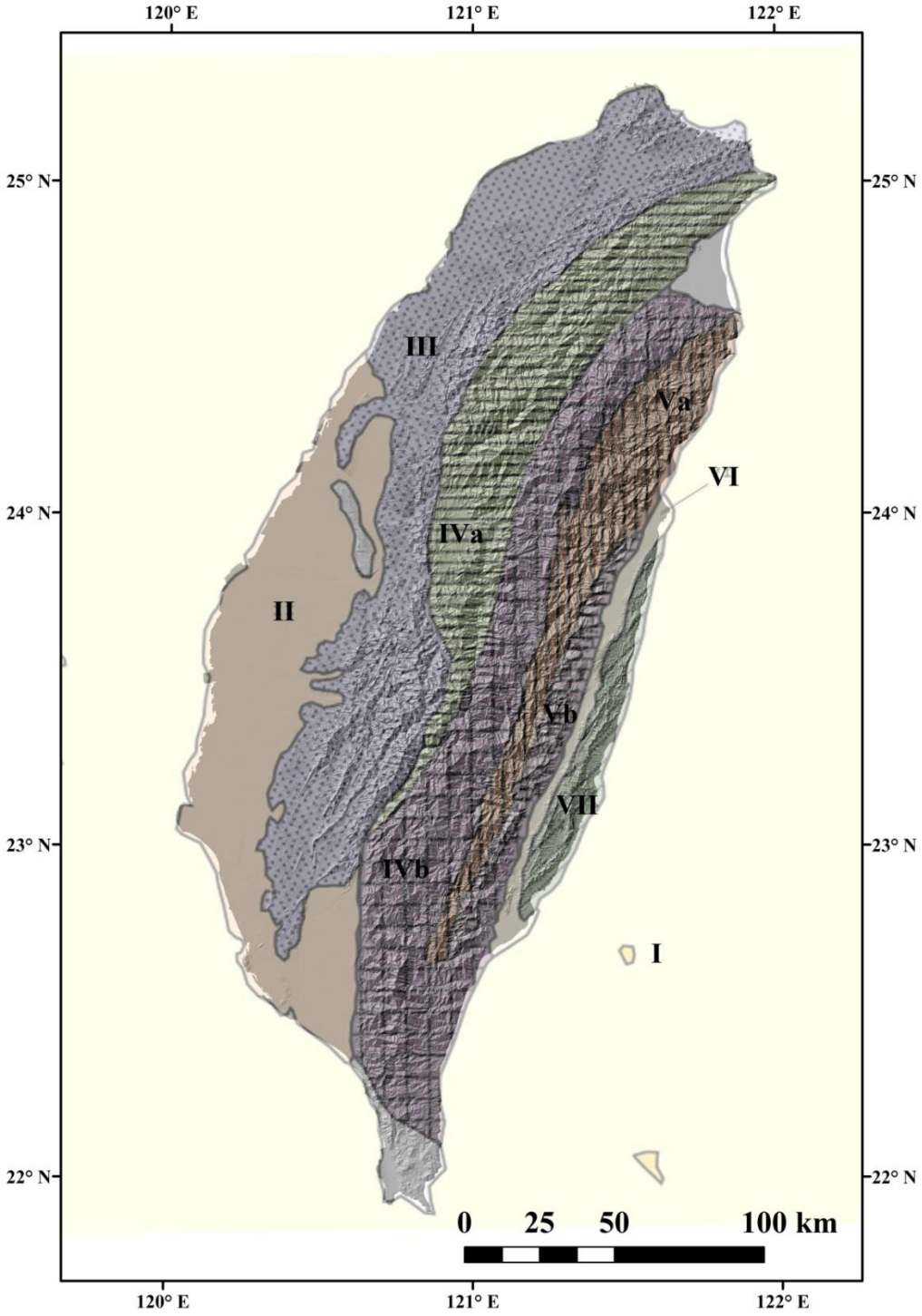

Fig. 2.3 Geology of Taiwan. I: Pleistocene basalt; II: Quaternary alluvial deposit; III: Neocene clastic rock; IV: Tertiary sub-metamorphic rock (a: argillite and slate; b: slate and phyllite); V: Pre-Tertiary metamorphic complex (a: schist, marble, and granite; b: schist and serpentine); VI: plate suture belt; VII: Neogene volcanic rock

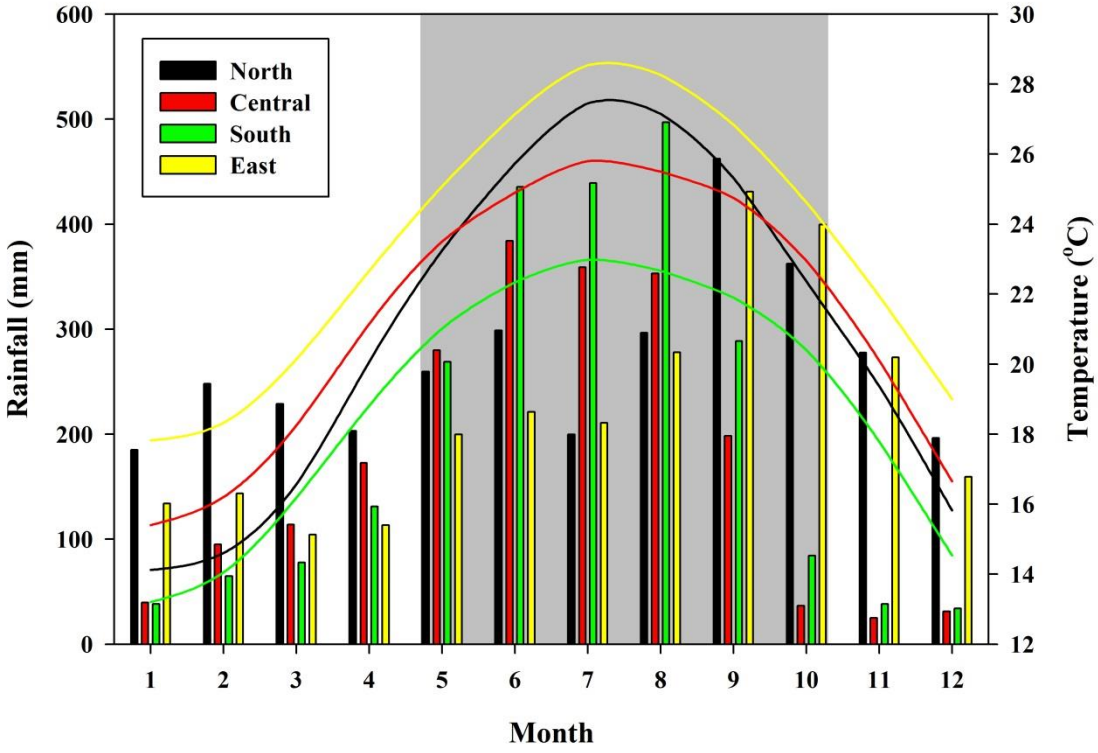

Fig. 2.4 Average monthly temperature (curved lines) and rainfall (bars) in different regions of Taiwan (averaged from 1981 to 2010). North: Taipei, Keelung, Taoyuan, Hsinchu, and Miaoli regions; Central: Taichung, Changhua, Nantou, and Yunlin regoins; South: Chiayi, Tainan, Kaohsiung, and Pingtung regions; East: Ilan, Hualien, and Taitung regions

Chapter 3 Data and methods

3.1 Mass movement data

This study analyzed 263 mass movements caused by 15 typhoons and nine rainstorm events during the seven-year period between 2006 and 2012 (Fig. 3.1; Table 3.1; Appendix). We collected mass movement data from the reports of the Soil and Water Conservation Bureau (SWCB) of Taiwan. These data include 172 landslides and 107 debris flows, with 16 events including both landslides and debris flows. The 16 events are landslides completely or partially mobilized to form debris flows during the same rainfall event. Mass movements occurred across Taiwan (Fig. 3.1), and these occurred during the wet season: one in May, 26 in June, 33 in July, 141 in August, 24 in September, and 38 in October (Fig. 3.2).

The SWCB has conducted detailed field surveys when rainfall-induced mass movement disasters such as damage of houses and roads occurred for preventing secondary disasters and quick recovery. The resultant reports contain information on the type, location, and approximate time (accuracy in hour) of each disaster event. They speculate the time based on real-time videos taken at observation stations, the time people informed disasters, and interviews with residents. They investigate the extent of affected areas and the damaged condition of residents and constructions. Types of disaster in these reports are classified into three: landslides**,** debris flows, and floods. Among them, landslides are the slide type of mass movements and different from the flow type. Therefore, we selected landslides and debris flows for our analysis. Falls or topples are more related to the gravity, so only a few cases of these types were reported, and all of them occurred during the time with almost no rainfall.

Therefore, we carefully checked all reports (n = 292), and excluded some data that were not caused by rainfall (almost no rainfall during mass movements). In addition, this study also collected 19 mass movements occurred in 2013 but only used for verifying the results of *SWI* (Fig. 3.1; Appendix). In the dataset used, only a few mass movements distributed in very high mountainous areas, because the SWCB only reported mass movements which directly affected residences and infrastructures.

Although mass movements occur frequently in Taiwan, there is yet no complete inventory with very detailed information. The relatively high integrity and consistency of the data collected by the SWCB indicate that at this moment the data are the best for analyzing the relation between mass movements and rainfall conditions over Taiwan.

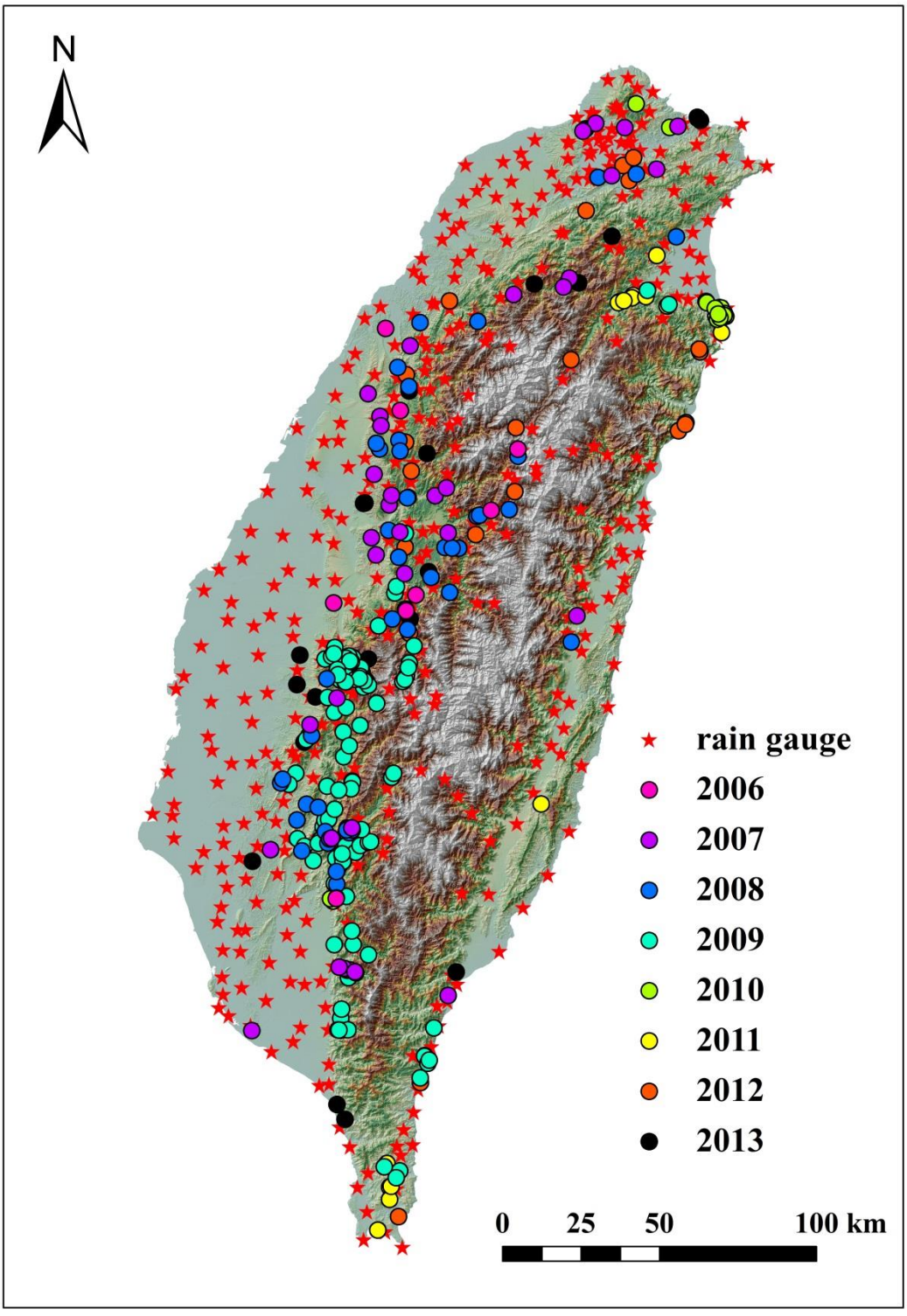

Fig. 3.1 Distribution of rain gauges and mass movements that occurred between 2006 and 2013.

Table 3.1 Typhoons and rainstorm events during 2006–2012.

Year	2006	2007	2008	2009	2010	2011	2012
Event	Rainstorm (6/9)	Rainstorm (6/4)	Typhoon Kalmaegi (7/16–18)	Typhoon Morakot (8/5–10)	Typhoon Lionrick (8/31–9/2)	Rainstorm (7/19)	Rainstorm (5/4)
		Rainstorm (8/9)	Typhoon Fun-Wong (7/26–29)	Typhoon Parma (10/3–6)	Rainstorm (9/24)	Typhoon Nanmadol (8/27–31)	Rainstorm (6/10)
		Typhoon Sepat (8/16–19)	Typhoon Sinlaku (9/11–16)		Rainstorm (10/16)	Rainstorm (10/1)	Typhoon Saola (7/30–8/6)
		Typhoon Wipha (9/17–19)	Typhoon Jangmi (9/26–29)		Typhoon Fanapi (9/17–20)		Typhoon Tembi (8/21–28)
		Typhoon Krosa (10/4–7)			Typhoon Megi (10/21–23)		

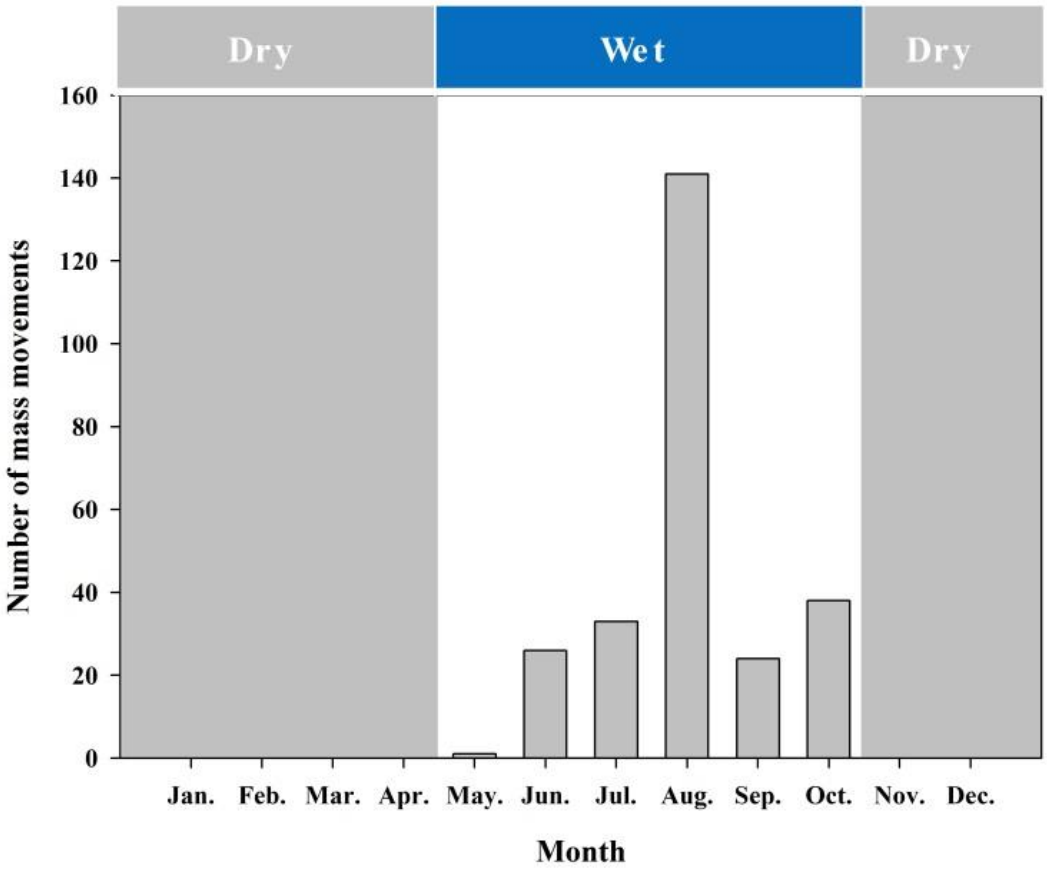

Fig. 3.2 Number of mass movements in each month.

3.2 Rainfall data

Taiwan's Central Weather Bureau has installed more than 400 rain gauges with a density of approximately one gauge every 76 km^2 (Fig. 3.1) that record hourly data. The apparatuses of these rain gauges are the tilting-bucket type which can be used for automated observations. Since rain gauges were not always located close to mass movement sites and relatively few rain gauges were distributed in mountainous areas, we selected the nearest five rain gauges for each mass movement and conducted a kriging interpolation using the ordinary kriging and the spherical semivariogram model with a variable search radius to estimate rainfall at each mass movement location. Then we obtained the hourly rainfall value at the location of each mass

movement from the beginning to the end of a rainfall event. As is common in Taiwan, one continuous rainfall event was considered to begin when hourly rainfall surpassed 4 mm and to end when hourly rainfall decreased to below 4 mm over the next six consecutive hours (e.g., Chang et al., 2011) (Fig. 3.3a).

We calculated the mean rainfall intensity (*I*, mm/h), rainfall duration (*D*, h), and peak rainfall intensity (mm/h) from the beginning of a rainfall event to the time of mass movement occurrence. Some previous studies have used one week's antecedent rainfall for analyzing the antecedent soil moisture and found that it is an important factor for triggering landslides (Crosta 1998; Jakob et al. 2006). Therefore, we also examined rainfall totals for 168 hours (one week) before the beginning of a rainfall event which caused mass movements and used it as the antecedent rainfall.

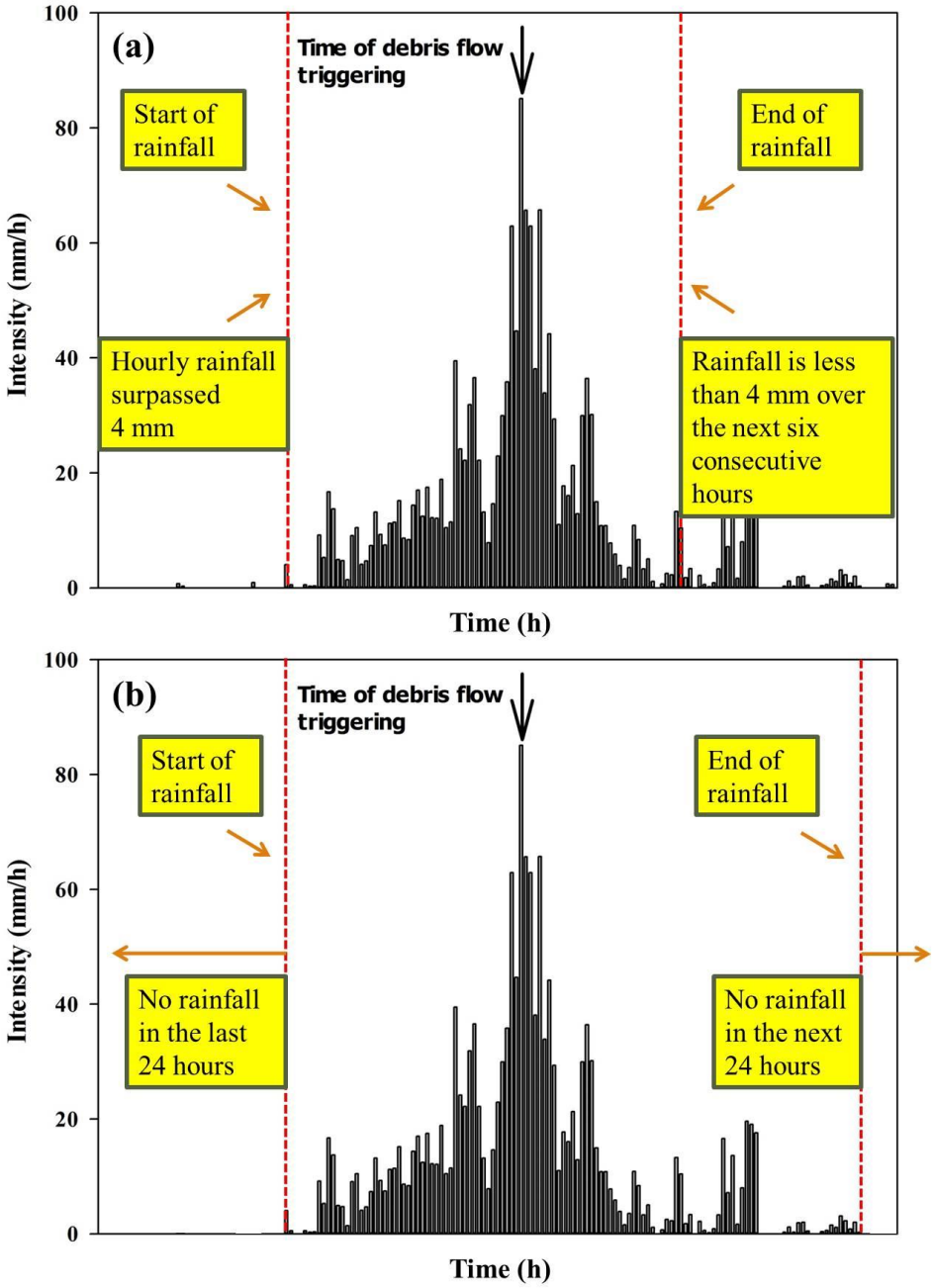

Fig. 3.3 Definitions of one rainfall event. (a) Rainfall begins when hourly rainfall surpassed 4 mm and to end when hourly rainfall decreased to below 4 mm over the next 6 consecutive hours. (b) Rainfall period delimited by a non-rainfall period of more than 24 h.

3.3 Topographic and geological data

Topographic data such as elevation and slope are derived from a 10-m DTM of Taiwan. The DTM was measured and produced by the Aerial Survey Office, Forestry Bureau of Taiwan. They used the analytical photogrammetric method for three-dimensional phase of aerial photographs and mapping elevation points. Raster grids were sampled to produce the DTM with the Transverse Mercator projection. Units of the plane coordinate and elevation are in meters.

Although several geologic maps of Taiwan were published in the early 20th century by Japanese geologists, newer 1:500,000 geologic maps with explanatory text have been published since 1984 based on the assessment and screening of all relevant data (Ho, 1988). This paper utilizes the 1:500,000 maps.

3.4 *I–D* thresholds

The *I–D* threshold for mass movements is defined as the lower bound of rainfall conditions for a mass movement to occur on a plot of the *I–D* relationship, namely minimum-level of the rainfall conditions (e.g., Guzzetti et al., 2007). In early years, the lower bound line was determined manually (e.g., Caine, 1980; Larsen and Simon, 1993; Chien-Yuan et al., 2005). However, more recently, mathematical and/or statistical criteria have been used to objectively determine the lower bound line. Guzzetti et al. (2007) were the first to propose the Bayesian inference method for determining *I–D* thresholds; Brunetti et al. (2010) proposed a frequentist approach; and Saito et al. (2010a) adopted the quantile-regression method.

Although many different methods were proposed, the general form of the relationship between rainfall intensity and duration is:

$$I = \kappa D^{-\varepsilon} \quad (3.1)$$

where κ is a scaling constant (intercept), and ε is the shape parameter (slope).

Like all landslide inventories, the data we analyzed contain inherent uncertainties including measurement errors, erosional or geographical censoring, and reporting biases (Kirschbaum et al., 2012; Korup et al., 2012; Petley, 2012). We therefore determined thresholds by the frequentist statistical method and the random sampling method, which are statistically robust approaches. Brunetti et al. (2010) suggested the frequentist statistical method for the definition of objective empirical-rainfall thresholds. The method firstly plots the empirical rainfall data in a logarithmic coordinate (*I*–*D* plot) and to find out the regression line for the plotted data. Next, the difference $\delta(D)$ between mean rainfall intensity for each data and the generalized rainfall intensity based on the regression line is calculated and used to determine the probability density function in a Gaussian form. Lastly, thresholds corresponding to different exceedance probabilities are defined based on the fitted distribution of $\delta(D)$. Following this method, we determined 5% as the standard *I*–*D* threshold. We also used the robust random sampling method due to its resistance to errors and outliers. To establish the threshold line equation, two-thirds of the data were randomly sampled, and this was repeated one hundred times, allowing us to calculate the mean and standard deviation of κ and ε in Eq. (3.1).

This study determined thresholds for all mass movements, landslides only, and debris flows only according to the statistical methodology mentioned above. As a result, the threshold for all mass movements can be higher than that for landslides only or debris flows only. This may be confusing because the threshold for all data should not be philosophically higher than that for a portion of data. Therefore,

discussion of, this study focuses on thresholds for landslides only and debris flows only.

Regional *I–D* thresholds are limited by their specificity to a certain region. They cannot be easily applied to other areas because the topographic, lithological, meteorological, and climatological characteristics of one region may vary from those of another (Jakob and Weatherly, 2003; Guzzetti et al., 2007, 2008). For example, the limited surface vegetation and the accumulation of regolith on slopes during long dry periods allow a relatively short and weak rainfall event to initiate mass movements in arid areas. Therefore, rainfall intensity (*I*) was divided by the mean annual precipitation (*MAP*) (Aleotti, 2004; Guzzetti et al., 2007, 2008; Dahal and Hasegawa, 2008; Saito et al., 2010a) to offset regional effects and obtain comparable rainfall thresholds for different areas. The relationship between rescaled rainfall intensity (I_{MAP}) and rainfall duration (I_{MAP}–*D* condition) was analyzed using the same procedure described for non-rescaled values.

The *MAP* of mountainous areas in Taiwan spatially varies but is greater than 3000 mm (Shieh, 2000). Therefore, for mountainous regions we divided *I* by a *MAP* value of 3000 mm to obtain I_{MAP} and allow us to conservatively examine average conditions. The *I–D* and I_{MAP}–*D* thresholds for Taiwan were then compared with previously reported threshold values compiled by Saito et al. (2010a).

We also adopted the principal component analysis (PCA) to *I–D* conditions of each mass movement. The rainfall condition associated with mass movements in Taiwan can be objectively grouped into two types: short duration–high intensity (SH) and long duration–low intensity (LL) types along with the first principal component (PC).

Although this study focuses on rainfall parameters and does not discuss topographic and geologic conditions in detail, we also briefly examine topographic

conditions such as elevation and slope and geologic conditions represented by four main lithological domains (sedimentary rocks, metamorphic rocks, igneous rocks, and alluvium) when a significant deviation from the generally expected influence of rainfall is observed. As the mass movements are point data, we overlayed them with the 10-m DTM and the geological map of Taiwan for deriving topographic and geologic conditions of each mass movement point.

3.5 Time difference between mass movements and peak rainfall intensity

To account for the effect of temporal rainfall intensity variations on mass movements, we calculated the time difference (T_d) between mass movements and peak rainfall intensity (maximum hourly rainfall) as follows:

T_d = time of a mass movement - time of peak rainfall intensity (3.2)

Positive T_d values indicate that mass movements occurred after peak rainfall intensity, and negative T_d values indicate the opposite conditions.

3.6 Soil water index

The soil water index (*SWI*) was proposed by Okada et al. (2001) from the Japan Meteorological Agency (JMA). This index uses a calculated value of the total water depth of a three-layer tank model with fixed parameters (Sugawara et al., 1974; Ishihara and Kobatake, 1979) (Fig. 3.4).

The tank model is a hydrological model to calculate water discharge. The

formula of *SWI* is as follows:

$$SWI = S_1 + S_2 + S_3 \tag{3.3}$$

where S_1, S_2, and S_3 are the remaining water heights (mm) for each tank which can be calculated as below:

$$S_1\,(t+\Delta t) = (1 - \beta_1 \Delta t) \times S_1\,(t) - q_1\,(t) \times \Delta t + R \tag{3.4}$$

$$S_2\,(t+\Delta t) = (1 - \beta_2 \Delta t) \times S_2\,(t) - q_2\,(t) \times \Delta t + \beta_1 \times S_1\,(t) \times \Delta t \tag{3.5}$$

$$S_3\,(t+\Delta t) = (1 - \beta_3 \Delta t) \times S_3\,(t) - q_3\,(t) \times \Delta t + \beta_2 \times S_2\,(t) \times \Delta t \tag{3.6}$$

where t is time (h); β_1, β_2, and β_3 show the coefficient of permeability (1/h) for each tank; R is rainfall (mm) q_1, q_2, and q_3 are runoff (mm/h) from side holes for each tank which can be calculated as below:

$$q_1\,(t) = \alpha_1\,\{S_1\,(t) - L_1\} + \alpha_2\,\{S_1\,(t) - L_2\} \tag{3.7}$$

$$q_2\,(t) = \alpha_3\,\{S_2\,(t) - L_3\} \tag{3.8}$$

$$q_3\,(t) = \alpha_4\,\{S_3\,(t) - L_4\} \tag{3.9}$$

where α_1, α_2, α_3, and α_4 show the outflow coefficient (1/h) for each tank; L_1, L_2, L_3, and L_4 represent the outflow height (mm) for each tank.

Okada (2007) indicated that, for predicting the occurrence of mass movements,

not the absolute value of *SWI* but the relative rank order of current *SWI* is important; the latter considers the previous largest value and 2nd largest value and so on in the same region during 10 years. The rank order of the *SWI* includes the concept of recursive time of mass movements in relation to the rainfall intensity and antecedent rainfall in the region. According to Okada (2007), the rank order of the *SWI* remains unchanged in many cases even if the parameters of the tank model change. The fixed parameters (α, β, and L) were identified by the statistical analysis of the relationship between rainfall and discharge in the granitic region in Japan (Table 3.2). Although both Japan and Taiwan are characterized by complex geological conditions, *SWI* only represents the conceptual soil water contents and the value will not change much when the parameters are adjusted to different types of geology. Therefore, the Japanese government applies *SWI* using the fixed parameters for the whole of Japan in spite of various geological conditions. For this reason, this paper applies *SWI* to Taiwan using the same parameters as in Japan.

In this study, values of *SWI* were calculated from one month before each mass movement (Fig. 3.5). For the analysis of *SWI*, we defined one continuous rainfall event as the rainfall period delimited by a non-rainfall period of more than 24 h as is commonly applied in Japan (Fig. 3.3b). This is suitable because *SWI* is the dynamic conceptual soil water content for a long time period, representing a long-term rainfall event.

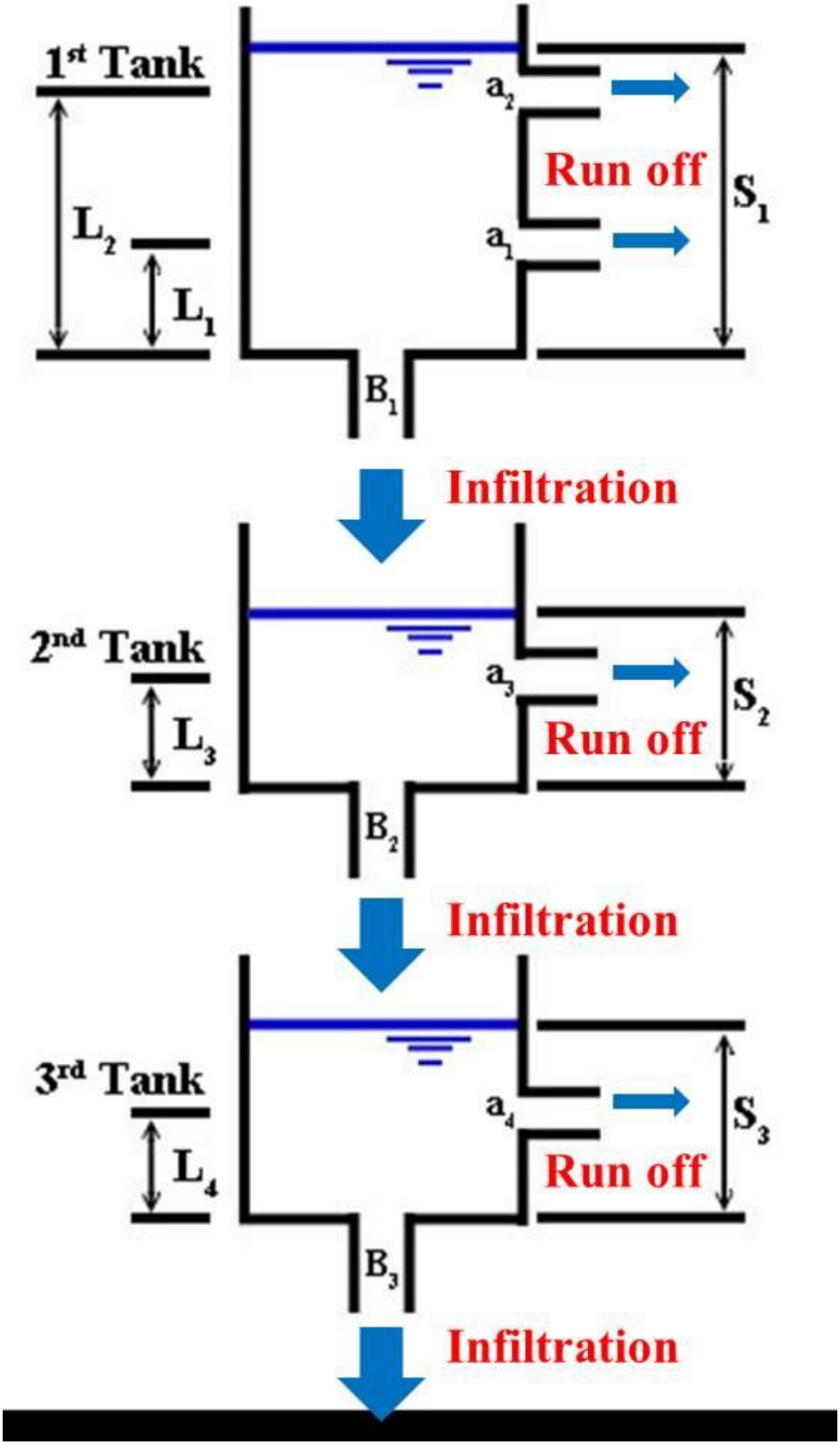

Fig. 3.4 Three-layer tank model.

Table 3.2 Parameters of *SWI*.

Tank	First	Second	Third
Outflow height (mm)	$L_1 = 15$ / $L_2 = 60$	$L_3 = 15$	$L_4 = 15$
Outflow coefficient (1/h)	$\alpha_1 = 0.1$ / $\alpha_2 = 0.15$	$\alpha_3 = 0.05$	$\alpha_4 = 0.01$
Coefficient of permeability (1/h)	$\beta_1 = 0.12$	$\beta_2 = 0.05$	$\beta_3 = 0.01$

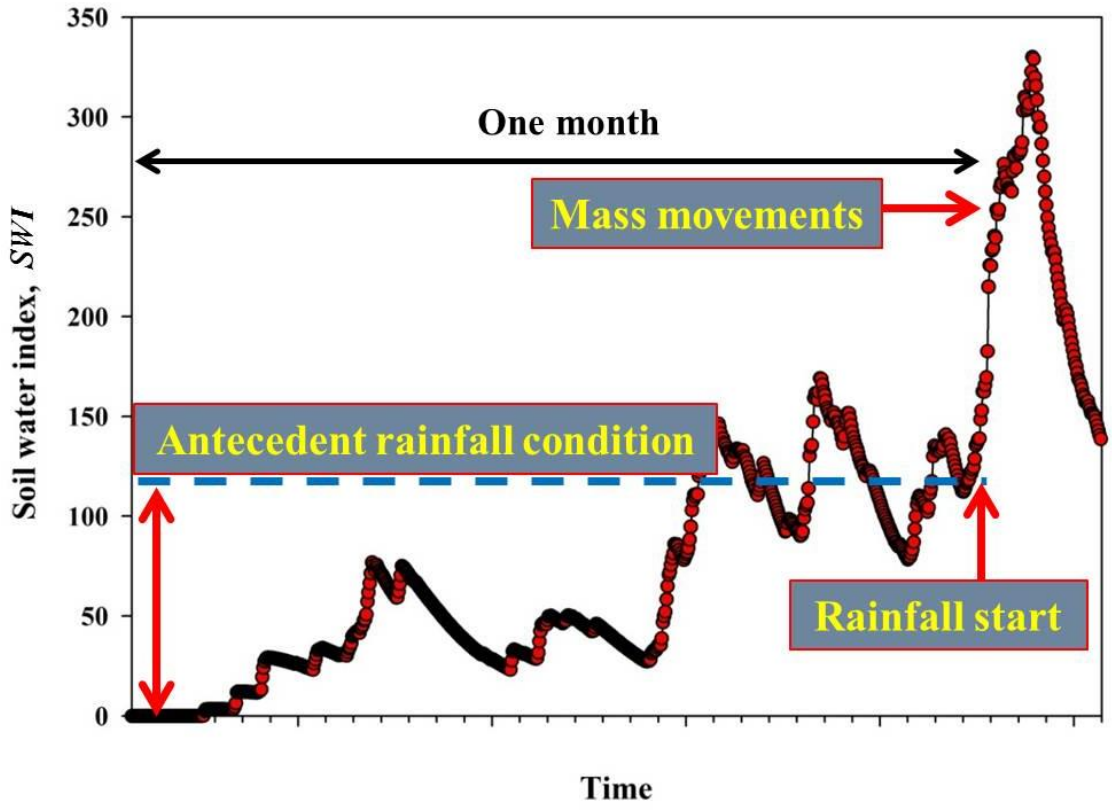

Fig. 3.5 Example of change in *SWI*.

3.7 Landslide size and magnitude

As mentioned in Section 3.1, the mass movement data collected in this study includes 172 landslides and 107 debris flows. However, the areal extent of each debris flow is difficult to identify on satellite images. Therefore, we selected the 172 landslides for mapping. The mapping was conducted using FORMOSA–II images which can be previewed at the website of the Center for Space and Remote Sensing Research, Nation Central University, Taiwan (http://earth.csrsr.ncu.edu.tw/CSRSR/QUERY3/QueryScreen.htm). After mapping the landslides, we calculated the area of each landslide. The volume and depth of each landslide were also estimated using the empirical formula of the relationship between landslide area and volume (Guzzetti et al., 2009):

$$V_L = 0.074 \times A_L^{1.450} \quad (3.10)$$

where A_L is the area in m^2, and V_L is the volume in m^3.

Eq. 3.10 was empirically obtained through a worldwide literature search by Guzzetti et al. (2009). They collected areas and volumes of 677 landslides occurred in different lithological, morphological and climatic settings, and were triggered by different causes, including rainfall, earthquakes, and rapid snowmelt. Therefore, it is possible to apply Eq. 3.10 also to Taiwan.

Many previous studies have found that the frequency–area distribution of landslides correlates well with a power-law relation (Hovius et al., 2000; Guzzetti et al., 2002; Malamud et al., 2004a,b). Differences in the shape of frequency–area distribution between different areas reflect regional characteristics. The frequency–area distribution was obtained using the landslide area data and the probability density

function:

$$P(A_L) = \frac{1}{N_{LT}} \frac{dN_L}{dA_L} = CA_L^{-\gamma} \quad (3.11)$$

where N_{LT} is the total number of landslides, dN_L is the number of landslides with area between A_L and $A_L + dA_L$, C is the scaling constant (intercept), and γ is the shape parameter (slope).

Malamud et al. (2004a) and Guzzetti et al. (2009) proposed the use of the total number or total volume of landslides to measure the magnitude of a landslide event. However, standardization is needed to compare landslide intensity among regions with different areal extent. Therefore, this study uses the average volume of landslides for calculating the magnitude scale:

$$m_L = \log V_a \quad (3.12)$$

where V_a is the average volume of landslides in m^3.

3.8 Estimation of sediment discharge

In Taiwan there are over 250 hydrometric stations, installed by the Water Resources Agency (WRA). To measure the suspended sediment discharge in main rivers, the WRA collects river water samples by using a DH-48 depth integrating suspended sediment sampler at each station, two to three times per month on average. Each sample is filtered, dried, and weighed, and the concentration of suspended sediment is recorded in parts per million (ppm). A rating-curve relationship of the type

is set between the measured sediment discharge (S_d) and daily water discharge (Q),

$$S_d = aQ^b \tag{3.13}$$

where a and b are constants for a given region (Walling, 1977; Cohn, 1995).

For each of the 17 main rivers (Fig. 2.1), we chose a hydrometric station that represents sediment discharge of the river (Fig. 2.1). The principle of the choice is either the station near the boundary between the mountain and the plain, or the most downstream station in a catchment. Sediment discharge during a typhoon event can be estimated using the rating-curve method and daily water discharge measured by the WRA (Dadson et al., 2004). This study estimated sediment discharge during the 15 typhoon events.

Although the sediment discharge includes suspended sediment discharge and bedload, the latter spatial distribution varies greatly and frequent measurements are difficult to carry out. In Taiwan, there is no routine observation of bedload. Therefore, this study focuses on suspended sediment discharge.

Chapter 4 Results of basic analyses

4.1 Rainfall conditions and *I–D* thresholds

Mean rainfall intensity for all investigated mass movements ranged from 8.9 to 64.8 mm/h with an average of 21.7 mm/h, and rainfall duration ranged between 2 and 71 h with an average of 33.2 h. Cumulative rainfall was as low as 60.3 mm and as high as 1916.5 mm with an average of 668.8 mm. Antecedent rainfall was between 1.8 and 707.7 mm with an average of 124.9 mm (Table 4.1). The *I–D* correlation (Fig. 4.1) revealed that an increase in rainfall duration caused a reduction in the rainfall intensity required to trigger a mass movement.

Average mean rainfall intensity, duration, cumulative rainfall, and antecedent rainfall for debris flows were 23.2 mm/h, 33.5 h, 692.6 mm, and 101.1 mm, respectively, and those for landslides were 20.7 mm/h, 32.5 h, 652.4 mm, and 142.2 mm, respectively (Table 4.1). A t-test and resultant *p*-values indicate that the mean rainfall intensity and antecedent rainfall significantly differ between landslides and debris flows (Table 4.1). Fig. 4.1 also shows that the *I–D* correlation line for debris flows is higher than that for landslides.

Fig. 4.2 shows the time difference (T_d) between mass movements and peak rainfall intensity. Approximately 16% of mass movements occurred very close to the time of peak rainfall intensity (within ± 30 min), and most mass movements (75%) occurred within ± 7 hours of the time of peak rainfall intensity.

As previously stated, we utilized the frequentist method with random sampling to delineate the *I–D* thresholds for all mass movements, landslides only, and debris flows only (Fig. 4.1). The resultant equations for these three conditions were as follows:

$$I = 18.10(\pm 2.67)D^{-0.17(\pm 0.04)} \quad (2 \leq D \leq 71 \text{ h; all mass movements}) \tag{4.1}$$

$$I = 13.25(\pm 2.76)D^{-0.08(\pm 0.06)} \quad (2 \leq D \leq 71 \text{ h; landslides only}) \tag{4.2}$$

$$I = 26.92(\pm 6.67)D^{-0.26(\pm 0.07)} \quad (2 \leq D \leq 68 \text{ h; debris flows only}) \tag{4.3}$$

The equation for all mass movements indicates that for short duration rainfall events (e.g., 2 h), high rainfall intensity (e.g., > 16.1 mm/h) can potentially trigger mass movements. For a long duration rainfall events (e.g., 71 h), low rainfall intensity (e.g., < 8.8 mm/h) may also trigger mass movements.

Saito et al. (2010a) compiled *I–D* thresholds for various locations around the world. For this study, we added the *I–D* thresholds for Taiwan to their graph (Fig. 4.3), revealing that the *I–D* threshold for Taiwan is generally higher than the thresholds for other areas.

Table 4.1 Rainfall conditions for mass movements during 2006–2012.

Rainfall conditions	Mean intensity (mm/h)		Duration (h)		Cumulative rainfall (mm)		Antecedent rainfall (mm)	
	Mass movements		Mass movements		Mass movements		Mass movements	
	Landslides	Debris flows	Landslides	Debris flows	Landslides	Debris flows	Landslides	Debris flows
Average	21.7		33.2		668.8		124.9	
	20.7	23.2	32.5	33.5	652.4	692.6	142.2	101.1
	$p < 0.05$		$p > 0.05$		$p > 0.05$		$p < 0.05$	
Max.	64.8		71.0		1916.5		707.7	
	64.8	58.8	71.0	68.0	1733.5	1916.5	707.3	707.7
Min.	8.9		2.0		60.3		1.8	
	8.9	9.9	2.0	2.0	60.3	64.0	1.8	3.5

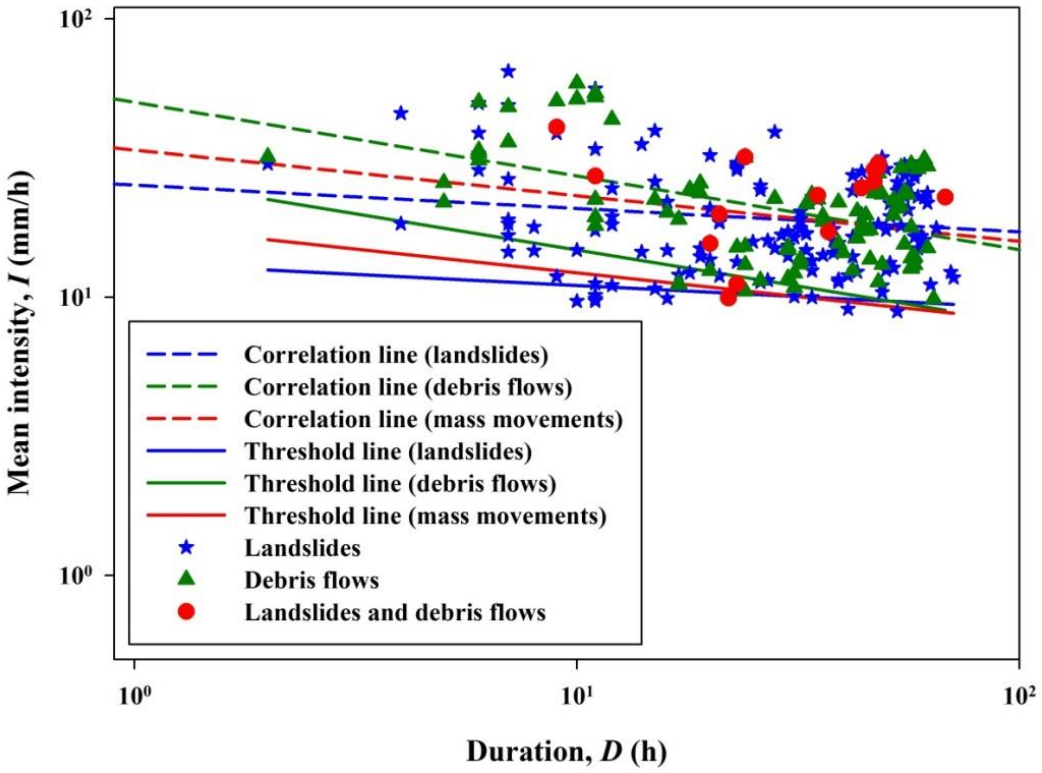

Fig. 4.1 *I–D* correlations and thresholds for all mass movements, landslides only, and debris flows only during 2006–2012.

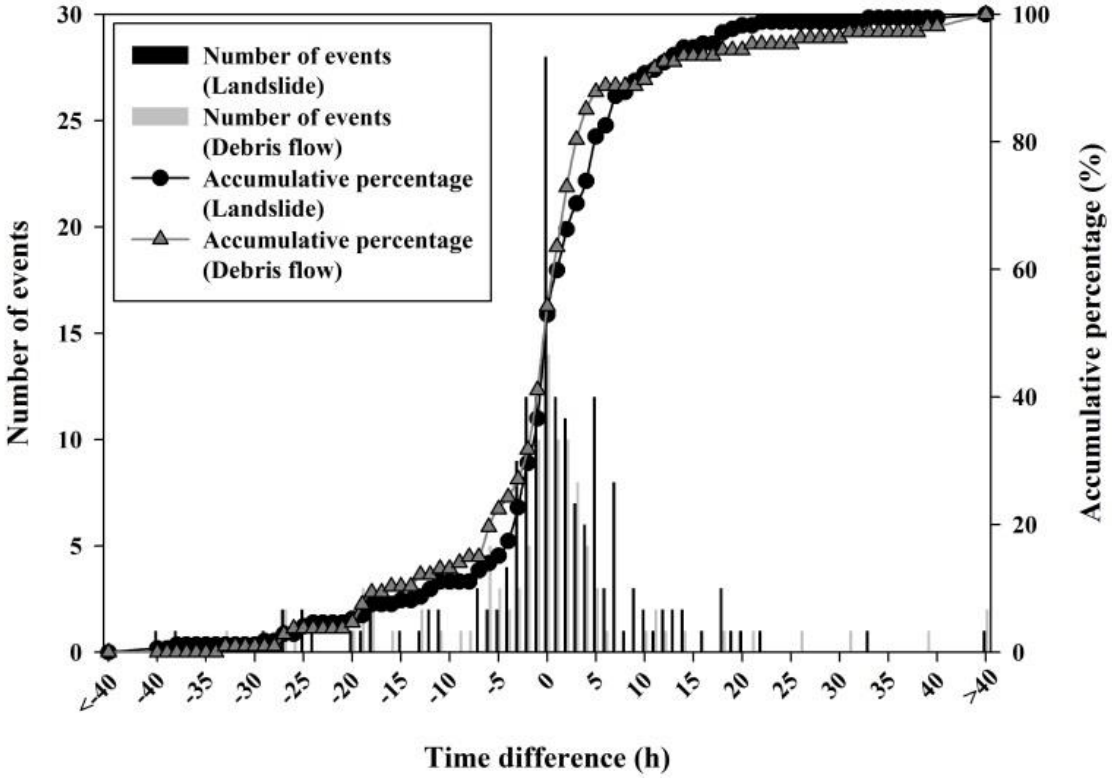

Fig. 4.2 Time differences between mass movement occurrences and peak rainfall intensity during 2006–2012.

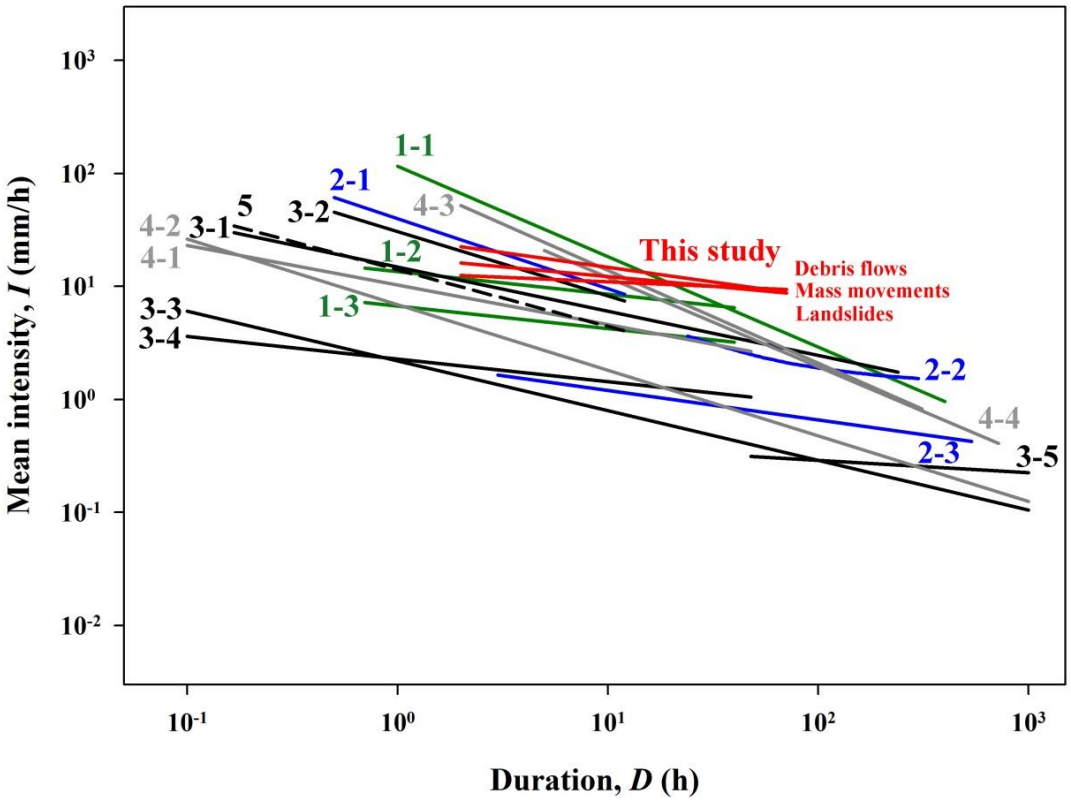

Fig. 4.3 Comparison of *I–D* thresholds. Green lines: thresholds for Taiwan. Blue lines: thresholds for Japan. Black lines: global thresholds. Gray lines: thresholds for humid (sub)tropics or Asian monsoon regions. Dashed line: other regional threshold. 1-1: Chien-Yuan et al., 2005; 1-2 & 1-3: Jan and Chen, 2005; 2-1 & 3-2: Jibson, 1989; 2-2: Hong et al., 2005; 2-3: Saito et al., 2010a; 3-1: Caine, 1980; 3-3, 3-4 & 3-5: Guzzetti et al., 2008; 4-1 & 4-2: Guzzetti et al., 2008, Cfa (climate of humid subtropical east coast in Köppen's system); 4-3: Larsen and Simon, 1993, Puerto Rico; 4-4: Dahal and Hasegawa, 2008, Nepal Himalaya; 5: Cannon et al., 2008, Southern California.

4.2 I_{MAP}–D thresholds

We rescaled mean rainfall intensity by dividing it by a *MAP* value of 3000 mm. Fig. 4.4 shows the I_{MAP}–D thresholds for Taiwan, and the new thresholds for all mass movements, landslides only, and debris flows only are described by the following equations:

$$I_{MAP} = 0.0060(\pm 0.0009)D^{-0.17(\pm 0.04)} \quad (2 \leq D \leq 71 \text{ h; all mass movements}) \tag{4.4}$$

$$I_{MAP} = 0.0044(\pm 0.0009)D^{-0.08(\pm 0.06)} \quad (2 \leq D \leq 71 \text{ h; landslides only}) \tag{4.5}$$

$$I_{MAP} = 0.0090(\pm 0.0022)D^{-0.26(\pm 0.07)} \quad (2 \leq D \leq 68 \text{ h; debris flows only}) \tag{4.6}$$

We also added the I_{MAP}–D thresholds for mass movements in Taiwan to the graph provided by Saito et al. (2010a). After rescaling, the I_{MAP}–D threshold for Taiwan was generally lower than that of other areas (Fig. 4.5).

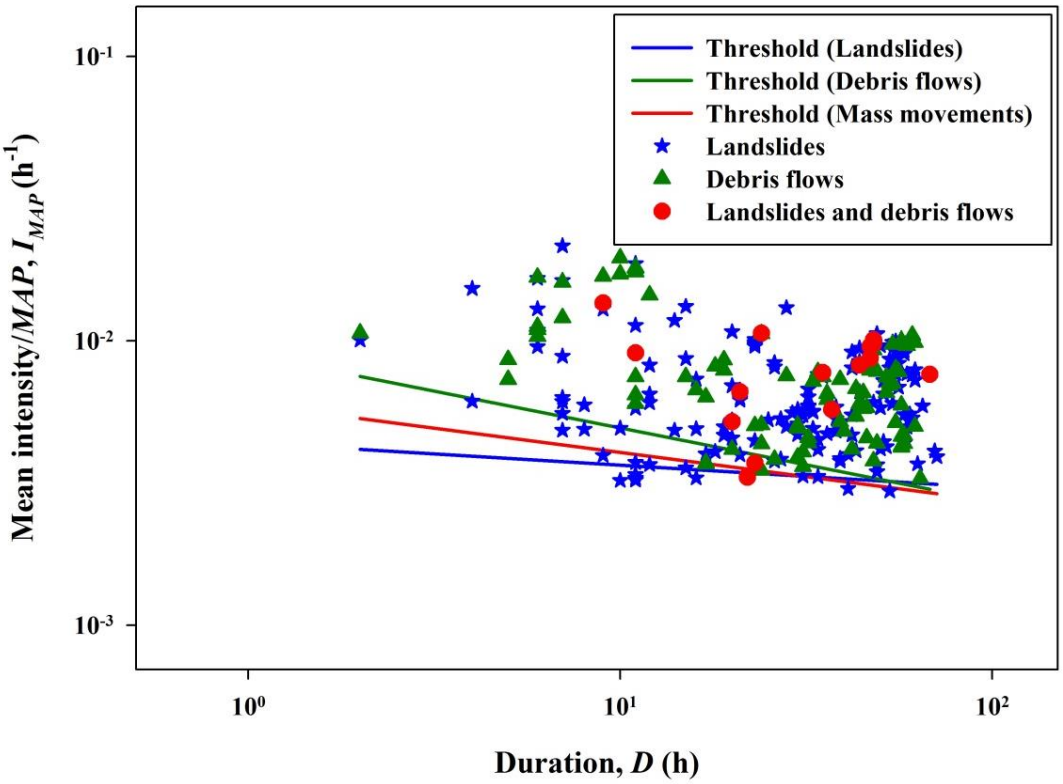

Fig. 4.4 I_{MAP}–D thresholds for all mass movements, landslides only, and debris flows only during 2006–2012.

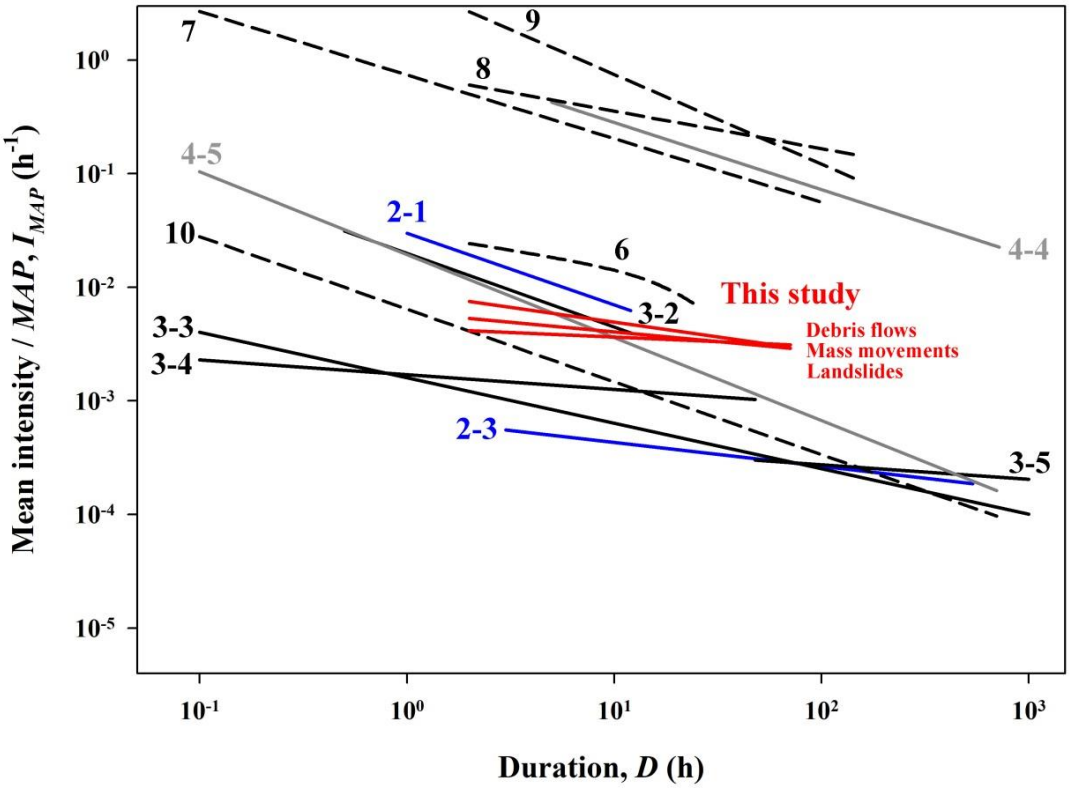

Fig. 4.5 Comparison of I_{MAP}–D thresholds. Blue lines: thresholds for Japan. Black lines: global thresholds. Gray lines: thresholds for humid (sub)tropics or Asian monsoon regions. Dashed lines: other regional thresholds. 2-1 & 3-2: Jibson, 1989; 2-3: Saito et al., 2010a; 3-3, 3-4 & 3-5: Guzzetti et al., 2008; 4-4: Dahal and Hasegawa, 2008, Nepal Himalaya; 4-5: Guzzetti et al., 2007, Mild mid-latitude climates; 6: Cannon, 1988, San Francisco; 7: Bacchini and Zannoni, 2003, Cancia, Dolomites, Italy; 8 & 9: Aleotti, 2004, Piedmont, Italy; 10: Guzzetti et al., 2007, Central and Southern Europe.

4.3 Differences in thresholds for landslides and debris flows

The calculated *I–D* and I_{MAP}–*D* correlations for landslides and debris flows revealed that debris flows tend to occur under more severe rainfall conditions than landslides (i.e., high intensity). In addition, t-tests revealed that the κ and ε of the *I–D* and I_{MAP}–*D* thresholds for landslides (Eqs. 4.2 and 4.5) and debris flows (Eqs. 4.3 and 4.6) are statistically different at the 5% significance level. However, Figs. 4.1 and 4.4 also demonstrate that the *I–D* correlation lines and thresholds for landslides and debris flows get closer as *D* increases; their difference becomes negligible once *D* reaches approximately 50 h.

4.4 Two types of rainfall conditions

For *I* and *D* of each mass movement event during 2006–2012, PCA was adopted to classify the rainfall conditions (Fig. 4.6). Two types of *I–D* conditions along with the positives and negatives of the first PC, whose proportion of variance was 71.8%, and those along with the second PC was 28.2%. Positives of the first PC score (120 mass movement events) mainly occur when rainfall persists for 20–40 h from the beginning of rainfall, i.e., SH rainfall. Conversely, negatives (143 mass movement events) mainly occur when rainfall persists for 80–200 h, i.e., LL rainfall.

In Fig. 4.6, we also plotted rainfall conditions of 19 mass movements occurred in 2013. According to the result shown in Fig. 4.6, the rainfall conditions of the 19 mass movements were classified into 14 SH types and 5 LL types.

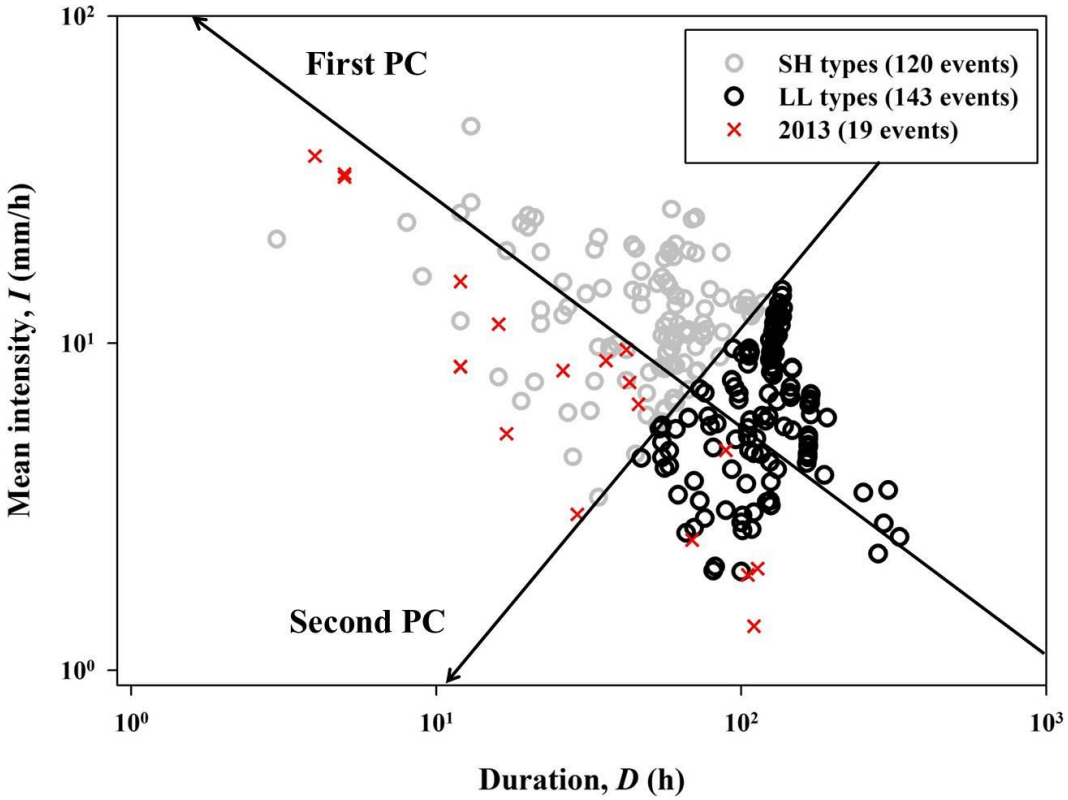

Fig. 4.6 PCA for *I–D* conditions of mass movements. Gray circles and black circles are SH and LL types, respectively, and red crosses are data for 2013.

4.5 Changes in *SWI*

During 2006–2012, the changes in *SWI* (Table 4.2) show that *SWI* at the moment before a rainfall event, which triggered mass movements, was 17.5 on average, ranging from 0 to 104.95. At the moment of mass movements, *SWI* was 336.81 on average, ranging from 68.63 to 645.04. Their differences were 319.31 on average, ranging from 47.79 to 639.08. In 2013, *SWI* at the moment before the rainfall events was 36 on average, ranging from 3.8 to 91.9. At the moment of mass movements, *SWI* was 154.4 on average, ranging from 81.7 to 220.7. The differences were 118.4 on average, ranging from −10.2 to 213.4. The values of *SWI* in 2013, except for that

before the rainfall event, were all smaller than those during 2006–2012. Fig. 4.6 also shows that the rainfall conditions in 2013 tend to be lower than in the other years.

Table 4.2 Changes in *SWI* during 2006–2012 and in 2013.

	SWI (2006–2012)			*SWI* (2013)		
Moment	Before rainfall	Mass movement	Difference	Before rainfall	Mass movement	Difference
Average	17.5	336.8	319.3	36	154.4	118.4
Max.	105	645	639.1	91.9	220.7	213.4
Min.	0	68.6	47.8	3.8	81.7	-10.2

4.6 Landslide area, volume, depth, and magnitude

Table 4.3 shows the landslide area, volume and depth based on the landslide mapping and calculated using the above-noted empirical formula (Eq. 3.10). During 2006–2012, the landslide area was 7.0×10^4 m^2 on average, ranging from 6.3×10^2 to 3.1×10^6 m^2. The volume was 2.4×10^6 m^3 on average, ranging from 8.9×10^2 to 1.9×10^8 m^3. The depth was 7.3 m on average, ranging from 1.4 to 62.0 m. Most of landslides (91.9%) have areas between 10^3 and 10^5 m^2 (Fig. 4.7). There are two particularly large landslides caused by Typhoon Morakot in 2009. The largest one occurred in Jiaxian District, Kaohsiung City with the area of 3.13×10^6 m^2, mean rainfall intensity of 23.3 mm/h, duration of 57 h, and cumulative rainfall of 1327.3 mm (Fig. 4.8). The second largest one occurred in Wutai Township, Pingtung County with the area of 2.11×10^6 m^2, mean rainfall intensity of 16.8 mm/h, duration of 29 h, and cumulative rainfall of 485.9 mm (Fig. 4.9).

From the estimated landslide volume, this study measured the magnitude of a landslide using Eq. 3.12. The resultant magnitude during 2006–2012 in Taiwan is m_L = 6.4.

Table 4.3 Area, volume and depth of landslides during 2006–2012.

	Average	Min.	Max.
Area (m^2)	7.0×10^4	6.3×10^2	3.1×10^6
Volume (m^3)	2.4×10^6	8.9×10^2	1.9×10^8
Depth (m)	7.3	1.4	62.0

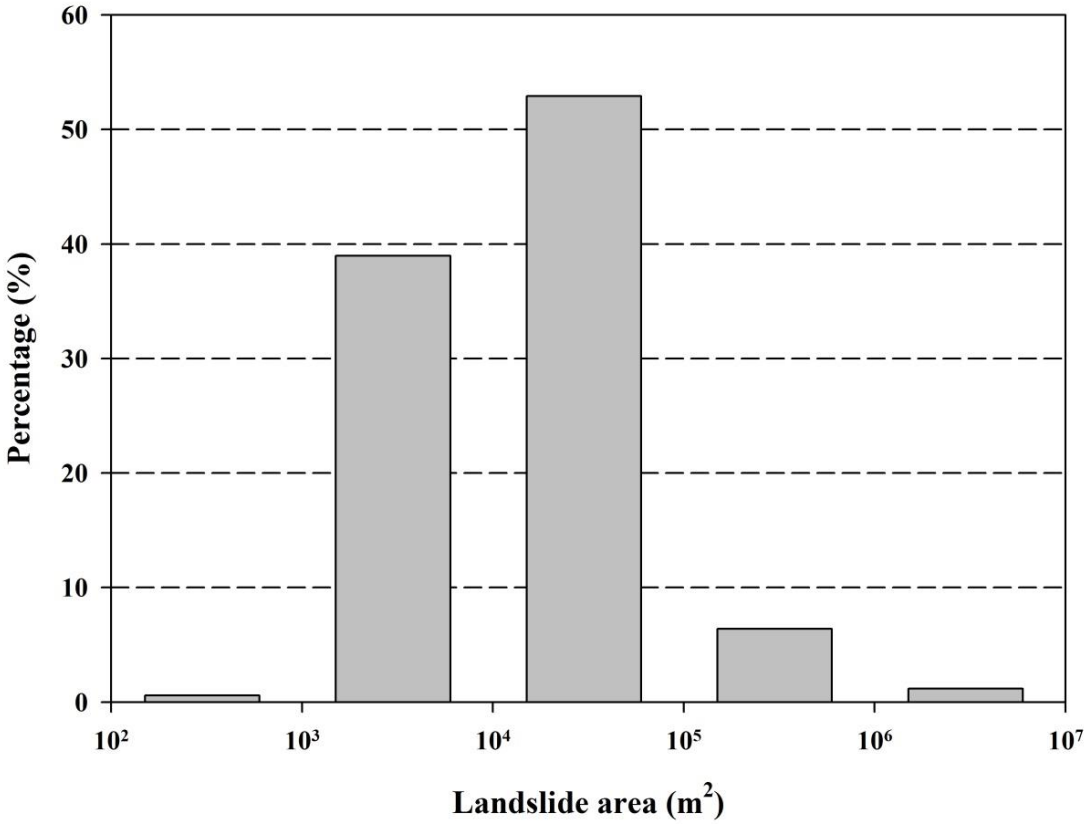

Fig. 4.7 Distribution of landslide area during 2006–2012.

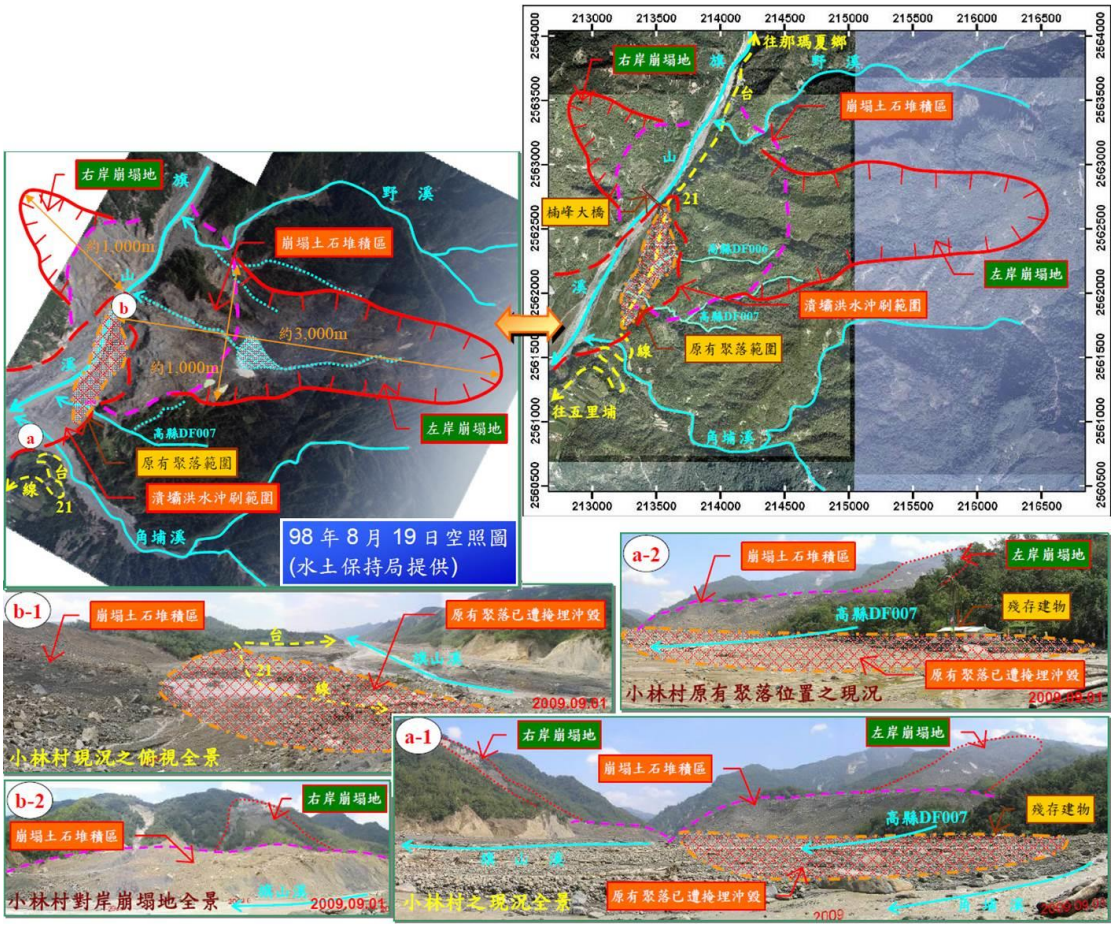

Fig. 4.8 Information on the largest landslide that occurred in Jiaxian District, Kaohsiung City, from the report of the SWCB.

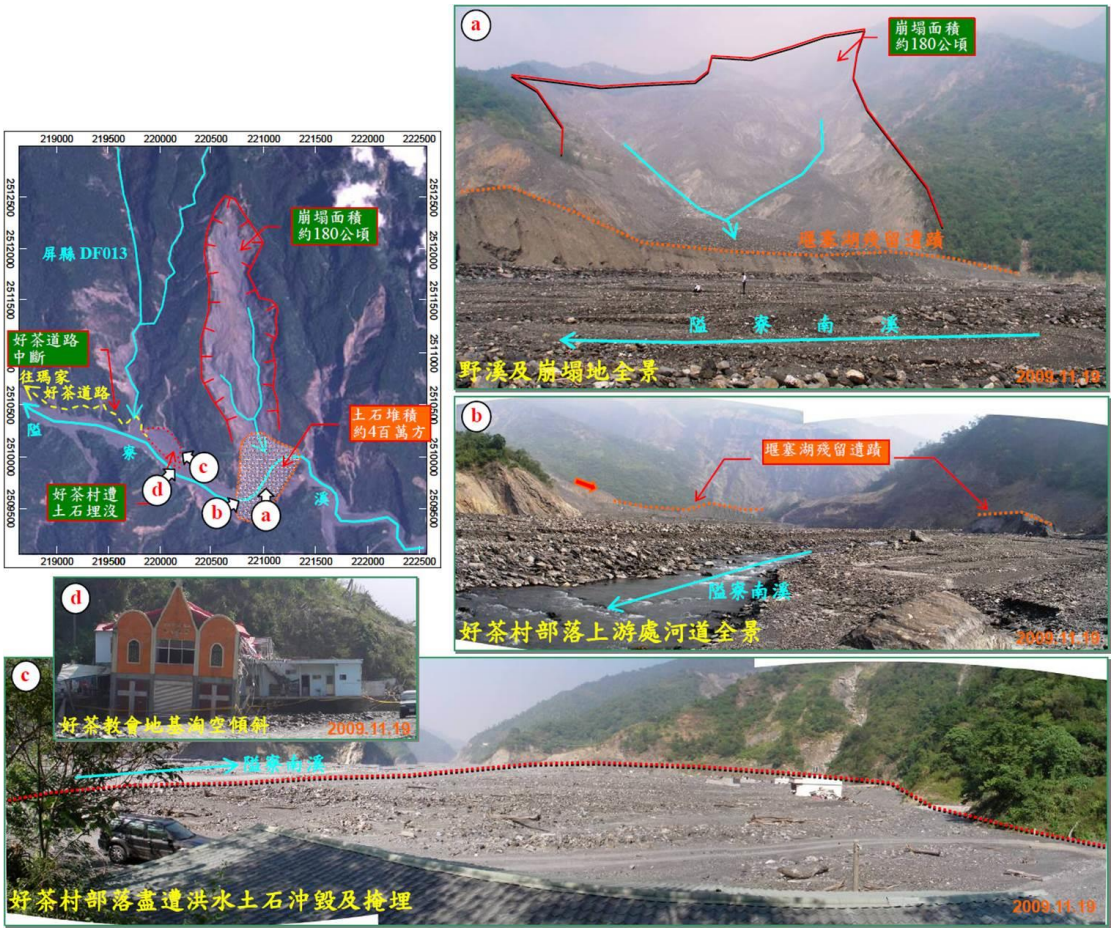

Fig. 4.9 Information on the second largest landslide that occurred in Wutai Township, Pingtung County from the report of the SWCB.

4.7 Frequency–area distribution of landslides

The areas of all 172 mapped landslides exhibit a frequency–area distribution that can be described by a power-law over more than three orders of area magnitude with a good fit (R^2 = 0.91) (Fig. 4.10):

$$P(A_L) = 292.5A_L^{-1.1} \ (6.3\times10^2 \text{ m}^2 < A_L < 3.1\times10^6 \text{ m}^2) \quad (4.7)$$

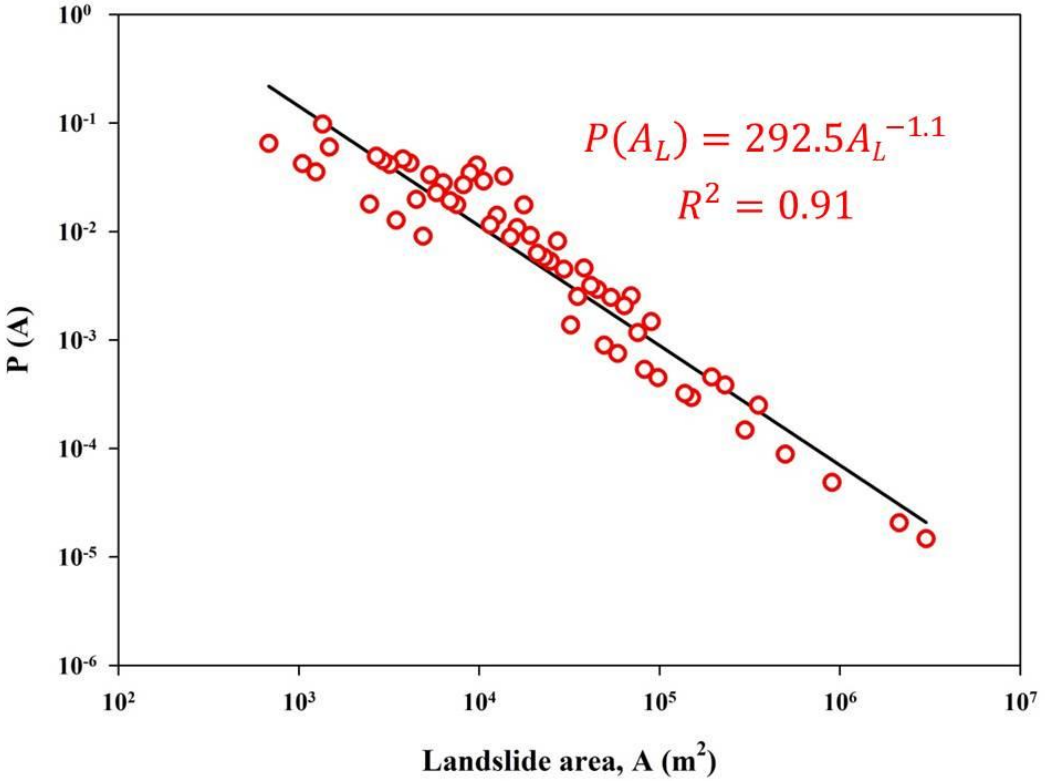

Fig. 4.10 Frequency–area distribution of 172 landslides in Taiwan during 2006–2012.

4.8 Sediment discharge of the 17 main rivers during typhoon events

Fig. 4.11–4.14 show the sediment discharge of the 17 main rivers during the 15 typhoon events and the related rainfall conditions, the cumulative rainfall and the average daily rainfall, calculated from the nearest rain gauge of each hydrometric station.

4.8.1 Northern rivers

During the 15 typhoon events, sediment discharge in the Xindian River ranged from 353 to 3.556×10^5 t with an average of 8.179×10^4 t. The maximum sediment discharge appeared during Typhoon Sinlaku in 2008 with a cumulative rainfall of

631.5 mm and an average daily rainfall of 105.3 mm. In the Tahan River, sediment discharge ranged from 1667 to 1.540×10^6 t with an average of 2.479×10^5 t. The maximum sediment discharge appeared during Typhoon Sinlaku in 2008 with a cumulative rainfall of 868.5 mm and an average daily rainfall of 144.8 mm. In the Touchien River, sediment discharge ranged from 4 to 8874 t with an average of 2016 t. The maximum sediment discharge appeared during Typhoon Krosa in 2007 with a cumulative rainfall of 727 mm and an average daily rainfall of 181.8 mm.

4.8.2 Central rivers

During the 15 typhoon events, in the Taan River, sediment discharge ranged from 164 to 1.055×10^4 t with an average of 4100 t. The maximum sediment discharge appeared during Typhoon Saola in 2012 with a cumulative rainfall of 794.5 mm and an average daily rainfall of 158.9 mm. In the Tachia River, sediment discharge ranged from 177 to 2.632×10^4 t with an average of 5505 t. The maximum sediment discharge appeared during Typhoon Morakot in 2009 with a cumulative rainfall of 815 mm and an average daily rainfall of 135.8 mm. In the Wu River, sediment discharge ranged from 411 to 5.714×10^4 t with an average of 2.395×10^4 t. The maximum sediment discharge appeared during Typhoon Morakot in 2009 with a cumulative rainfall of 815 mm and an average daily rainfall of 135.8 mm. In the Choshui River, sediment discharge ranged from 2.779×10^4 to 1.345×10^8 t with an average of 2.037×10^7 t. The maximum sediment discharge appeared during Typhoon Morakot in 2009 with a cumulative rainfall of 658 mm and an average daily rainfall of 109.7 mm.

4.8.3 Southern rivers

During the 15 typhoon events, in the Tsengwen River, sediment discharge ranged from 109 to 9.676×10^6 t with an average of 8.839×10^5 t. The maximum sediment discharge appeared during Typhoon Morakot in 2009 with a cumulative rainfall of 1088 mm and an average daily rainfall of 181.3 mm. In the Erhjen River, sediment discharge ranged from 303 to 4.291×10^6 t with an average of 5.346×10^5 t. The maximum sediment discharge appeared during Typhoon Nanmadol in 2011 with a cumulative rainfall of 333 mm and an average daily rainfall of 66.6 mm. In the Kaoping River, sediment discharge ranged from 6.989×10^4 to 2.870×10^8 t with an average of 2.084×10^7 t. The maximum sediment discharge appeared during Typhoon Morakot in 2009 with a cumulative rainfall of 1126.5 mm and an average daily rainfall of 187.8 mm. In the Linpien River, sediment discharge ranged from 3200 to 4.257×10^6 t with an average of 6.370×10^5 t. The maximum sediment discharge appeared during Typhoon Morakot in 2009 with a cumulative rainfall of 877.5 mm and an average daily rainfall of 146.3 mm. In the Sihjhong River, sediment discharge ranged from 22 to 5.961×10^5 t with an average of 8.864×10^4 t. The maximum sediment discharge appeared during Typhoon Megi in 2010 with a cumulative rainfall of 223.5 mm and an average daily rainfall of 74.5 mm.

4.8.4 Eastern rivers

During the 15 typhoon events, in the Peinan River, sediment discharge ranged from 2.436×10^4 to 2.618×10^7 t with an average of 3.706×10^6 t. The maximum sediment discharge appeared during Typhoon Tembi in 2012 with a cumulative rainfall of 415.2 mm and an average daily rainfall of 51.9 mm. In the Hsiukuluan

River, sediment discharge ranged from 5249 to 2.517×10^7 t with an average of 3.788×10^6 t. The maximum sediment discharge appeared during Typhoon Tembi in 2012 with a cumulative rainfall of 265.5 mm and an average daily rainfall of 33.2 mm. In the Hualien River, sediment discharge ranged from 4663 to 3.568×10^7 t with an average of 4.958×10^6 t. The maximum sediment discharge appeared during Typhoon Sepat in 2007 with a cumulative rainfall of 352.5 mm and an average daily rainfall of 88.1 mm. In the Hoping River, sediment discharge ranged from 124 to 2.551×10^7 t with an average of 3.284×10^6 t. The maximum sediment discharge appeared during Typhoon Fung-Wong in 2008 with a cumulative rainfall of 392.5 mm and an average daily rainfall of 98.1 mm. In the Lanyang River, sediment discharge ranged from 643 to 2.217×10^7 t with an average of 4.263×10^6 t. The maximum sediment discharge appeared during Typhoon Jangmi in 2008 with a cumulative rainfall of 248 mm and an average daily rainfall of 62 mm.

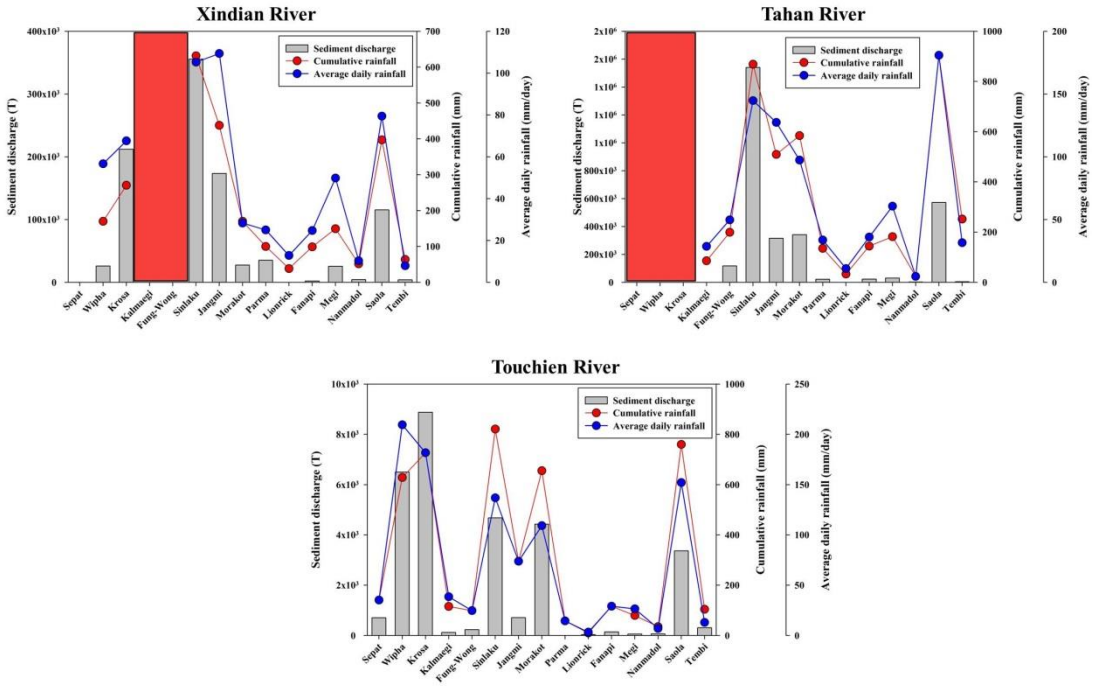

Fig. 4.11 Sediment discharge of northern rivers during typhoon events and the related rainfall conditions. Red background means no available data.

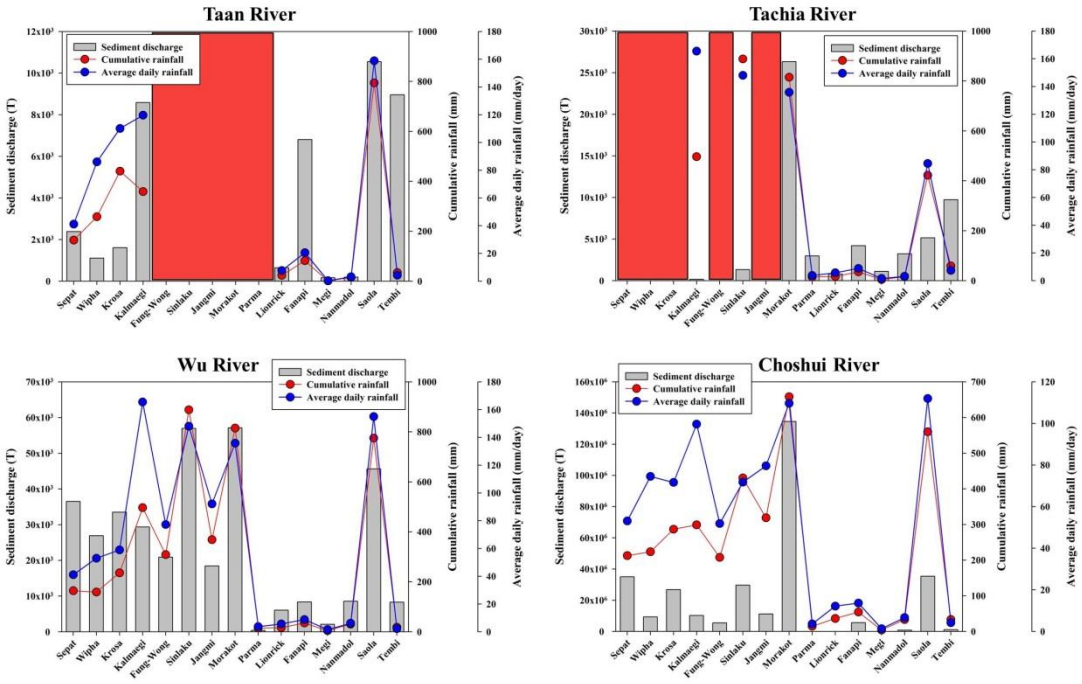

Fig. 4.12 Sediment discharge of central rivers during typhoon events and the related rainfall conditions. Red background means no available data.

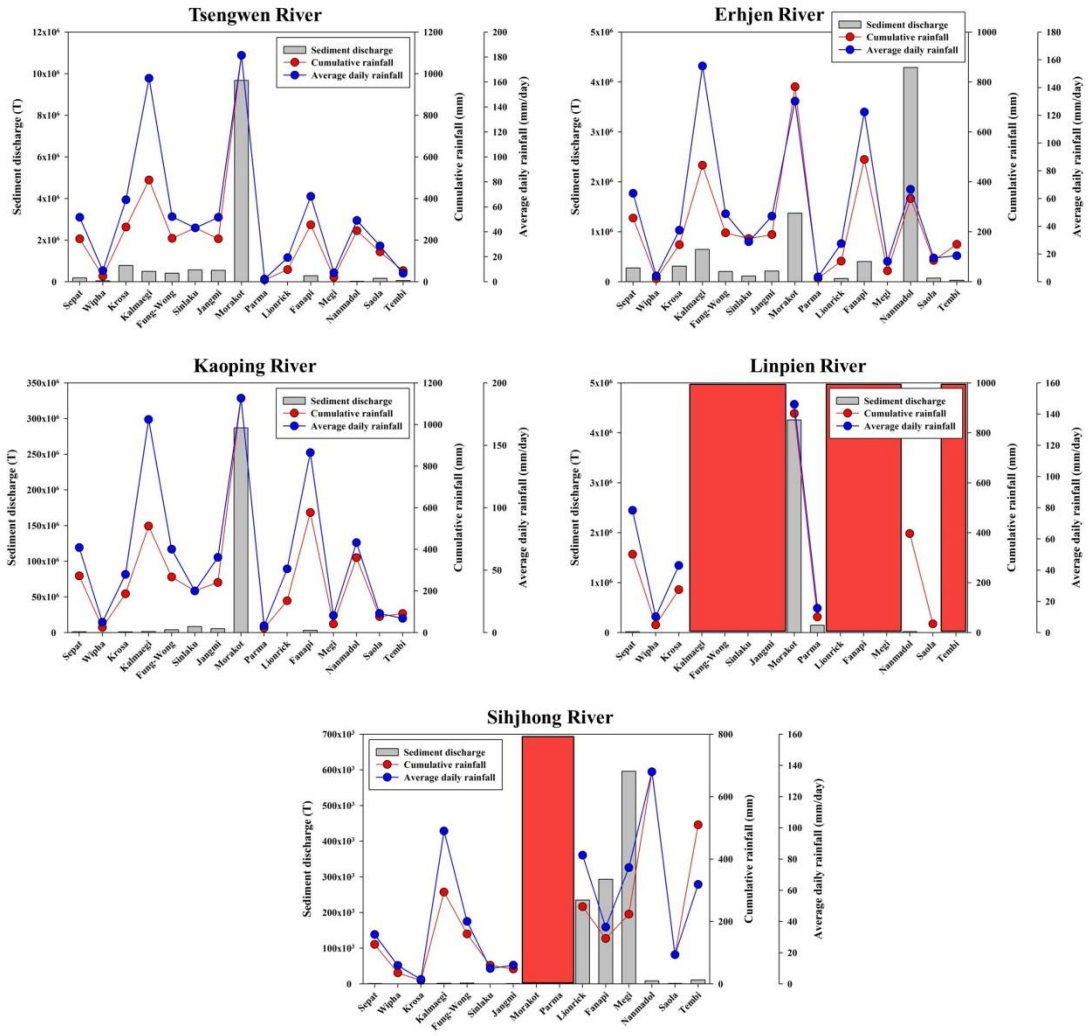

Fig. 4.13 Sediment discharge of southern rivers during typhoon events and the related rainfall conditions. Red background means no available data.

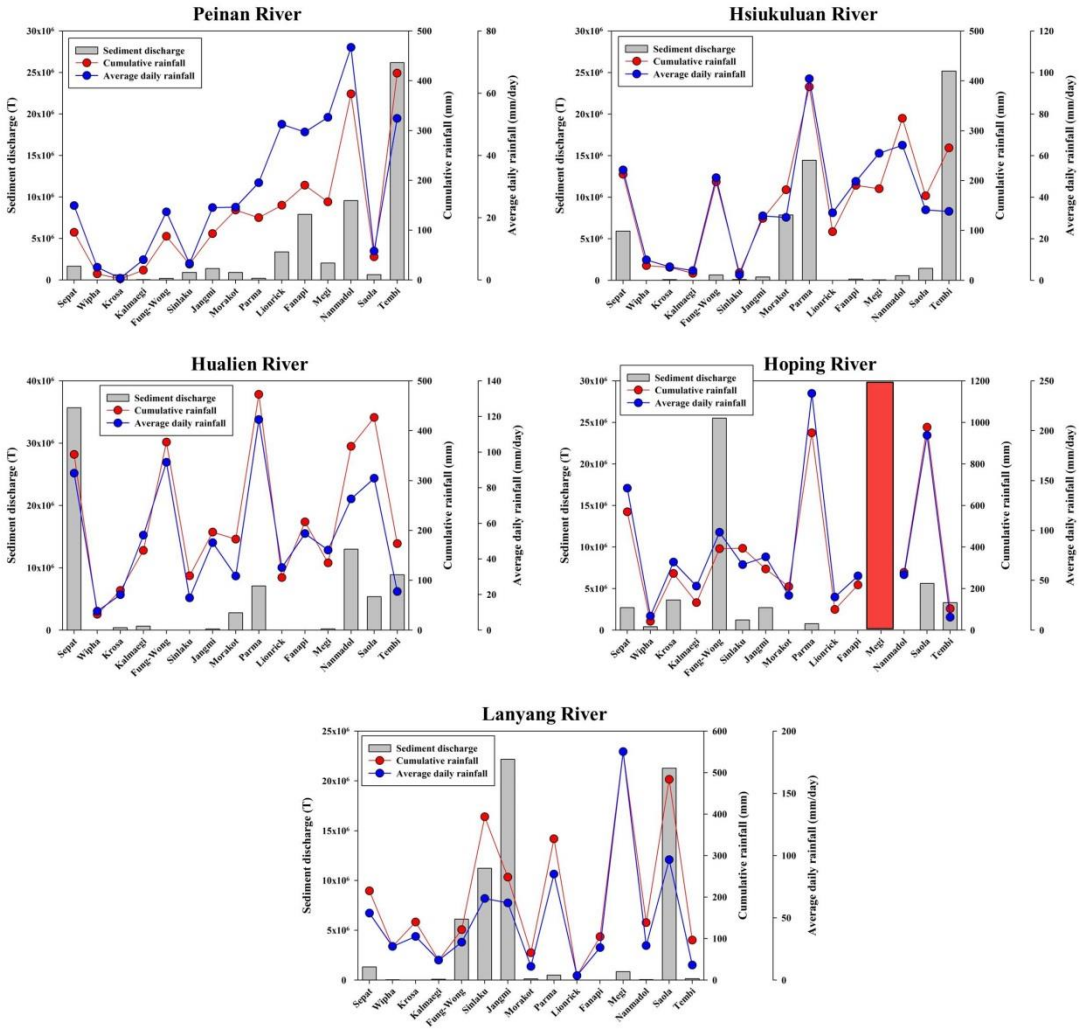

Fig. 4.14 Sediment discharge of eastern rivers during typhoon events and the related rainfall conditions. Red background means no available data.

Chapter 5 Assessment of mass movement occurrences

5.1 *I–D* thresholds and rainfall conditions for mass movements

5.1.1 Thresholds for landslides and debris flows

The difference in the *I–D* and I_{MAP}–*D* thresholds between landslides and debris flow as well as data in Table 1 indicates that a higher mean rainfall intensity is required to flush surface materials and cause a debris flow for short duration rainfall events. Although these trends may include reporting biases of our mass movement inventory, we ruled out reporting biases based on the unaltered trends that we obtained using the frequentist statistical method and the random sampling methods. Our results reflect the fact that relatively abundant water is needed along channels and streams to trigger a debris flow. A long duration rainfall event leads to a gradual increase in groundwater level, soil moisture, and pore water pressure (Wieczorek and Glade 2005), and flow along channels and streams increases concurrently. Therefore, similar rainfall intensity levels can trigger both landslides and debris flows if rainfall duration is sufficiently long. In addition, landslides may completely or partially mobilize to form debris flows (Iverson et al. 1997), which also applies to the 16 cases in Taiwan, and the condition of their occurrence is comparable to that for debris flows (Figs. 4.1 and 4.4). This observation further confirms the above statement.

5.1.2 Comparing the obtained thresholds with those from previous studies

Jan and Chen (2005) established *I–D* thresholds for debris flows in the Chenyoulan river catchment in central Taiwan before and after the 1999 Chi-Chi earthquake. The threshold determined in this study for the whole of Taiwan was similar to the threshold for the Chenyoulan river catchment before the Chi-Chi earthquake (1-2 in Fig. 4.3), lower than the threshold for Taiwan from 1989 to 2001 (1-1 in Fig. 4.3), and higher than the threshold for the Chenyoulan river catchment just after the Chi-Chi earthquake (1-3 in Fig. 4.3). These results suggest that the rainfall threshold for mass movements in Taiwan decreased in 1999 when the Chi-Chi earthquake generated an enormous quantity of loose material, which resulted in a rapid decrease of the mass movement rainfall threshold for this region. Our results indicate that the threshold recovered to pre-earthquake values during 2006–2012. Many previous studies reported similar decreases in both the maximum rainfall intensity and critical cumulative rainfall required to trigger mass movements after the Chi-Chi earthquake (Lin et al. 2003; Chang et al. 2009; Shieh et al. 2009; Chen 2011). As observed in this study, these values gradually regained to the pre-earthquake conditions after several years (Lin et al. 2003; Chang et al. 2009; Shieh et al. 2009; Chen 2011).

The slope of the rainfall threshold line for debris flows as determined in this study is similar to the value calculated by Jan and Chen (2005). However, our slope is quite different from that reported in Chien-Yuan et al. (2005), which utilized data from 61 debris flows that occurred between 1989 and 2001. Chien-Yuan et al. (2005) obtained data from newspapers and interviews with local residents, and the *I–D* threshold was visually defined rather than statistically determined. The differences in

the threshold line slope between our study and Chien-Yuan et al. (2005) are likely attributable to their relatively small sample size and their subjective method for establishing *I–D* thresholds. Comparatively, we determined the *I–D* threshold using 107 debris flow events and employed statistical methods to ensure the validity of our results. Nevertheless, our study along with the studies performed by Chien-Yuan et al. (2005) and Jan and Chen (2005) reported thresholds for debris flows that were larger than thresholds for landslides.

Our *I–D* thresholds for Taiwan tend to be higher than those for other areas of the world, particularly for long duration rainfall events (Fig. 4.3). As Taiwan is characterized by high-relief topography and complex geology (Fig. 2.1) that facilitate mass movements, the above observation seems contradictory. In Taiwan, high cumulative precipitation amounts and frequent heavy storms, particularly those associated with typhoons (Wu and Kuo, 1999), have created landforms that are well adjusted to the extreme climatic conditions of the region. Therefore, since unconsolidated hillslope materials are limited, strong rainfall is needed to trigger mass movements. Several studies on mass movements in Japan also found that hillslopes in regions with high cumulative precipitation displayed greater resistance to rainfall than hillslopes in regions with low cumulative precipitation (Omura, 1980, 1982). Saito and Matsuyama (2012) confirmed this for Japan using *MAP* data. They found that because the *MAP* is extremely high in the eastern part of the Kii Peninsula, Japan, it is not prone to landslides even with the high cumulative rainfall and maximum hourly rainfall intensity due to the typhoon event. Therefore, the higher *I–D* threshold for Taiwan relative to other areas of the world is acceptable. In addition, the gentle slope of threshold in Taiwan may indicate that the rainfall intensity plays a much more important role in triggering mass movements. This observation further confirms the above statement that landforms are well adjusted to the extreme climatic conditions.

Mass movements then triggered only when the rainfall intensity reaches a certain value.

As indicated above, the I_{MAP}–D threshold is useful for eliminating biases caused by regionally varied rainfall conditions. Even though we used a relatively conservative *MAP* value of 3000 mm to rescale the data, the I_{MAP}–D threshold for Taiwan was generally lower than in other areas. Therefore, the steep topography and highly deformed underlying bedrock of Taiwan likely contribute to the frequent mass movements in the region. In summary, analysis of both I–D and I_{MAP}–D thresholds is useful for examining the effects of topography, geology, and hillslope adjustment to rainfall conditions on mass movements.

5.1.3 Mass movements in relation to rainfall peaks and antecedent rainfall

I–D plots represent average rainfall event conditions and do not necessarily reflect high rainfall intensities at the time of a mass movement occurrence. Therefore, predicting the exact time of mass movements using only I–D thresholds is difficult. Many studies have found that peak rainfall intensity occurs very close to the time of mass movement occurrence (Aleotti 2004; Chien-Yuan et al. 2005; Guzzetti et al. 2007, 2008; Dahal and Hasegawa 2008; Saito et al. 2010a,b). Thus, analyzing peak rainfall intensity in conjunction with I–D thresholds is useful for characterizing mass movements.

Most mass movement occurrences investigated were concentrated around the time of peak rainfall intensity; approximately 75% of mass movements occurred within seven hours from the rainfall peak (Fig. 4.2). To focus on the remaining 25% of mass movements that occurred significantly before and after the rainfall peak, we

classified the mass movements into three groups: $T_d < -7$ (Group 1 = G1), $T_d = -7$ to 7 (G2), and $T_d > 7$ (G3). Table 5.1 shows average peak intensity, mean intensity, duration, and antecedent rainfall for these three groups.

G2 had the highest peak and mean intensities for both landslides and debris flows and the difference from the other groups is statistically significant in most cases. The antecedent rainfall for landslides in G2 was also significantly higher. This indicates that G2 includes typical landslides in terms of not only the large event number but also their mechanisms directly related to hillslope hydrology. Landslide occurrence is highly relevant to soil moisture contents (Terlien 1998; Wu and Chen 2009) and antecedent rainfall elevates the moisture contents (Glade 1997; Crosta 1998; Crozier 1999; Glade et al. 2000; Jakob et al. 2006). Therefore, the combination of abundant antecedent rainfall and high intensity rainfall can easily trigger landslides, especially around the time of rainfall peak. In addition, during or just after the rainfall peak, high intensity rainfall flushed large amounts of debris in rivers, triggering debris flows. In this case, abundant antecedent rainfall is not a requirement, because debris flows can be caused from river-bed material saturated with surface water (Berti et al. 1999; Coe et al. 2008), not necessarily hillslope material saturated with underground soil water.

G3 had the longest rainfall duration for both landslides and debris flows. Although G3 is characterized by low peak and mean rainfall intensities, rainfall continued for a long period, resulting in mass movements long after the rainfall peak. Terlien (1998) also indicated that when there is no significant antecedent rainfall and rainfall intensity is low, triggering landslides with high soil moisture content often requires a long duration rainfall event.

According to Table 5.1, G1 does not correspond to any strong, abundant or long rainfall, meaning that the mass movements occurred in spite of relatively small

impacts of the corresponding rainfall and antecedent rainfall. This is an unexpected result; our first assumption had been that such mass movements well before the rainfall peak reflect abundant antecedent rainfall, which was found to be invalid. For G1, the role of factors other than rainfall, such as local topography or geology highly susceptible to mass movements, seems to be more important. However, the result may be due to the definition of antecedent rainfall. Although we considered the period of 168 hours in computing the amount of antecedent rainfall, even earlier rainfall might have affected the mass movements in G1. Indeed, the definition of antecedent rainfall is a difficult task (Crozier 1999; Glade et al. 2000; Dahal and Hasegawa 2008). To discuss these issues, the effects of topography and geology are examined in the next section.

Fig. 5.1 shows changes in *SWI* for the G1, G2, and G3 mass movements. From the beginning of rainfall to the occurrence of mass movements, the three group present similar trends of changes in *SWI*. This means that in spite of small influence of the corresponding rainfall and antecedent rainfall on the G1 mass movements, changes in soil water contents show the sign of mass movements (see detailed discussion in Section 5.2). Table 5.2 shows average values of *SWI* for G1, G2, and G3. Values of *SWI* before a rainfall event are almost the same for the three groups. However, the average value of *SWI* at the moment of mass movements for G1 is much lower than those for the other two groups. Since the G1 mass movements occurred significantly before the rainfall peak, without very strong rainfall, soil water contents cannot increase much. This again proves that other factors may be more important in the occurrence of the G1 mass movements.

Table 5.1 Average rainfall conditions of different T_d groups. Bold values show significantly higher values for one group than the other groups identified using t-test between two groups ($p < 0.05$).

Rainfall condition groups	Peak intensity (mm/h)		Mean intensity (mm/h)		Duration (h)		Antecedent rainfall (mm)	
	Landslides	Debris flows	Landslides	Debris flows	Landslides	Debris flows	Landslides	Debris flows
G1: T_d < -7 (n = 19, 16)	71.5	65.6	16.8	13.7	32.6	29.9	79.4	102.0
G2: T_d = -7 to 7 (n = 131, 79)	80.7	**90.3**	**21.9**	**25.9**	30.8	32.2	**159.3**	90.1
G3: T_d > 7 (n = 22, 12)	60.4	56.6	18.7	18.1	**45.6**	**46.9**	94.7	172.0

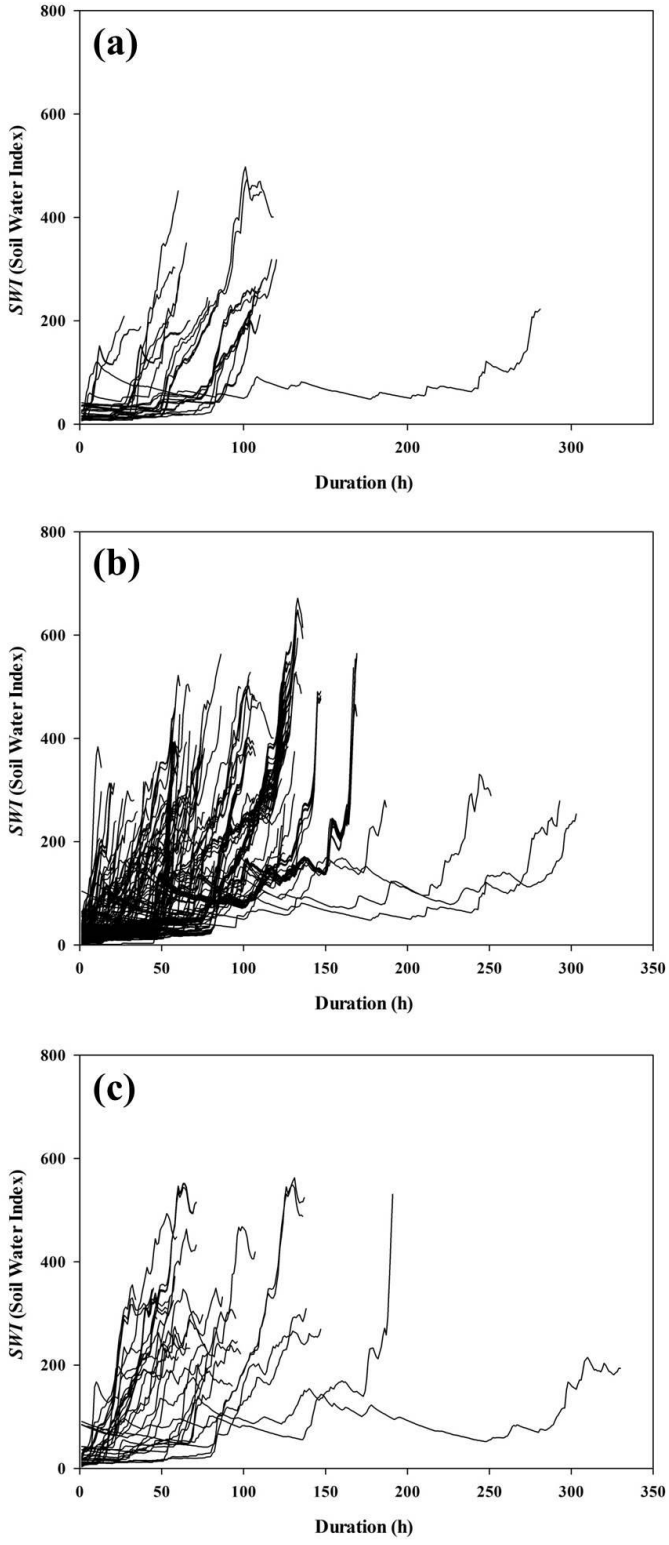

Fig. 5.1 Changes in *SWI* for (a) G1, (b) G2, and (c) G3 mass movements.

Table 5.2 Average values of *SWI* for the G1, G2, and G3 mass movements.

Group	Before rainfall	Mass movement	Difference
G1	14.2	258.8	244.5
G2	17.4	351.2	333.8
G3	20.8	326.8	306.0

5.1.4 Topographic and geological conditions for G1 mass movements

As mentioned in Section 5.1.3, an unexpected result came out for G1 – the mass movements occurred significantly before the rainfall peak in spite of relatively small impacts of the corresponding rainfall and antecedent rainfall. Using the 10-m DTM and the geological map of Taiwan, the frequency distributions of elevation, slope and geology for the whole of Taiwan, all the 263 mass movements, and the G1 mass movements are summarized (Fig. 5.2). The percentage of the G1 mass movements below 500 m in elevation and below 10° in slope are less than those for all mass movements. For higher and steeper areas, the percentage of the G1 mass movements is always larger than that of all mass movements. This indicates that the G1 mass movements tended to occur under severer topographical conditions. In addition, the G1 mass movements occurred more in the domain of sedimentary rocks whose strength is usually weaker than that of metamorphic rocks. These observations suggest that the topographical and geological conditions more favorable for erosion induced the G1 mass movements in spite of relatively small impacts of the corresponding and antecedent rainfall.

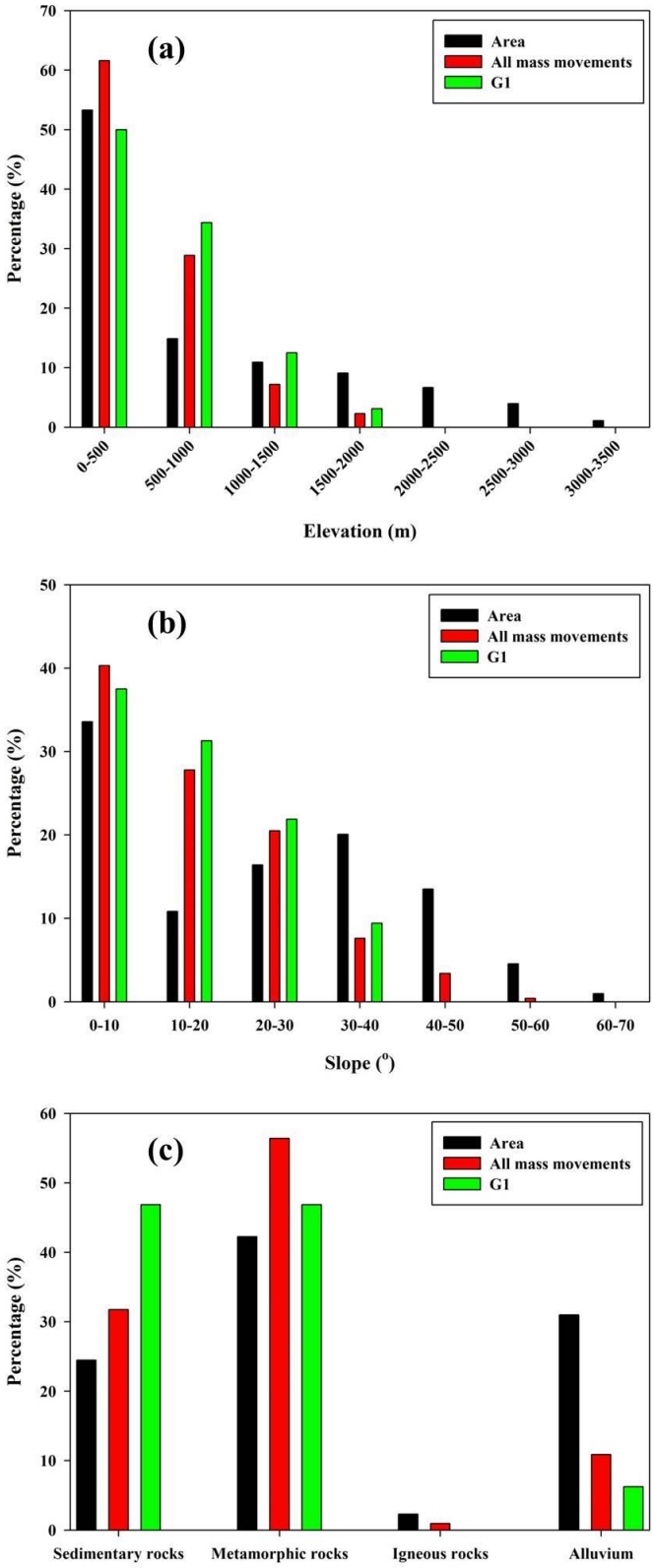

Fig. 5.2 Frequency distribution of (a) elevation, (b) slope, and (c) lithological domains for the whole of Taiwan, all mass movements, and G1 mass movements.

5.2 Soil water index

5.2.1 Antecedent rainfall condition based on *SWI*

The *SWI* values before a rainfall event which triggered mass movements can be regarded as an indicator of antecedent rainfall condition. We compared *SWI* with the mean rainfall intensity, duration and cumulative rainfall (Fig. 5.3). The results suggest that the two values of *SWI* before the rainfall event, 20 and 40, represent rainfall conditions for triggering mass movements. When *SWI* is above 40, rainfall conditions needed for triggering mass movements are lower than 15 mm/h in mean intensity, shorter than 100 h in duration, and less than 1000 mm in cumulative rainfall. When *SWI* is between 20 and 40, rainfall conditions needed are up to 30 mm/h in mean intensity, 150 h in duration, and 1500 mm in cumulative rainfall. When *SWI* is below 20, rainfall conditions needed are up to 30 mm/h in mean intensity, 350 h in duration, and 2000 mm in cumulative rainfall. The above statement indicates that the upper bound of rainfall conditions for triggering mass movements can be defined on the basis of *SWI*. This means the *SWI* can be used as the indicator for assessing the effect of antecedent rainfall on mass movements. However, it is difficult to define the lower bound, because some mass movements occur under quite low impacts of rainfall.

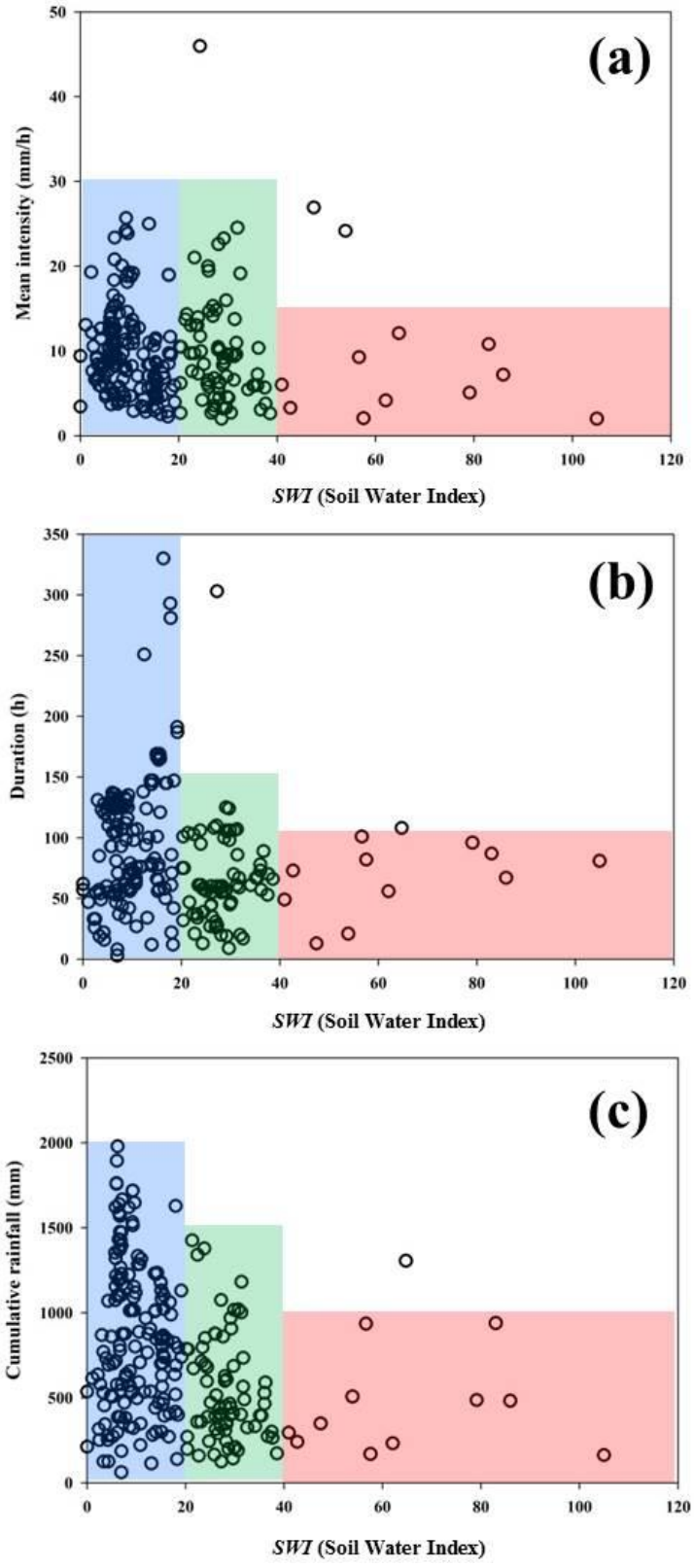

Fig. 5.3 Comparing *SWI* with the mean intensity (a), duration (b) and cumulative rainfall (c) during 2006–2012.

5.2.2 Changes in *SWI* for the two types of rainfall condition

Fig. 5.4 shows hourly changes of *SWI* for the SH and LL rainfall types from the beginning of rainfall events to mass movement occurrences, based on the data for the years 2006–2012. Non-parametric median regressions were adopted to determine the general trends of *SWI* of these two types (SH and LL curves in Fig. 5.4). The SH type shows that *SWI* rises rapidly within 100 h of duration and exceeded 150 for more than 90% of events. This result shows that a rapid increase of soil water contents with short duration is responsible for mass movements initiation in the SH type.

SWI of the LL type gently rises to about 150 and tends to be stable during 100–300 h. Although the LL curve is not located at the high domain where mass movements are initiated, the temporal change of *SWI* for each event is large. Many events were associated with high values of *SWI*, which reveals that heavy rainfall also occurs during long-term rainfall. This raises soil water contents and causes mass movements. Therefore, gentle rise of *SWI* over a long duration from the beginning of a rainfall event, followed by heavy rainfall, is critical for mass movement initiation for the LL type.

The changes in *SWI* for the mass movements with very large positive first PC values significantly differ from those with very large negative first PC values, and are with the SH and LL general curves. In addition, 80% of the events of SH type occurred with durations shorter than 72 h and 80% of the events of LL type occurred with durations longer than 93 h. Therefore, the classification of the two types is generally acceptable. The remaining 20% of the events of each type belonged to the transitional zone of the two types, and allocation of one of the types was only operational. Further studies are needed to improve the classification methodology.

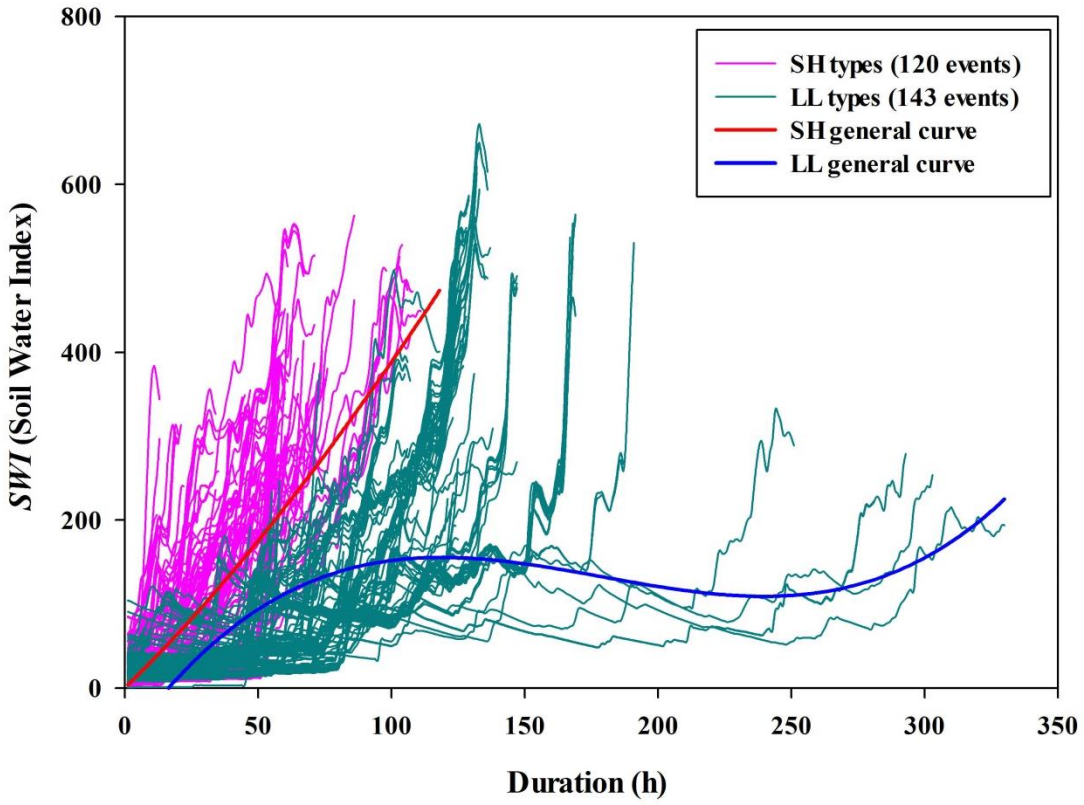

Fig. 5.4 Changes in *SWI* between two types of rainfall condition during 2006–2012.

5.2.3 Verification of inferences on *SWI*

The observations in Sections 5.2.1 and 5.2.2 based on data for 2006–2012 were tested by analyzing 19 rainfall-induced mass movements in 2013. The rainfall conditions of the 19 mass movements were classified into 14 SH types and 5 LL types (Fig. 4.6). Their *SWI* values before rainfall events and rainfall condition of mass movements were plotted (Fig. 5.5). Most of them correspond to the upper bound of rainfall conditions, confirming that *SWI* can be used as the indicator of antecedent conditions and to detect the upper bound of rainfall conditions for mass movements. The changes in *SWI* of the mass movements in 2013 also follow the trends of the predefined SH and LL curves (Fig. 5.6). These results verify the observations in Sections 5.2.1 and 5.2.2.

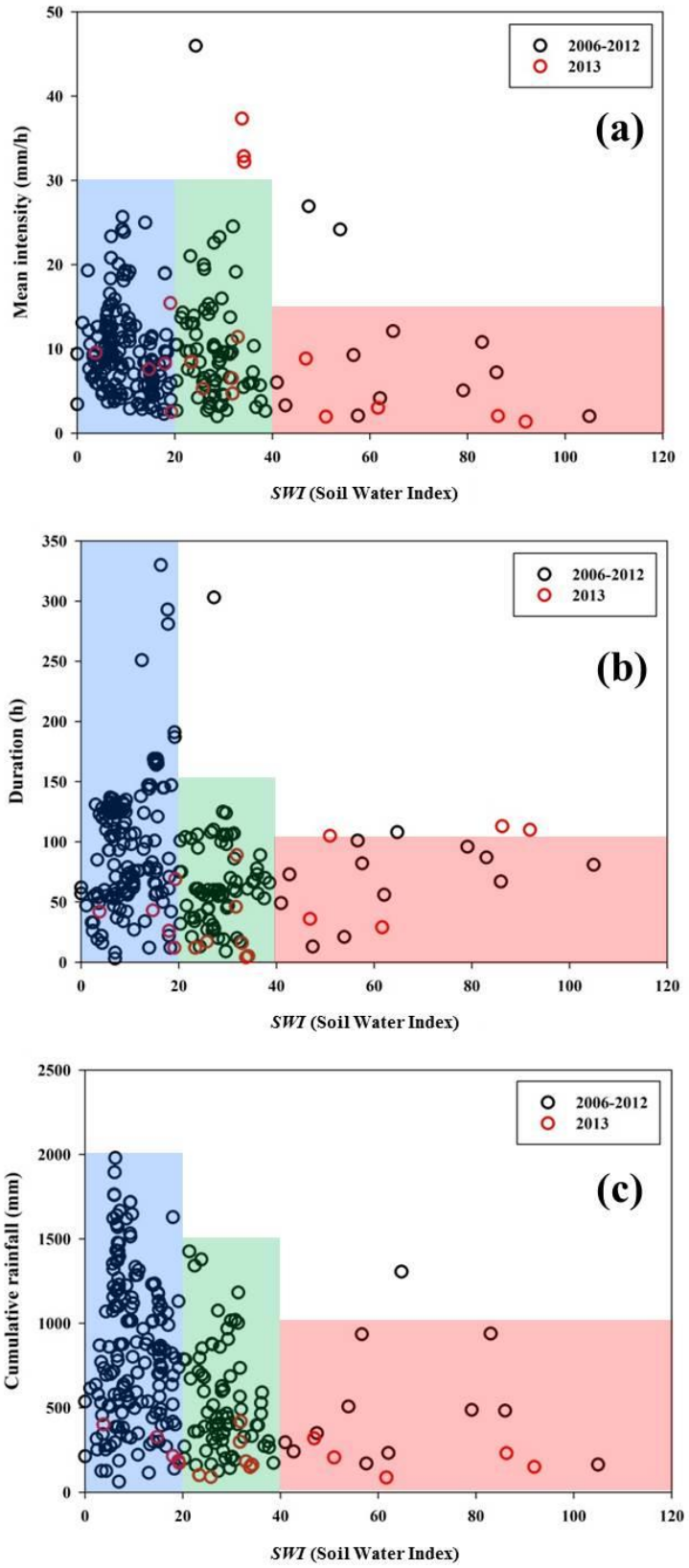

Fig. 5.5 Verification of the *SWI* analysis using data for 2013. (a) mean intensity, (b) duration, and (c) cumulative rainfall.

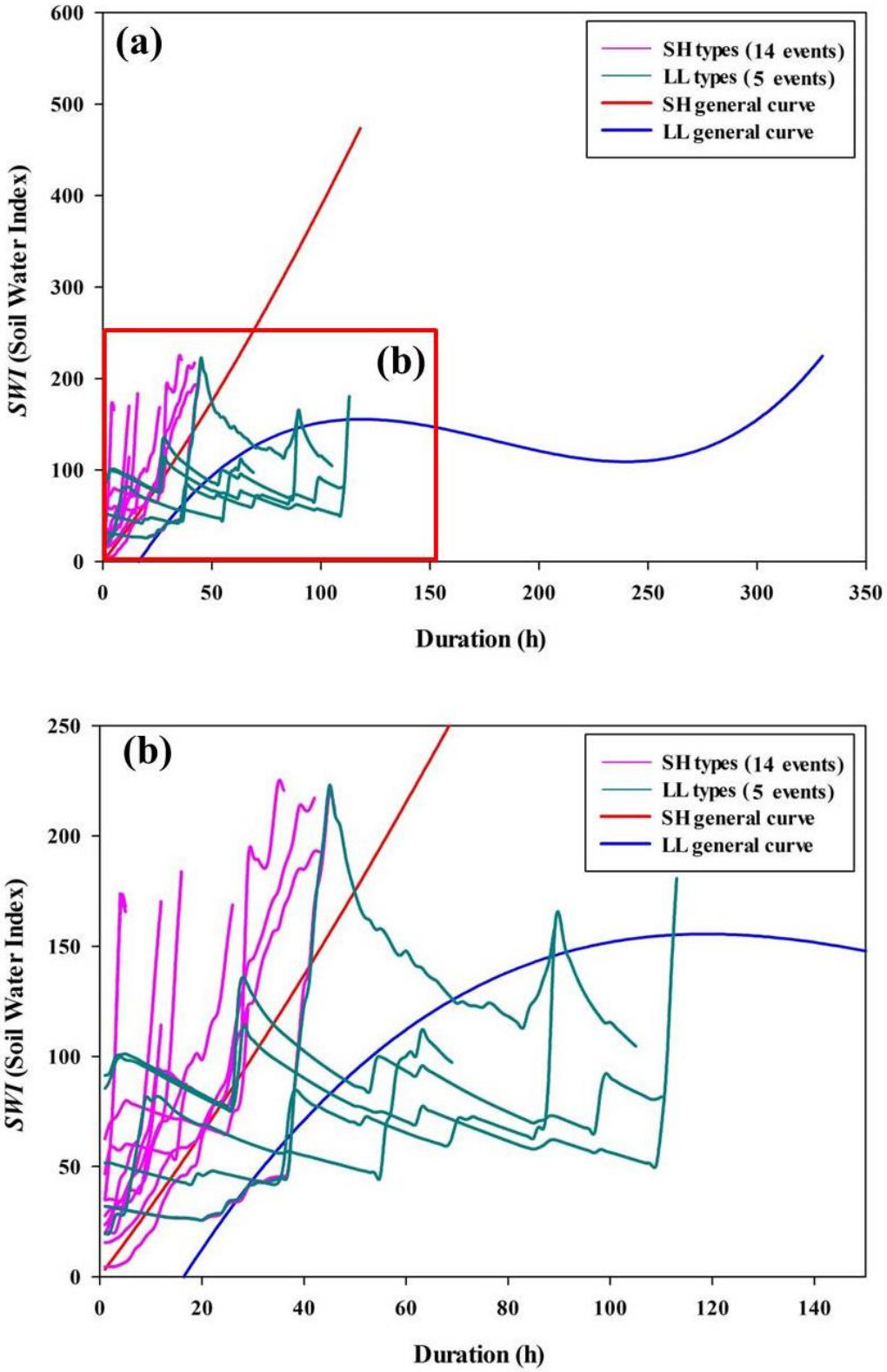

Fig. 5.6 Verification of the changing trends of *SWI* for the two types of rainfall conditions using data for 2013.

5.3 Contributions of the *I–D* threshold and *SWI* to mass movement warnings

Both *I–D* thresholds and *SWI* contribute to mass movement warnings. For the *I–D* threshold, once the rainfall conditions exceed the threshold, it can provide warnings of a potential mass movement hazard. *SWI* of the LL type often increased rapidly before mass movements (Fig. 5.4), which can also be used for warnings. This phenomenon cannot be found in the *I–D* threshold because the *I–D* plot represents average event rainfall and does not necessarily reflect sporadic high rainfall intensities. Thus, predicting the exact time of mass movements using only the *I–D* threshold is difficult. On the other hand, *SWI* is a long-term and dynamic index that reflects antecedent rainfall and temporal rainfall intensity variations. Therefore, *SWI* is suitable for real-time monitoring. However, effective usage of *SWI* may be sometimes difficult because it requires a more complex procedure than the *I–D* threshold including the early determination of the SH or LL type for each event. Therefore, the combined use of the *I–D* threshold and *SWI* is recommended to local authorities for making appropriate decisions to prevent mass movement hazards.

Chapter 6 Assessment of landslide magnitudes and sediment discharge in rivers

6.1 Landslide magnitudes

6.1.1 Landslide size and rainfall conditions

Fig. 6.1a shows rainfall conditions of landslides in which the circle size represents the size of landslide area. Large landslides tend to be associated with longer duration rainfalls. The landslides were classified into three groups with similar landslide numbers, according to the landslide area: 1) <9000 m^2, 2) 9000–24000 m^2, and 3) >24000 m^2. The three groups contain 58, 58, and 56 landslides, respectively. Fig. 6.1b shows the density of data distribution of these three groups: the data of group 1 are distributed very widely but with the increase of landslide area (groups 2 to 3), data distributions become more centralized at longer duration rainfalls. This phenomenon is consistent with some previous studies that deep and large slides usually occur only due to long-duration, moderate-intensity storms that provide a high ground water level, soil moisture, and pore water pressure; whereas, shallow and small slides that remove only soils over bedrock can occur even by short duration storms (Wieczorek, 1987; Larsen and Simon, 1993).

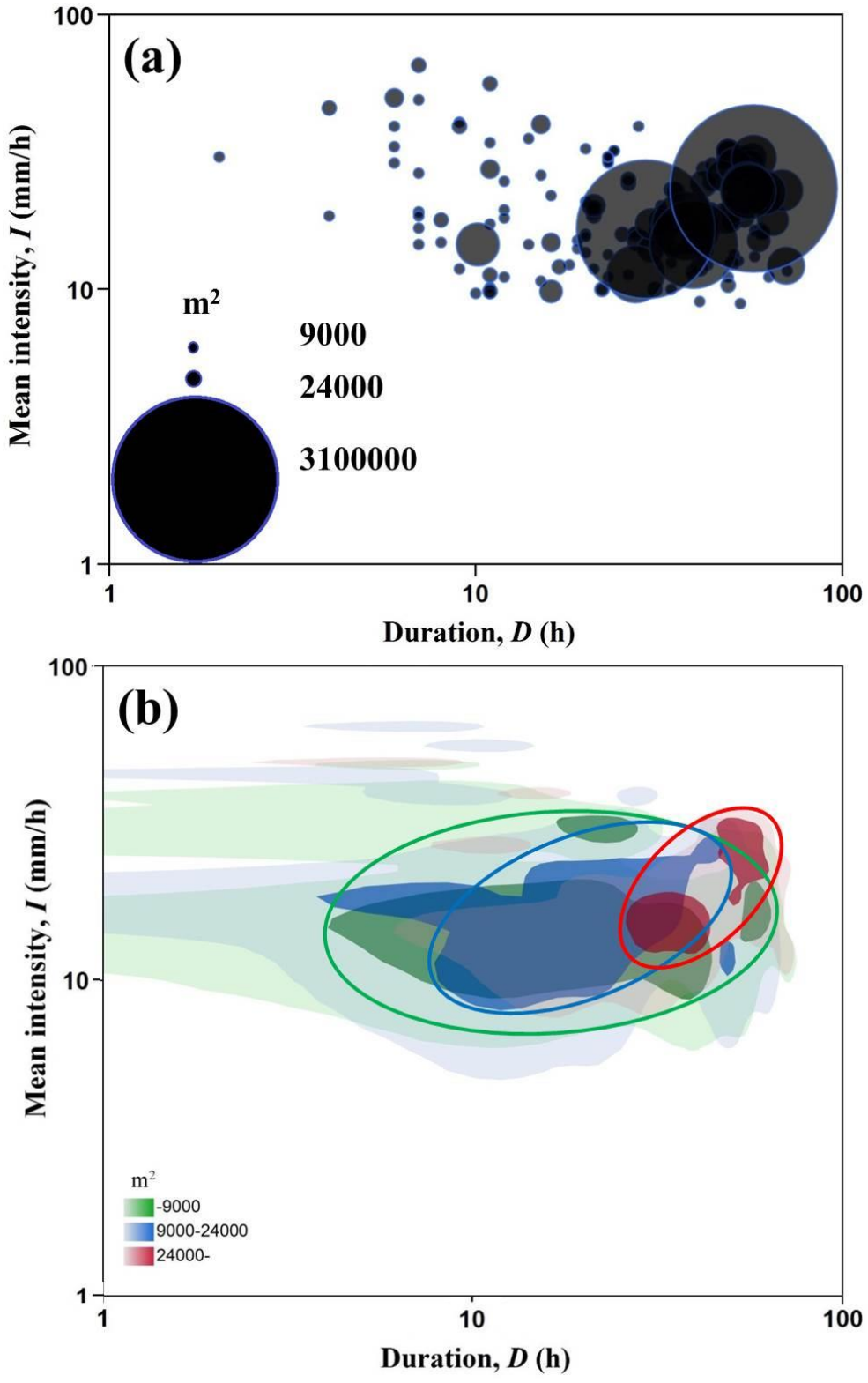

Fig. 6.1 Rainfall duration–intensity relationship for landslides during 2006–2012. (a) Landslide size and rainfall conditions. Circle size represents the size of landslide area. (b) Rainfall conditions for three groups of landslide area.

6.1.2 Frequency and area of landslides

Many previous studies have demonstrated that the frequency–area distribution correlates well with a power-law relation but only for medium to large landslides (Sugai et al., 1994; Hovius et al., 2000; Guzzetti et al., 2002; Malamud et al., 2004a,b). The distribution from medium to small landslides often shows a deviation from a power-law (so-called rollover) (Hovius et al., 2000; Guzzetti et al., 2002; Malamud et al., 2004a,b). However, in this study, the distribution only displayed the segment for medium to large landslides (6.3×10^2 m^2 < A_L < 3.1×10^6 m^2) without a significant rollover (Fig. 4.10). The SWCB may not have reported small-scale landslides because they focused on the landslides which caused disasters such as the damage of houses or roads.

Researchers have investigated the frequency–area relationship of landslides for different areas in the world. Fujii (1969) studied 800 landslides caused by various heavy rainfall events in Japan and found that the slope of the frequency–area distribution (γ) is 1.96. Hovius et al. (1997) obtained γ = 2.17 for 4984 landslides in the mountainous area along the Alpine fault in New Zealand. Hungr et al. (1999) dealt with 1937 rockfalls and rock slides along the main transportation route of southwestern British Columbia and found γ = 1.75 ± 0.30. Malamud and Turcotte (1999) noted that 1130 landslides in the Challana Valley, Bolivia yielded γ = 2.6; In the Akaishi Range, central Japan, 3243 landslides yielded γ = 3.0; and in the Eden Canyon, Alameda, USA, 709 landslides yielded γ = 3.3. Dai and Lee (2001) analyzed 2811 landsides in Hong Kong and found that γ is 2.2. Guzzetti et al. (2002) studied two data sets of landslides in central Italy and found that γ is 2.5. They then concluded that many landslide inventories satisfy γ = 2.5 ± 0.5.

However, in this study, γ for Taiwan is 1.1. Hovius et al. (2000) have studied

1040 landslides in the Ma-An and Wan-Li catchments, eastern Taiwan, and found that γ is 1.7. Both values for Taiwan are much lower than those in the other areas. The lower values for Taiwan indicate that if the same total area or total number of landslides occurred, the proportion of large landslides is higher in Taiwan. It may reflect high-relief topography, complex geology, high cumulative precipitation amounts and frequent heavy storms in Taiwan that lead to frequent deep and large landslides. The difference in γ between eastern Taiwan (Hovius et al., 2000) and the whole of Taiwan (this study) could be related to massive and intact metamorphic rocks in the former, which may lower the possibility of large landslides.

Table 6.1 Slope of landslide frequency–area distributions.

Reference	Area	Slope (γ)
This study	Taiwan	1.1
Hovius et al. (2000)	Eastern Taiwan	1.7
Fujii (1969)	Japan	1.96
Hovius et al. (1997)	New Zealand	2.17
Hungr et al. (1999)	British Columbia	1.75 ± 0.30
Malamud and Turcotte (1999)	Bolivia	2.6
	Central Japan	3.0
	USA	3.3
Dai and Lee (2001)	Hong Kong	2.2
Guzzetti et al. (2002)	Central Italy	2.5

6.1.3 Magnitude of landslide events

As noted, the magnitude scale of all studied landslide in Taiwan (m_L) during 2006–2012 is 6.4. We also picked up two major representative landslide events (Table 6.2). One was caused by Typhoon Morakot in 2009, including 73 landslides. The other was caused by Typhoon Megi in 2010, including 21 landslides. The average volume of landslides of these two events are 5.4×10^6 and 5.6×10^4, respectively, and the magnitude scale of landslide events are m_L = 6.7 and 4.8, respectively. Concerning their rainfall conditions, the mean intensity for the two events and 2006–2012 are almost the same: 21–23 mm/h. However, the rainfall duration and cumulative rainfall are quite different; both increases as m_L increase. This indicates that, under the same rainfall intensity, longer duration and greater cumulative rainfall will cause larger landslides, which sounds reasonable. Therefore, the magnitude scale can be used to assess the characteristics of past landslide events.

Table 6.2 Comparison of magnitude scale and rainfall conditions of two major events and all events during 2006–2012.

Event	2009 Typhoon Morakot (n = 73)	2010 Typhoon Megi (n = 21)	2006–2012 (n = 172)
Area (m^2)	1.4×10^5	1.0×10^4	7.0×10^4
Volume (m^3)	5.4×10^6	5.6×10^4	2.4×10^6
m_L	6.7	4.8	6.4
Mean intensity (mm/h)	21.7	22.7	20.9
Duration (h)	46.6	22.2	32.9
Cumulative rainfall (mm)	1020.5	501.2	663.8

6.2 Sediment discharge

6.2.1 Sediment discharge and rainfall conditions

According to sediment discharge of the 17 main rivers during the 15 typhoon events (Fig. 4.11–4.14), high sediment discharge during a typhoon event was usually accompanied with high cumulative rainfall and high average daily rainfall. Therefore, this study compared the sediment discharge with cumulative rainfall and average daily rainfall (Fig. 6.2). Except the Tachia River, all the main rivers presented a positive correlation between the sediment discharge and cumulative rainfall or average daily rainfall. When sediment discharge is compared with cumulative rainfall, the correlation (R^2 = 0.54 on average) is better than that with average daily rainfall (R^2 = 0.47 on average). This is because the sediment discharge is mainly controlled by

water discharge (Lin et al., 2011) and the total rainfall better reflects water discharge via the precipitation into rivers than a shorter daily rainfall.

Dadson et al. (2004) pointed out that suspended-sediment concentrations in rivers within ~40 km of the 1999 Chi-Chi earthquake were four times as much as the decadal background values even four years after the earthquake. Since the Tachia River is located near the epicenter, the unique relationships between sediment discharge and rainfall conditions for the river could be related to the effect of the Chi-Chi earthquake. However, some rivers closer to the epicenter than the Tachia River such as the Choshui River still showed positive correlations between sediment discharge and rainfall conditions. Therefore, further investigations are needed to fully understand the uniqueness of the Tachia River.

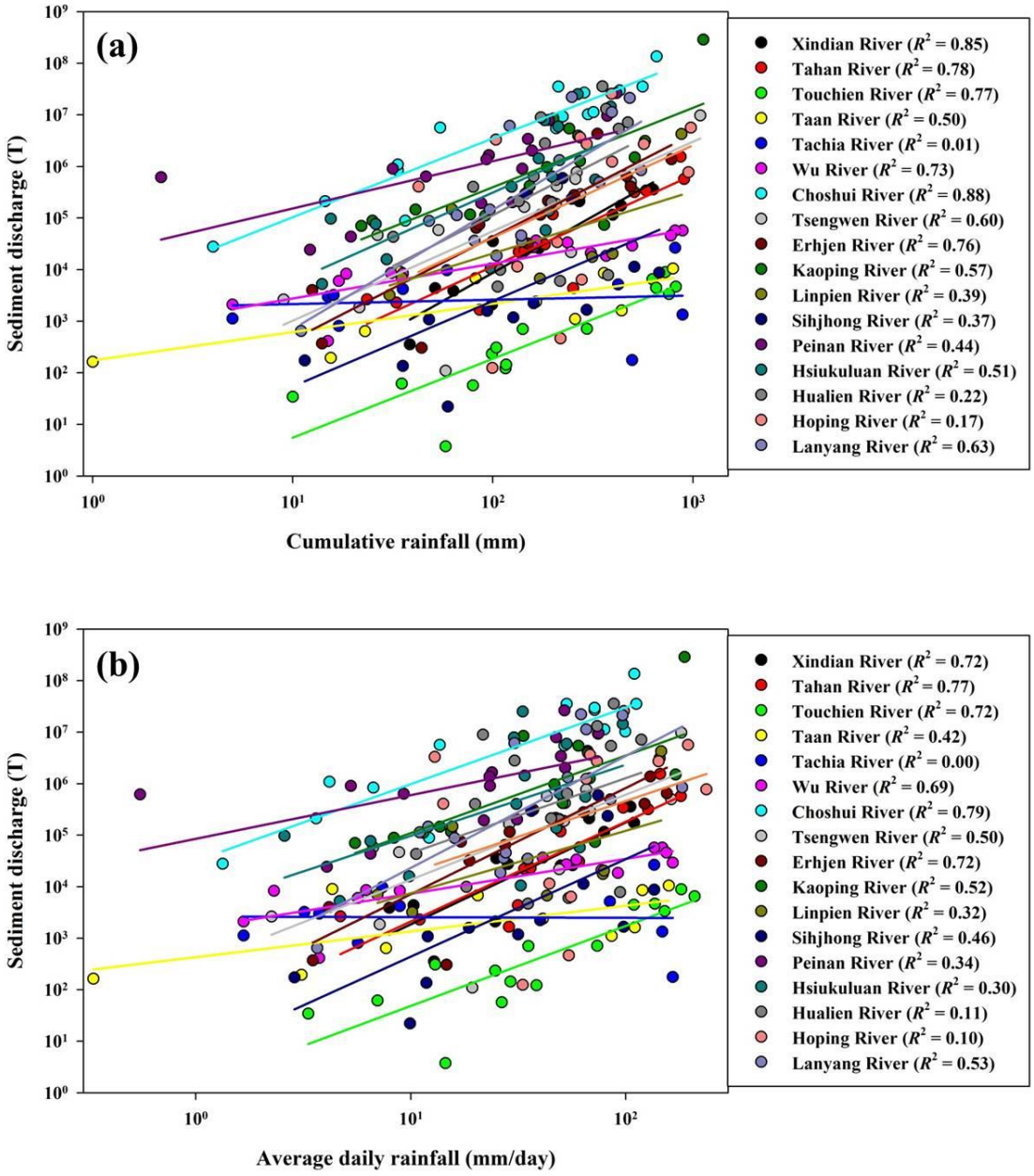

Fig. 6.2 Relationships between sediment discharge and rainfall conditions of the 17 main rivers. (a) Cumulative rainfall and (b) average daily rainfall

6.2.2 Characteristics of the sediment discharge between rivers

Table 6.3 summarizes the equation of the regression line for each river shown in Fig. 6.2a. The exponent of the regression line in the form of a power function is

related to the sensitivity of sediment discharge to river discharge. The large exponent means sediment discharge of the river will increase drastically when rainfall intensity increases. On the other hand, the coefficient of the regression line is related to the inherent ability to transport sediment of a river. In other words, the large coefficient means the river still has a high sediment discharge even under a relatively small amount of rainfall. Table 6.3 shows that the exponent and coefficient are quite different among the rivers. We then discuss reasons for these differences using the area and mean slope of river catchments. There are a positive correlation between the coefficient and catchment area, and a slight positive correlation between the coefficient and mean slopes (Fig. 6.3a,b). These results seem to be reasonable because a larger area and a steeper mean slope of a river catchment leads to more sediment yields. Fig. 6.4 shows the 17 river catchments in Taiwan with the distribution of average coastal suspended sediment flux estimated by Dadson et al. (2003). It appears that the high sediment flux is usually associated with the large catchments, confirming the above inference. In addition, the exponent and the coefficient are negatively correlated (Fig. 6.3c), indicating that a river catchment with relatively small sediment yields even starts to produce a lot of sediments when precipitation becomes intense. This mechanism seems to be one of reasons for the wide distribution of high sediment flux along the Taiwanese coasts as shown in Fig. 6.4.

Table 6.3 Regression equations for the relationship between sediment discharge and the cumulative rainfall for each river.

River	Equation
Xindian	$S_d = 19.7 \times E^{2.0}$
Tahan	$S_d = 24.5 \times E^{1.9}$
Touchien	$S_d = 0.2 \times E^{1.5}$
Taan	$S_d = 174.0 \times E^{0.5}$
Tachia	$S_d = 1776.1 \times E^{0.1}$
Wu	$S_d = 575.1 \times E^{0.7}$
Choshui	$S_d = 3106.2 \times E^{1.5}$
Tsengwen	$S_d = 19.0 \times E^{1.7}$
Erhjen	$S_d = 4.4 \times E^{2.0}$
Kaoping	$S_d = 335.0 \times E^{1.5}$
Linpien River	$S_d = 80.6 \times E^{1.2}$
Sihjhong	$S_d = 1.2 \times E^{1.7}$
Peinan	$S_d = 18653.0 \times E^{0.9}$
Hsiukuluan	$S_d = 109.8 \times E^{1.7}$
Hualien	$S_d = 12.4 \times E^{2.0}$
Hoping	$S_d = 11.2 \times E^{1.8}$
Lanyang	$S_d = 3.5 \times E^{2.3}$

S_d: sediment discharge; E: cumulative rainfall

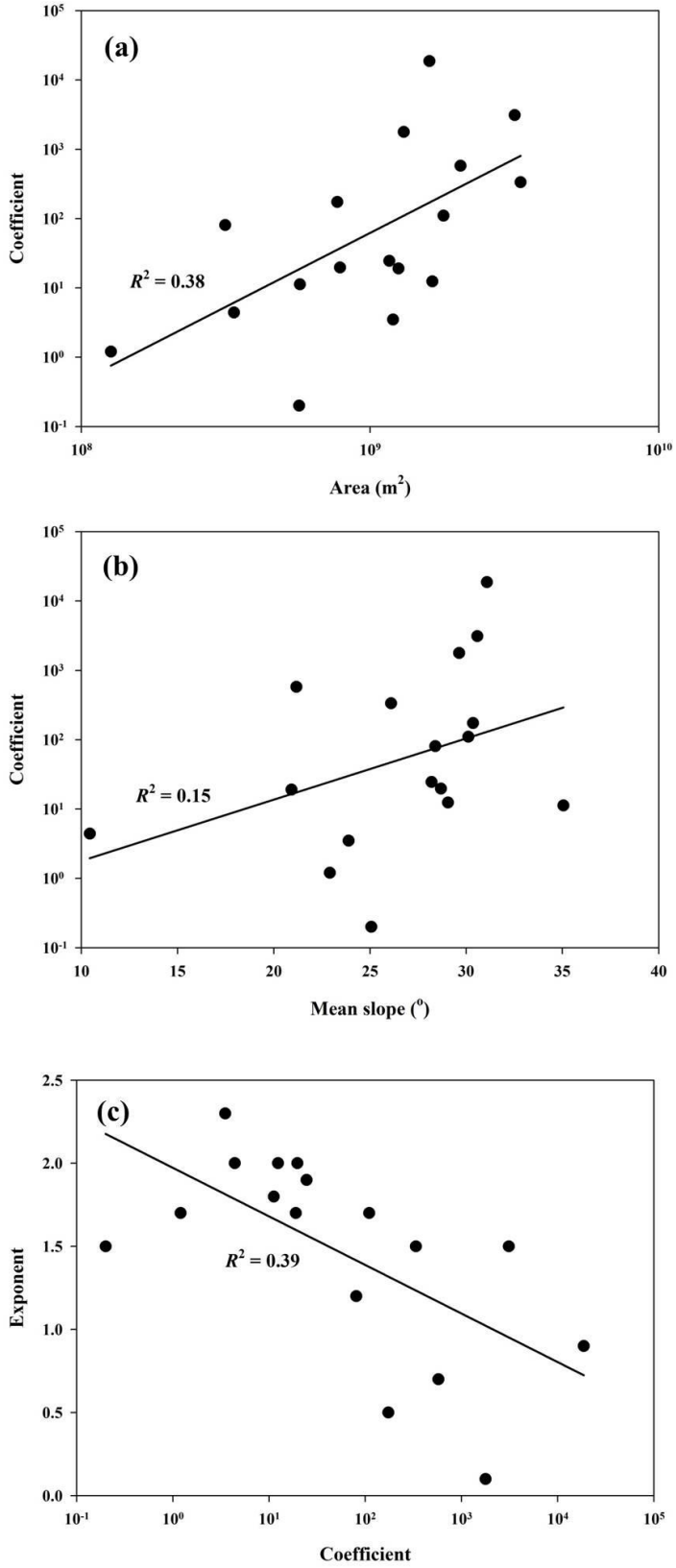

Fig. 6.3 Correlations between (a) coefficient and area, (b) coefficient and mean slope, and (c) exponent and coefficient of each river.

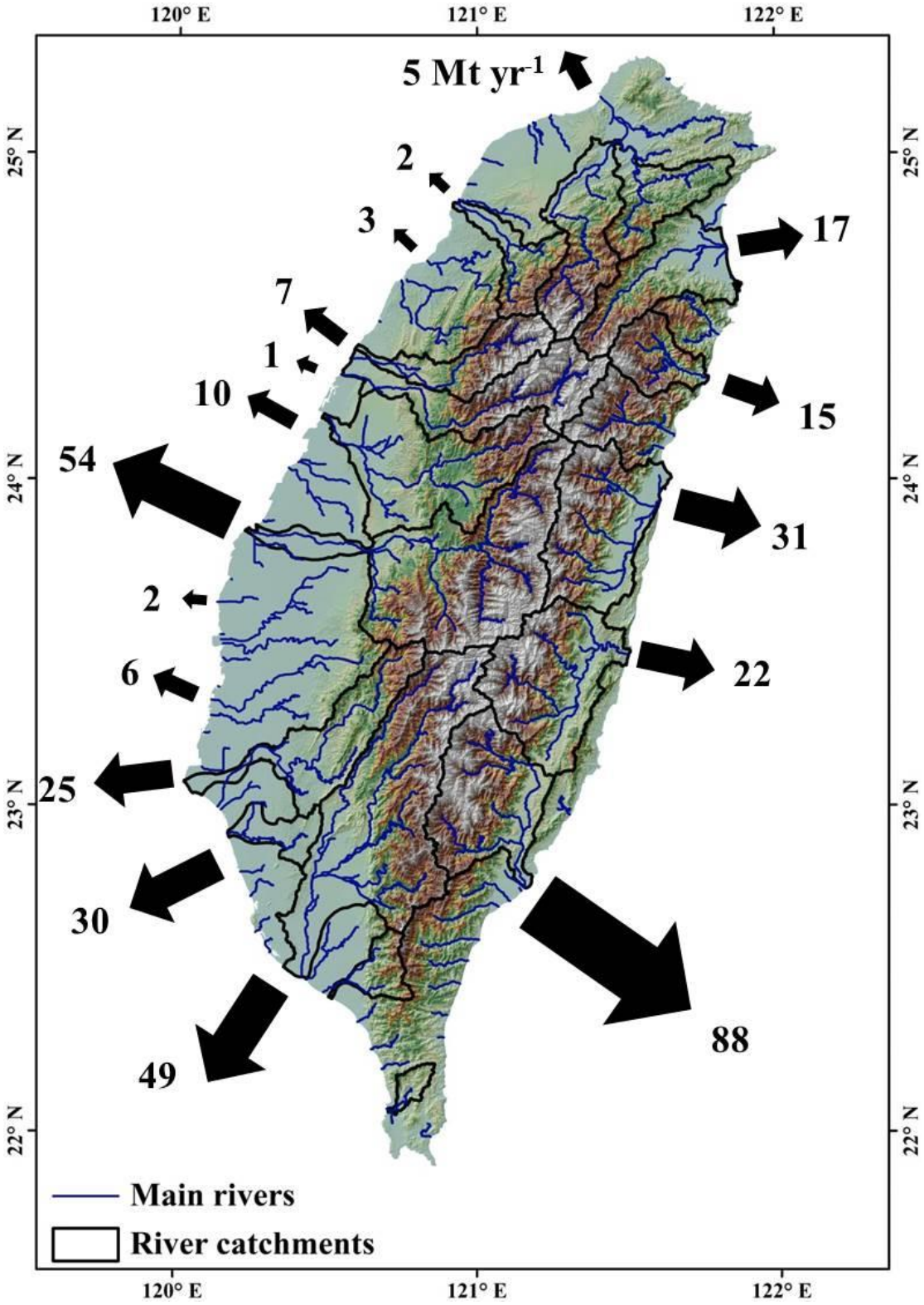

Fig. 6.4 The 17 major river catchments in Taiwan and the distribution of average annual coastal suspended sediment flux according to Dadson et al. (2003)

6.3 Effects of landslides debris on sediment discharge in rivers

To examine how landslide debris affects sediment discharge in rivers, we compared the average sediment discharge with the average area of landslides during the 14 typhoon events (Fig. 6.5). They are positively correlated with R^2 = 0.42. This indicates that when larger landslides are caused by heavier rainfall during a typhoon event, more loose materials from the latest landslide debris are flushed into rivers, resulting in higher sediment discharge. However, the correlation is not very high and is lower than that between sediment discharge and rainfall conditions described in Section 6.2.1. This means that the latest landslides caused by each of the 14 typhoon events do not constitute an only single source of sediment discharge; debris on slopes and river-bed materials that already existed before the event are also sources of sediment discharge. Previous studies in Taiwan also pointed out that some of landslide debris are not delivered to rivers during the single rainfall event that induced the landslides but are successively delivered to rivers by following heavy storms (Dadson et al., 2004; Lin et al., 2011).

However, it can also be said that a large amount of landslide debris is quickly transported into rivers in Taiwan. As noted, the proportion of large landslides is high in Taiwan. Dadson et al. (2004) indicated that, when the lowest point of a landslide reaches a location with the drainage area > 1 km^2, produced sediment are delivered to channels. This means debris of large landslides have higher opportunity to reach such locations and supply sediment to rivers. A reasonably good positive correlation shown in Fig. 6.5 reflects this mechanism.

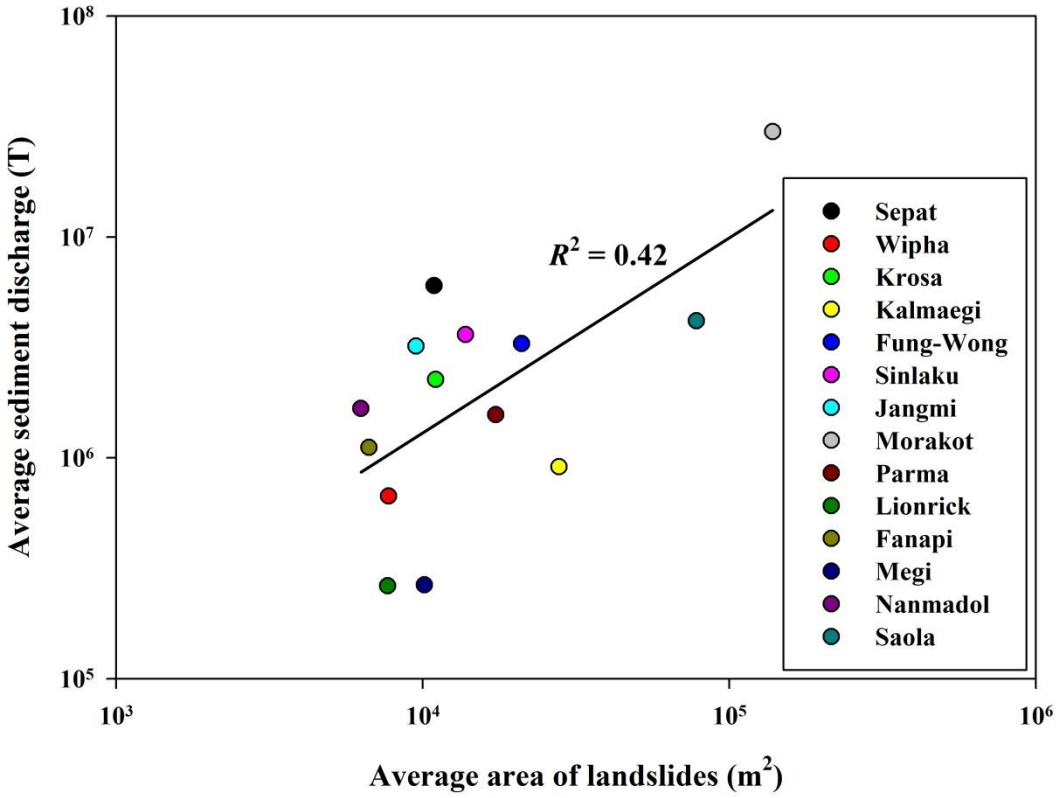

Fig. 6.5 Relationship between the average sediment discharge and the average area of landslides during each typhoon event.

Chapter 7 Conclusions

This study established empirical *I–D* thresholds for mass movements in Taiwan from data for landslides and debris flows, and these thresholds were compared with those for other areas in the world. For short duration rainfall events, higher mean rainfall intensities were required to trigger debris flows, while long duration rainfall events can trigger both landslides and debris flows with almost the same rainfall intensity. *I–D* thresholds for mass movements in Taiwan tended to be higher than those for other areas, but the rescaled I_{MAP}–*D* thresholds, which the rainfall intensity rescaled by a *MAP* of 3,000 mm, tended to be lower. These results reflect the rainfall characteristics of the region along with the topographic and geological conditions of Taiwan. This study has also demonstrated the importance of peak rainfall intensity in that most mass movements (74.9%) occurred within seven hours from the rainfall peak. Antecedent rainfall is also important in triggering such landslides from saturated hillslope material, whereas it is less important in triggering debris flows from material on the river bed. Other events that occurred significantly before or after the rainfall peak may be related to duration of rainfall and non-meteorological factors such as local topography and geology.

This study is the first to apply the *SWI* index to Taiwan which has been used by the Japan Meteorological Agency to assess mass movement hazards in Japan. For different values of *SWI* before rainfall events, the rainfall conditions needed for triggering mass movements, such as the rainfall intensity and duration, are different. When higher values of *SWI* are observed before rainfall events, the upper limit of rainfall conditions needed for triggering mass movements will be lower. Therefore, *SWI* can be used as the indicator of the antecedent rainfall condition. We classified

rainfall condition for triggering mass movements into two types, SH and LL, based on PCA. The two types performed differently in determining changes of *SWI*. The SH type is associated with a rapid increase of *SWI* within a short duration, and the LL type is with a gradual rise and subsequent constancy of *SWI*. Thus, a rapid increase of soil water contents with short duration is responsible for mass movement initiation in the SH type; while the gentle rise of *SWI* over a long duration, followed by heavy rainfall, is critical for mass movement initiation in the LL type. All the observations were successfully verified by analyzing 19 mass movements that occurred in 2013. Therefore, we recommend the use of *SWI* for real-time prediction of mass movements in Taiwan, to allow relevant authorities to establish a usable warning system. At the same time, *I–D* thresholds provide a widely applicable general guideline for mass movements. The use of both *SWI* and the *I–D* threshold seems to be useful to build a comprehensive warning system.

The areas of 172 landslides were mapped using FORMOSA–II images and their volumes and depths were estimated using an empirical formula. We found that deep landslides usually occurred due to long duration and moderate intensity rainfall, whereas shallow landslides occurred due to short duration and high intensity rainfall. Shallow landslides can occur even during a short rainfall event because flushing surface materials is easier; whereas deep landslides need a high groundwater level, soil moisture, and pore water pressure caused by a prolonged rainfall. The frequency–area correlation of the landslides is expressed by a power-law relation having an exponent of −1.1. This exponent value is lower than those for other areas around the world, indicating that the proportion of large landslides is exceptionally high in Taiwan. This may be because Taiwan is characterized by high-relief topography, complex geology, high cumulative precipitation amounts and frequent heavy storms. This study also proposed a landslide-event magnitude scale, and its average for all

landslides during 2006–2012 was estimated to be 6.4. We also found that the magnitude scale can be used to assess historical landslide events.

The sediment discharge of the 17 main rivers in Taiwan during 15 typhoon events was estimated using the rating-curve method. Positive correlations between sediment discharge and rainfall magnitudes for each river indicate that sediment discharge increased due to heavy rainfall during a typhoon event. The correlation is better when the sediment discharge is compared with the cumulative rainfall than the average daily rainfall, indicating that the amount of sediment discharge during a typhoon event is mainly controlled by total rainfall amount. The differences in correlation lines for different rivers clearly show that the catchments with larger areas and steeper slopes produce more sediment. However, the results also indicate that even catchments with relatively small sediment yields start to provide quite high sediment flux when rainfall intensity becomes higher.

A positive correlation between the average sediment discharge and the average area of landslides during typhoon events indicates that landslides caused during a typhoon event lead to higher sediment discharge. However, the relatively low correlation means that the landslides caused by the latest typhoon event do not constitute a single source of sediment discharge, and landslide debris staying on slopes since previous heavy storms and river-bed materials are also important sources of river sediment.

Further studies are necessary in various aspects such as building a more complete mass movement inventory for each typhoon event to enable detailed analyses on the *I–D* thresholds and *SWI*; performing multivariate analyses for geomorphological, geological and other environmental factors affecting mass movements along with rainfall characteristics to obtain a more comprehensive statistical model; and analyzing the effects of debris produced in different periods and stored in various

locations in a catchment using a sediment budget approach. Such trials will help us better understand how landslides are triggered and affect sediment discharge in rivers under the highly dynamic erosional condition of Taiwan.

Acknowledgement

I would like to express my special appreciation to my advisor Prof. TAKASHI OGUCHI, the Center for Spatial Information Science, The University of Tokyo. I would like to thank him for encouraging my research and for allowing me to grow as a research scientist. His advice on both research as well as on my career have been priceless. Besides my advisor, I would like to thank the rest of my thesis committee: Prof. KAORU SAITO, Prof. TOMOCHIKA TOKUNAGA, Prof. TOSHIHIKO SUGAI, and Prof. YUICHI S. HAYAKAWA, the University of Tokyo, for their insightful comments that broaden my research from various perspectives. I would also like to thank Dr. HITOSHI SAITO, the College of Economics, Kanto Gakuin University for his technical support with data analysis and scientific advices. I would also like to thank Prof. YUICHI S. HAYAKAWA, the Center for Spatial Information Science, The University of Tokyo for his various supports including a solution to my financial difficulty.

Special thanks also go to my family. Words cannot express how grateful I am to my mother, father, brother, and sister for all of the sacrifices that made on my behalf. Their prayer has been supporting me. I would also like to thank all of my friends and colleagues including the members of the laboratory of Dr. OGUCHI, who supported me at various stages of producing this thesis including data collection, data analyses and writing drafts. Finally I would like express my sincere appreciation to my beloved girlfriend AI-TI who spent sleepless nights with me and was always my support in the moments when there was no one else to answer my queries.

References

Aleotti P (2004) A warning system for rainfall-induced shallow failures. Engineering Geology 73:247–265

Aleotti P, Chowdhury R (1999) Landslide hazard assessment: summary review and new perspectives. Bulletin of Engineering Geology and the Environment 58:21–44

Ayalew L, Yamagishi H (2005) The application of GIS-based logistic regression for landslide susceptibility mapping in the Kakuda–Yahiko Mountains, Central Japan. Geomorphology 65:15–31

Bacchini M, Zannoni A (2003) Relations between rainfall and triggering of debris-flow: case study of Cancia (Dolomites, Northeastern Italy). Natural Hazards and Earth System Sciences 3:71–79

Berti M, Genevois R, Simoni A, Tecca PR (1999) Field observations of a debris flow event in the Dolomites. Geomorphology 29:265–274

Bishop AW (1955) The use of the slip circle in the stability analysis of slopes. Geotechnique 5:7–17

Bou Kheir R, Chorowicz J, Abdallah C, Dhont D (2008) Soil and bedrock distribution estimated from gully form and frequency: a GIS-based decision-tree model for Lebanon. Geomorphology 93:482–492

Brunetti MT, Peruccacci S, Rossi M, Luciani S, Valigi D, Guzzetti F (2010) Rainfall thresholds for the possible occurrence of landslides in Italy. Nat. Hazards Earth Syst. Sci 10:447–458

Caine N (1980) The rainfall intensity–duration control of shallow landslides and debris flows. Geografiska Annaler. Series A. Physical Geography 62:23–27

Cannon S (1988) Regional rainfall–threshold conditions for abundant debris-flow

activity. In: Ellen SD, Wieczorek GF (eds) Landslides, floods, and marine effects of the storm of January 3–5, 1982, in the San Francisco Bay Region, California: US Geological Survey Professional Paper, vol. 1434, pp. 35–42

Cannon S, Gartner J, Wilson R, Bowers J, Laber J (2008) Storm rainfall conditions for floods and debris flows from recently burned areas in southwestern Colorado and southern California. Geomorphology 96:250–269

Chang CW, Lin PS, Tsai CL (2011) Estimation of sediment volume of debris flow caused by extreme rainfall in Taiwan. Engineering Geology 123:83–90

Chang FJ, Chiang YM, Lee WS (2009) Investigating the impact of the Chi-Chi earthquake on the occurrence of debris flows using artificial neural networks. Hydrol. Process 23:2728–2736

Chang JC, Slaymaker O (2002) Frequency and spatial distribution of landslides in a mountainous drainage basin: Western Foothills, Taiwan. Catena 46:285–307

Chang K, Chiang S (2009) An integrated model for predicting rainfall-induced landslides. Geomorphology 105:366–373

Chang TC, Chao RJ (2006) Application of back-propagation networks in debris flow prediction. Engineering Geology 85:270–280

Chen H, Chen RH, Lin ML (1999) Initiative anatomy of Tungmen debris flow, eastern Taiwan. Environmental and Engineering Geoscience 5:459–473

Chen H, Su DI (2001) Geological factors for hazardous debris flow in Hoser, central Taiwan. Environmental Geology 40:1114–1124

Chen JC (2011) Variability of impact of earthquake on debris-flow triggering conditions: case study of Chen-Yu-Lan watershed, Taiwan. Environmental Earth Sciences 64:1787–1794

Cheng JD, Huang YC, Wu HL, Yeh JL, Chang CH (2005) Hydrometeorological and landuse attributes of debris flows and debris floods during typhoon Toraji, July

29–30, 2001 in central Taiwan. Journal of Hydrology 306:161–173

Chien-Yuan C, Tien-Chien C, Fan-Chieh Y, Wen-Hui Y, Chun-Chieh T (2005) Rainfall duration and debris-flow initiated studies for real-time monitoring. Environmental Geology 47:715–724

Chuang SC, Chen H, Lin GW, Lin CW, Chang CP (2009) Increase in basin sediment yield from landslides in storms following major seismic disturbance. Engineering Geology 103:59–65

Claessens L, Knapen A, Kitutu MG, Poesen J, Deckers JA (2007) Modelling landslide hazard, soil redistribution and sediment yield of landslides on the Ugandan footslopes of Mount Elgon. Geomorphology 90:23–35

Clague JJ, Evans SG (2003) Geologic framework of large historic landslides in Thompson River Valley, British Columbia. Environmental & Engineering Geoscience 9:201–212

Coe J, Kinner D, Godt J (2008) Initiation conditions for debris flows generated by runoff at Chalk Cliffs, central Colorado. Geomorphology 96:270–297

Cohn TA (1995) Recent advances in statistical methods for the estimation of sediment and nutrient transport in rivers. Reviews of Geophysics 33:1–18

Crosta G (1998) Regionalization of rainfall thresholds: an aid to landslide hazard evalution. Environmental Geology 35:131–145

Crozier MJ (1999) Prediction of rainfall-triggered landslides: a test of the antecedent water status model. Earth Surface Processes and Landforms 24:825–833

Dadson SJ, Hovius N, Chen H, Dade WB, Hsieh ML, Willett SD, Hu JC, Horng MJ, Chen MC, Stark CP, Lague D, Lin JC (2003) Links between erosion, runoff variability and seismicity in the Taiwan orogeny. Nature 426:648–651

Dadson SJ, Hovius N, Chen H, Dade WB, Lin JC, Hsu ML, Lin CW, Horng MJ, Chen TC, Milliman J, Stark CP (2004) Earthquake-triggered increase in sediment

delivery from an active mountain belt. Geology 32:733–736

Dadson S, Hovius N, Pegg S, Dade WB, Horng MJ, Chen H (2005) Hyperpycnal river flows from an active mountain belt. Journal of Geophysical Research 110:F04016

Dahal R, Hasegawa S (2008) Representative rainfall thresholds for landslides in the Nepal Himalaya. Geomorphology 100:429–443

Dai FC, Lee CF (2001) Frequency-volume relation and prediction of rainfall-induced landslides. Engineering Geology 59:253–266

Dai FC, Lee CF (2002) Landslide characteristics and slope instability modeling using GIS, Lantau Island, Hong Kong. Geomorphology 42:213–228

Dai FC, Lee CF, Ngai YY (2002) Landslide risk assessment and management and management–an overview. Engineering Geology 64: 65–87

Dietrich WE, Reiss R, Hsu ML, Montgomery DR (1995) A process-based model for colluvial soil depth and shallow landsliding using digital elevation data. Hydrological Processes 9:383–400

Dou J, Oguchi T, Hayakawa YS, Uchiyama S, Saito H, Paudel U (2014) GIS-based landslide susceptibility mapping using a certainty factor model and its validation in the Chuetsu area, central Japan. Landslide Science for a Safer Geoenvironment, Springer International Publishing:419–424

Fellenius W (1927) Erdstatische Berechnungen mit Reibung and Kohasion. Ernst, Berlin

Finlay PJ, Fell R, Maguire PK (1997) The relationship between the probability of landslide occurrence and rainfall. Canadian Geotechnical Journal 34: 811–824

Fujii Y (1969) Frequency distribution of landslides caused by heavy rainfall. Journal Seismological Society Japan 22: 244–247

Fuller CW, Willett SD, Hovius N, Slingerland R (2003) Erosion rates for Taiwan

mountain basins: new determinations from suspended sediment records and a stochastic model of their temporal variation. The Journal of Geology 11: 71–87

Glade T (1997) The temporal and spatial occurrence of rainstorm-triggered landslide events in New Zealand. Dissertation, Victoria University of Wellington

Glade T, Crozier M, Smith P (2000) Applying probability determination to refine landslide-triggering rainfall thresholds using an empirical "antecedent daily rainfall model". Pure and Applied Geophysics 157:1059–1079

Guzzetti F, Ardizzone F, Cardinali M, Rossi M, Valigi D (2009) Landslide volumes and landslide mobilization rates in Umbria, central Italy. Earth and Planetary Science Letters 279:222–229

Guzzetti F, Carrara A, Cardinali M, Reichenbach P (1999) Landslide hazard evaluation: a review of current techniques and their application in a multi-scale study, central Italy. Geomorphology 31:181–216

Guzzetti F, Malamud BD, Turcotte DL, Reichenbach P (2002) Power-law correlations of landslide areas in central Italy. Earth and Planetary Science Letters 195:169–183

Guzzetti F, Peruccacci S, Rossi M, Stark C (2007) Rainfall thresholds for the initiation of landslides in central and southern Europe. Meteorology and Atmospheric Physics 98:239–267

Guzzetti F, Peruccacci S, Rossi M, Stark C (2008) The rainfall intensity–duration control of shallow landslides and debris flows: an update. Landslides 5:3–17

Guzzetti F, Reichenbach P, Cardinali M, Galli M, Ardizzone F (2005) Probabilistic landslide hazard assessment at the basin scale. Geomorphology 72:272–299

Guzzetti F, Reichenbach P, Ardizzone F, Cardinali M, Galli M (2006) Estimating the quality of landslide susceptibility models. Geomorphology 81:166–184

Ho CS (1986) A synthesis of the geologic evolution of Taiwan. Tectonophysics 125:1–16

Ho CS (1988) An introduction to the geology of Taiwan, explanatory text of the geologic map of Taiwan. Central Geological Survey, the Ministry of Economic Affairs, Taipei, Taiwan

Hong Y, Hiura H, Shino K, Sassa K, Suemine A, Fukuoka H, Wang G (2005) The influence of intense rainfall on the activity of large-scale crystalline schist landslides in Shikoku Island, Japan. Landslides 2:97–105

Hovius N, Stark CP, Allen PA (1997) Sediment flux from a mountain belt derived by landslide mapping. Geology 25:231–234

Hovius N, Stark CP, Hao-Tsu C, Jiun-Chuan L (2000) Supply and removal of sediment in a landslide-dominated mountain belt: Central Range, Taiwan. The Journal of Geology 108:73–89

Hungr O, Evans SG, Hazzard J (1999) Magnitude and frequency of rock falls and rock slides along the main transportation corridors of southwestern British Columbia. Canadian Geotechnical Journal 36: 224–238

Ishihara Y, Kobatake S (1979) Runoff model for flood forecasting. Bulletin of Disaster Prevention Research Institute, Kyoto University 29:27–43

Iverson RM (2000) Landslide triggering by rain infiltration. Water Resources Research 36:1897–1910

Iverson RM, Reid ME, LaHusen RG (1997) Debris-flow mobilization from landslides. Annual Review of Earth and Planetary Sciences 25:85–138

Jakob M (2006) Hydrometeorological thresholds for landslide initiation and forest operation shutdowns on the north coast of British Columbia. Landslides 3:228–238

Jakob M, Weatherly H (2003) A hydroclimatic threshold for landslide initiation on the

North Shore Mountains of Vancouver, British Columbia. Geomorphology 54:137–156

Jan CD, Chen CL (2005) Debris flows caused by typhoon Herb in Taiwan. In: Jakob M, Hungr O (eds) Debris flow hazards and related phenomena, Berlin Heidelberg, Springer, pp 539–563

Janbu N, Bjerrum L, Kjaernsli B (1956) Stabilitestsbere Bning for Fyllinger Skjaeringer Ognaturlige Skraninger. Norwegian Geotechnical Publication, vol. 16, Norway, Oslo

Jiang X, Qiao J, Wang C, Zhao Y (2006) Computer simulation of landslides by the contact element method. Computers and Geosciences 32:434–441

Jibson R (1989) Debris flow in southern Puerto Rico. Geological Society of America, Special Paper, vol. 236, pp. 29–55

Keefer DK (1984) Landslides caused by earthquakes. Geological Society of America Bulletin 95:406–421

Keefer DK (2000) Statistical analysis of an earthquake-induced landslide distribution—the 1989 Loma Prieta, California event. Engineering Geology 58:231–249

Keefer DK, Wilson R, Mark R, Brabb E, Brown W, Ellen S, Harp E, Wieczorek G, Alger C, Zatkin R (1987) Real-time landslide warning during heavy rainfall. Science 238:921–925

Kim SK, Hong WP, Kim YM (1992) Prediction of rainfall-triggered landslides in Korea. In: Bell DH (ed) Landslides, Proceedings of the Sixth International Symposium on Landslides, Christchurch, 10–14 February 1992, v. 2, Balkema, Rotterdam, pp 989–994

Kirschbaum D, Adler R, Adler D, Peters-Lidard C, Huffman G (2012) Global distribution of extreme precipitation and high-impact landslides in 2010

relative to previous years. Journal of Hydrometeorology 13:1536–1551

Komac M (2006) A landslide susceptibility model using the analytical hierarchy process method and multivariate statistics in perialpine Slovenia. Geomorphology 74:17–28

Korup O, Gorum T, Hayakawa Y (2012) Without power? Landslide inventories in the face of climate change. Earth Surface Processes and Landforms 37:92–99

Larsen M, Simon A (1993) A rainfall intensity–duration threshold for landslides in a humid-tropical environment: Puerto Rico. Geografiska Annaler. Series A. Physical Geography 75:13–23

Lee S (2007) Landslide susceptibility mapping using an artificial neural network in the Gangneung area, Korea. International Journal of Remote Sensing 28:4763–4783

Lee S, Choi J (2004) Landslide susceptibility mapping using GIS and the weight-of-evidence model. International Journal of Geographical Information Science 18:789–814

Lee S, Lee M (2006) Detecting landslide location using KOMPSAT 1 and its application to landslide-susceptibility mapping at the Gangneung area, Korea. Advances in Space Research 38:2261–2271

Lee S, Ryu J, Kim I (2007) Landslide susceptibility analysis and its verification using likelihood ratio, logistic regression, and artificial neural network models: case study of Youngin, Korea. Landslides 4:327–338

Li YH (1976) Denudation of Taiwan island since the Pliocene epoch. Geology 4:105–107

Lin CW, Shieh CL, Yuan BD, Shieh YC, Liu SH, Lee SY (2003) Impact of Chi-Chi earthquake on the occurrence of landslides and debris flows: example from the Chenyulan River watershed, Nantou, Taiwan. Engineering Geology 71:49–61

Lin GW, Chen H, Chen YH, Horng MJ (2008) Influence of typhoons and earthquakes on rainfall-induced landslides and suspended sediments discharge. Engineering Geology 97:32–41

Lin GW, Chen H, Petley DN, Horng MJ, We SJ, Chuang B (2011) Impact of rainstorm-triggered landslides on high turbidity in a mountain reservoir. Engineering Geology 117:97–103

Lin GW, Chen H (2012) The relationship of rainfall energy with landslides and sediment delivery. Engineering Geology 125:108–118

Lin Z, Oguchi T, Chen YG, Saito K (2009) Constant-slope alluvial fans and source basins in Taiwan. Geology 37:787–790

Lumb P (1975) Slope failures in Hong Kong. Quarterly Journal of Engineering Geology and Hydrogeology 8:31–65

Malamud BD, Turcotte DL (1999) Self-organized criticality applied to natural hazards. Natural Hazards 20:93–116

Malamud BD, Turcotte DL, Guzzetti F, Reichenbach P (2004a) Landslide inventories and their statistical properties. Earth Surface Processes and Landforms 29:687–711

Malamud BD, Turcotte DL, Guzzetti F, Reichenbach P (2004b) Landslides, earthquakes, and erosion. Earth and Planetary Science Letters 229:45–59

Melchiorre C, Matteucci M, Azzoni A, Zanchi A (2008) Artificial neural networks and cluster analysis in landslide susceptibility zonation. Geomorphology 94:379–400

Morgenstem NR, Price VE (1965) The analysis of the stability of general slip surface. Geotechnique 15:79–93

Okada K (2007) Current State of Disaster Generation Risk Forecast by SOIL WATER INDEX. Tsuchi-to-kiso 55:4–6

Okada K, Makihara Y, Shimpo A, Nagata K, Kunitsugu M, Saito K (2001) Soil Water Index. Tenki 47:36–41

Omura H (1980) Fundamental study on forecasting of landslide area (I) – relation between total precipitation, resistance index and landslide area ratio –. Journal of the Japan Society of Erosion Control Engineering 33:15–25 (in Japanese with English abstract)

Omura H (1982) Forecast method of landslide area ratio by gamma distribution model. Journal of the Japan Society of Erosion Control Engineering 35:31–37 (in Japanese with English abstract)

Onodera T, Yoshinaka R, Kazama H (1974) Slope failures caused by heavy rainfall in Japan. Proc. 2nd Int. Congress of the Int Ass Eng Geol, v. 11, San Paulo 11, pp 1–10

Osanai N, Shimizu T, Kuramoto K, Kojima S, Noro T (2010) Japanese early-warning for debris flows and slope failures using rainfall indices with Radial Basis Function Network. Landslides 7:325–338

Pal M, Mather P (2003) An assessment of the effectiveness of decision tree methods for land cover classification. Remote Sensing of Environment 86:554–565

Petley D (2012) Global patterns of loss of life from landslides. Geology 40:927–930

Saito H, Korup O, Uchida T, Hayashi S, Oguchi T (2014) Rainfall conditions, typhoon frequency, and contemporary landslide erosion in Japan. Geology 42:999–1002

Saito H, Matsuyama H (2012) Catastrophic landslide disasters triggered by record-breaking rainfall in Japan: their accurate detection with normalized soil water index. SOLA 8:81–84

Saito H, Nakayama D, Matsuyama H (2009) Comparison of landslide susceptibility based on a decision-tree model and actual landslide occurrence: the Akaishi

Mountains, Japan. Geomorphology 109:108–121

Saito H, Nakayama D, Matsuyama H (2010a) Relationship between the initiation of a shallow landslide and rainfall intensity–duration thresholds in Japan. Geomorphology 118:167–175

Saito H, Nakayama D, Matsuyama H (2010b) Two types of rainfall conditions associated with shallow landslide initiation in Japan as revealed by Normalized Soil Water Index. SOLA 6:57–60

Salvucci GD, Entekabi D (1994) Explicit expressions for Green-Ampt (Delta function diffusivity) infiltration rate and cumulative storage. Water Resources Research 30:2661–2663

Sassa K (2005) Landslide disasters triggered by the 2004 Mid-Niigata Prefecture earthquake in Japan. Landslides 2:135–142

Schneevoigt N, van der Linden S, Thamm H, Schrott L (2008) Detecting Alpine landforms from remotely sensed imagery. A pilot study in the Bavarian Alps. Geomorphology 93:104–119

Schumm SA (1973) Geomorphic thresholds and the complex response of drainage systems. Fluvial Geomorphology 6:69–85

Shieh CL, Chen YS, Tsai YJ, Wu JH (2009) Variability in rainfall threshold for debris flow after the Chi-Chi Earthquake in central Taiwan, China. International Journal of Sediment Research 24:177–188

Shieh SL (2000) User's Guide for Typhoon Forecasting in the Taiwan Area (VIII). Central Weather Bureau, Taipei

Sidle CR (1992) A theoretical model of the effects of timber harvesting on slope stability. Water Resources Research 28:1897–1910

Sitar N, Anderson SA, Johnson KA (1992) Conditions leading to the initiation of rainfall-induced debris flows. Geotech. Engrg. Div. Specialty Conf.: Stability

and Perf. of Slopes and Embankments-II, ASCE, New York, N. Y., 834–839

Spencer E (1967) A method of analysis of the stability of embankments assuming parallel inter-slice forces. Geotechnique 12:11–26

Sugai T, Ohmori H, Hirano M (1994) Rock control on magnitude–frequency distribution of landslides. Transactions Japanese Geomorphological Union 15:233-251

Sugawara M, Ozaki E, Watanabe I, Katsuyama Y (1974) Tank model and its application to Bird Creek, Wollombi Brook, Bikin River, Kitsu River, Sanaga River and Namr Mune. Research Note of the National Research Center for Disaster Preventions 11:1–64

Teng LS (1990) Geotectonic evolution of late Cenozoic arc-continent collision in Taiwan. Tectonophysics 183:57–76

Terlien MT (1998) The determination of statistical and deterministic hydrological landslide-triggering thresholds. Environmental Geology 35:124–130

Walling DE (1977) Assessing the accuracy of suspended sediment raring curves for a small basin. Water Resources Research 13:531–538

Wang B, Ho L (2002) Rainy season of the Asian-Pacific summer monsoon. Journal of Climate 15:386–398

Wieczorek GF (1987) Effect of rainfall intensity and duration on debris flows in central Santa Cruz Mountains, California. Reviews in Engineering Geology 7:93–104

Wieczorek GF, Glade T (2005) Climatic factors influencing occurrence of debris flows. In Jakob M, Hunger O (eds) Debris-flow Hazards and Related Phenomena. Berlin, Springer-Verlag, pp 325–362

Wieczorek GF, Morgan BA, Campbell RH (2000) Debris-flow hazards in the Blue Ridge of central Virginia. Environmental & Engineering Geoscience 6:3–23

Willett SD, Fisher D, Fuller C, Yeh EC, Lu CY (2003) Erosion rates and orogenic wedge kinematics in Taiwan inferred from apatite fission track thermochronometry. Geology 31:945–948

Wilson RC (1989) Rainstorms, pore pressures, and debris flows: a theoretical framework. Landslides in semi-arid environment. Inland Geological Society, Riverside:101–117

Wilson RC, Wieczorek GF (1995) Rainfall thresholds for the initiation of debris flow at La Honda, California. Environmental & Engineering Geoscience 1:11–27

Wu CC, Kuo YH (1999) Typhoons affecting Taiwan: Current understanding and future challenges. American Meteorological Society Bulletin 80:67–80

Wu CH, Chen SC (2009) Determining landslide susceptibility in Central Taiwan from rainfall and six site factors using the analytical hierarchy process method. Geomorphology 112:190–204

Wu W, Sidle RC (1995) A distributed slope stability model for steep forested basins. Water Resources Research 31:2097–2110

Xu M, Watanachaturaporn P, Varshney P, Arora M (2005) Decision tree regression for soft classification of remote sensing data. Remote Sensing of Environment 97:322–336

Yalcin A (2008) GIS-based landslide susceptibility mapping using analytical hierarchy process and bivariate statistics in Ardesen (Turkey): comparisons of results and confirmations. Catena 72:1–12

Yu SB, Chen HY, Kuo LC (1997) Velocity field of GPS stations in the Taiwan area. Tectonophysics 274:41–59

Appendix

Mass movements data

Year	Type	Date	Time	Coordinate (TWD97)	
				X	Y
2006	Landslides	0609	05:00	271789	2676720
	Landslides	0609	15:00	263297	2657260
	Landslides	0609	17:00	213143	2627780
	Debris flows	0609	18:00	214028	2533860
	Landslides	0610	05:00	234380	2689060
	Debris flows	0610	06:00	213974	2533630
	Landslides	0610	08:00	229696	2715190
	Debris flows	0610	12:00	236220	2625280
2007	Landslides	0607	16:00	234203	2650390
	Landslides	0607	16:00	235738	2637140
	Landslides	0608	16:00	230811	2658990
	Landslides	0608	14:00	227902	2687190
	Landslides	0608	15:00	231561	2662090
	Debris flows	0809	02:00	249583	2502790
	Debris flows	0813	19:00	219720	2510320
	Debris flows	0813	19:00	217418	2510800
	Landslides	0813	07:00	249570	2650110
	Landslides	0813	19:00	219412	2510520
	Landslides	0813	19:00	218249	2510970
	Landslides	0813	19:00	216409	2511440

	Landslides	0813	19:00	214851	2511810
	Landslides	0813	16:00	220189	2510040
	Landslides	0813	16:00	219943	2510340
	Landslides	0814	03:00	193031	2549220
	Landslides	0818	23:00	205628	2589020
	Debris flows	0819	12:00	212422	2552870
	Landslides	0819	17:00	225171	2648550
	Debris flows	0820	12:00	218919	2556200
	Debris flows	0918	17:00	236220	2625280
	Landslides	0918	11:00	288208	2731260
	Landslides	0918	11:00	286320	2728360
	Landslides	0919	01:00	224102	2694400
	Landslides	1006	23:00	226019	2668790
	Landslides	1006	15:00	305861	2779170
	Landslides	1006	16:00	296554	2780540
	Landslides	1006	19:00	270450	2725990
	Landslides	1006	16:00	228165	2684230
2008	Debris flows	0717	19:00	196261	2570460
	Debris flows	0717	19:00	196930	2571660
	Debris flows	0717	20:00	201448	2558650
	Debris flows	0717	23:00	218800	2556180
	Debris flows	0717	23:00	202968	2548830
	Debris flows	0717	23:00	210442	2554980
	Landslides	0717	23:00	218553	2556000
	Landslides	0717	23:00	214131	2538220

	Landslides	0717	23:00	211288	2551310
	Landslides	0717	22:00	218035	2554600
	Landslides	0717	22:00	211807	2552650
	Debris flows	0718	00:00	204502	2563710
	Debris flows	0718	02:00	252972	2645180
	Debris flows	0718	02:00	244118	2635950
	Debris flows	0718	04:00	248620	2645430
	Debris flows	0718	04:00	250829	2645280
	Debris flows	0718	02:00	214016	2542260
	Debris flows	0718	02:00	217351	2556060
	Debris flows	0718	03:00	218572	2556140
	Debris flows	0718	03:00	219053	2555490
	Debris flows	0718	06:00	233929	2679630
	Debris flows	0718	00:00	208214	2562690
	Landslides	0718	11:00	234285	2676170
	Landslides	0718	02:00	230627	2650930
	Landslides	0718	06:00	271862	2674510
	Landslides	0718	03:00	217329	2555470
	Landslides	0718	02:00	206123	2585550
	Landslides, Debris flows	0718	08:00	227779	2676790
	Landslides	0718	05:00	233831	2642370
	Debris flows	0728	10:00	288784	2615330
	Landslides	0728	17:00	230627	2650930
	Debris flows	0914	02:00	322234	2744360

	Landslides	0914	20:00	297308	2763270
	Landslides	0914	10:00	236032	2625810
	Landslides	0914	20:00	237108	2696690
	Landslides	0914	04:00	210945	2603620
	Debris flows	0915	08:00	258755	2655420
	Debris flows	0915	05:00	259547	2655720
	Landslides	0915	11:00	269023	2657540
	Landslides	0915	11:00	226712	2678580
	Landslides	0915	15:00	233548	2702840
	Landslides	0915	01:00	240614	2717050
	Landslides	0928	21:00	309528	2764340
2009	Debris flows	0807	20:00	213302	2538430
	Debris flows	0807	21:00	217318	2555480
	Debris flows	0807	21:00	217520	2555430
	Landslides	0807	23:00	222637	2600970
	Landslides	0807	23:00	216875	2604190
	Landslides	0807	21:00	211218	2597660
	Debris flows	0808	15:00	240709	2476520
	Debris flows	0808	17:00	201599	2552700
	Debris flows	0808	18:00	236923	2607260
	Debris flows	0808	15:00	235152	2602760
	Debris flows	0808	21:00	236309	2604540
	Debris flows	0808	13:00	213351	2518960
	Debris flows	0808	20:00	215347	2495590
	Debris flows	0808	09:00	214010	2533640

	Debris flows	0808	20:00	210455	2554960
	Debris flows	0808	21:00	210209	2552670
	Debris flows	0808	16:00	219053	2571060
	Debris flows	0808	16:00	219088	2570760
	Debris flows	0808	17:00	218240	2555750
	Debris flows	0808	16:00	231588	2572270
	Debris flows	0808	22:00	219261	2610340
	Debris flows	0808	03:00	211034	2569400
	Debris flows	0808	02:00	216196	2586730
	Debris flows	0808	17:00	216297	2578850
	Debris flows	0808	22:00	217230	2603950
	Debris flows	0808	20:00	221915	2603490
	Debris flows	0808	21:00	221981	2605880
	Debris flows	0808	20:00	221733	2607120
	Debris flows	0808	20:00	214000	2542260
	Debris flows	0808	20:00	209757	2556470
	Landslides, Debris flows	0808	20:00	218120	2552950
	Landslides, Debris flows	0808	21:00	217292	2551280
	Landslides, Debris flows	0808	17:00	217200	2554780
	Landslides, Debris flows	0808	21:00	217010	2550440
	Debris flows	0808	04:00	215422	2491750

	Debris flows	0808	22:00	203840	2550330
	Landslides	0808	03:00	220186	2510030
	Landslides	0808	15:00	215792	2545890
	Landslides	0808	19:00	210309	2558590
	Landslides	0808	06:00	211503	2558840
	Landslides, Debris flows	0808	11:00	217706	2491850
	Landslides	0808	07:00	242082	2483450
	Landslides	0808	06:00	201060	2573560
	Landslides	0808	20:00	237189	2608590
	Landslides	0808	08:00	235770	2603460
	Landslides	0808	01:00	219375	2518970
	Landslides	0808	17:00	214968	2544220
	Landslides	0808	17:00	213813	2546470
	Landslides	0808	23:00	208755	2552250
	Landslides	0808	06:00	211501	2558910
	Landslides	0808	16:00	232221	2573550
	Landslides	0808	22:00	213065	2611860
	Landslides	0808	22:00	218015	2610860
	Landslides	0808	02:00	218092	2582330
	Landslides	0808	23:00	217186	2604360
	Landslides	0808	01:00	215025	2603620
	Landslides	0808	05:00	234180	2446910
	Landslides	0808	09:00	229222	2448250
	Landslides	0808	22:00	215620	2498440

	Landslides	0808	15:00	224234	2515720
	Landslides	0808	17:00	220139	2548370
	Landslides	0808	22:00	221506	2550490
	Landslides	0808	22:00	224124	2551580
	Landslides	0808	22:00	224914	2551730
	Landslides	0808	23:00	220029	2603480
	Landslides	0808	23:00	221590	2604390
	Landslides	0808	01:00	215131	2603360
	Landslides	0808	19:00	216683	2602780
	Landslides	0808	05:00	233025	2444780
	Landslides	0808	08:00	217859	2508450
	Landslides, Debris flows	0808	20:00	208242	2551290
	Landslides	0808	22:00	226801	2595820
	Landslides	0808	07:00	218911	2523350
	Debris flows	0809	01:00	243095	2481210
	Debris flows	0809	04:00	245059	2492460
	Debris flows	0809	02:00	238682	2614080
	Debris flows	0809	06:00	215812	2547380
	Debris flows	0809	05:00	206646	2545690
	Debris flows	0809	03:00	205377	2585680
	Debris flows	0809	06:00	223475	2602970
	Debris flows	0809	06:00	224230	2601580
	Debris flows	0809	03:00	222815	2603040
	Debris flows	0809	02:00	236875	2607220

	Debris flows	0809	01:00	221514	2588790
	Landslides, Debris flows	0809	17:00	218648	2568620
	Landslides	0809	00:00	214515	2491870
	Landslides	0809	06:00	217065	2610160
	Landslides	0809	01:00	198900	2570030
	Landslides	0809	02:00	232615	2630960
	Landslides	0809	05:00	235984	2649960
	Landslides	0809	10:00	227354	2620520
	Landslides	0809	00:00	214789	2491770
	Landslides	0809	04:00	216088	2545470
	Landslides	0809	06:00	221973	2555590
	Landslides	0809	06:00	215816	2547870
	Landslides	0809	09:00	214750	2568190
	Landslides	0809	04:00	217161	2534360
	Landslides	0809	07:00	210392	2609910
	Landslides	0809	00:00	218789	2609060
	Landslides	0809	03:00	218280	2609280
	Landslides	0809	06:00	212434	2610810
	Landslides	0809	06:00	213537	2612820
	Landslides	0809	05:00	213487	2613590
	Landslides	0809	06:00	213210	2611580
	Landslides	0809	04:00	204417	2584310
	Landslides	0809	02:00	221370	2603770
	Landslides	0809	01:00	214337	2606570

	Landslides	0809	02:00	216913	2602650
	Landslides	0809	06:00	214489	2604970
	Landslides	0809	01:00	213294	2592970
	Landslides	0809	02:00	243543	2482230
	Landslides	0809	06:00	213479	2562100
	Landslides	0809	05:00	211780	2552630
	Landslides, Debris flows	1005	18:00	313070	2727300
	Landslides	1006	01:00	319875	2722820
2010	Landslides	0901	13:00	242117	2483640
	Debris flows	0919	21:00	214010	2533640
	Debris flows	0919	18:00	213963	2534790
	Debris flows	0919	20:00	212968	2532830
	Debris flows	0919	21:00	212130	2533580
	Landslides	0919	23:00	217274	2491960
	Landslides	0919	21:00	217155	2553860
	Landslides	0924	06:00	309422	2786760
	Debris flows	1021	15:00	335878	2721790
	Landslides, Debris flows	1021	11:00	338007	2719080
	Landslides, Debris flows	1021	12:00	337348	2719520
	Landslides, Debris flows	1021	15:00	336005	2721870
	Landslides	1021	14:00	334851	2719170

	Landslides	1021	10:00	336446	2719510
	Landslides	1021	12:00	337519	2720080
	Landslides	1021	16:00	331735	2723800
	Landslides	1021	12:00	331957	2723390
	Landslides	1021	15:00	336091	2721790
	Landslides	1021	12:00	335577	2721340
	Landslides	1021	14:00	336496	2721740
	Landslides	1021	14:00	337400	2719870
	Landslides	1021	14:00	337536	2720000
	Landslides	1021	12:00	337533	2719390
	Landslides	1021	12:00	336867	2719530
	Landslides	1021	12:00	336987	2719030
	Landslides	1021	10:00	335347	2718090
	Landslides	1021	12:00	334663	2721610
	Landslides	1021	12:00	337457	2719360
	Landslides	1021	14:00	336155	2718630
	Landslides	1021	11:00	335578	2719810
2011	Landslides	0719	04:00	222154	2605800
	Landslides	0828	23:00	230932	2441750
	Debris flows	0829	07:00	230940	2437870
	Landslides	0829	04:00	231443	2442040
	Landslides	0829	14:00	230132	2449270
	Landslides	0830	11:00	227193	2428070
	Debris flows	1002	05:00	308508	2725720
	Debris flows	1002	05:00	308166	2724940

	Landslides, Debris flows	1002	10:00	304055	2723660
	Landslides, Debris flows	1002	10:00	303765	2723390
	Landslides	1002	04:00	305512	2724000
	Landslides, Debris flows	1002	19:00	279207	2563740
	Debris flows	1003	03:00	319315	2722340
	Landslides	1003	05:00	312526	2725370
	Landslides	1009	05:00	336604	2713870
2012	Debris flows	0503	16:00	237257	2618140
	Landslides	0610	22:00	270809	2663220
	Debris flows	0610	18:00	258340	2649550
	Debris flows	0610	16:00	215578	2547970
	Debris flows	0610	14:00	216247	2545580
	Landslides	0610	17:00	237827	2669770
	Landslides	0611	18:00	271204	2683570
	Landslides	0611	12:00	236869	2661400
	Landslides	0612	00:00	305246	2767080
	Landslides, Debris flows	0612	09:00	307217	2762280
	Debris flows	0612	11:00	222990	2603060
	Landslides	0612	05:00	308658	2769590
	Debris flows	0612	19:00	236873	2607210
	Landslides	0612	11:00	235926	2645590

	Debris flows	0802	08:00	293494	2752700
	Landslides	0802	12:00	288715	2705230
	Debris flows	0802	04:00	322954	2682570
	Debris flows	0802	04:00	325310	2685220
	Debris flows	0802	04:00	325135	2684680
	Debris flows	0802	02:00	329805	2707730
	Landslides	0802	02:00	329527	2708610
	Landslides	0803	00:00	250007	2723970
	Debris flows	0824	06:00	233765	2432400
2013	Landslides	0520	01:00	237469	2622640
	Landslides	0921	23:00	252150	2510260
	Landslides	0829	13:00	222684	2659540
	Landslides	0829	13:00	223067	2659640
	Landslides	0829	13:00	187252	2545560
	Landslides	0831	07:00	216721	2463340
	Debris flows	0829	12:00	214205	2468060
	Landslides	0831	17:00	328944	2782440
	Landslides	0831	17:00	329064	2782130
	Landslides	0831	16:00	329926	2781470
	Landslides	0829	06:00	202375	2611170
	Landslides	0901	04:00	293408	2778760
	Landslides	0901	05:00	301730	2744580
	Landslides	0829	06:00	203676	2583460
	Landslides	0829	03:00	201419	2601770
	Landslides	1006	16:00	291137	2729750

	Landslides	1006	15:00	277020	2729390
	Debris flows	0713	07:00	242875	2675370
	Debris flows	0713	07:00	243396	2637730